1998

Model verificaton of quantitative precipitation forecasts over California

Scott Archer
San Jose State University

INFORMATION TO USERS

This manuscript has been reproduced from the microfilm master. UMI films the text directly from the original or copy submitted. Thus, some thesis and dissertation copies are in typewriter face, while others may be from any type of computer printer.

The quality of this reproduction is dependent upon the quality of the copy submitted. Broken or indistinct print, colored or poor quality illustrations and photographs, print bleedthrough, substandard margins, and improper alignment can adversely affect reproduction.

In the unlikely event that the author did not send UMI a complete manuscript and there are missing pages, these will be noted. Also, if unauthorized copyright material had to be removed, a note will indicate the deletion.

Oversize materials (e.g., maps, drawings, charts) are reproduced by sectioning the original, beginning at the upper left-hand corner and continuing from left to right in equal sections with small overlaps. Each original is also photographed in one exposure and is included in reduced form at the back of the book.

Photographs included in the original manuscript have been reproduced xerographically in this copy. Higher quality 6" x 9" black and white photographic prints are available for any photographs or illustrations appearing in this copy for an additional charge. Contact UMI directly to order.

UMI

A Bell & Howell Information Company
300 North Zeeb Road, Ann Arbor MI 48106-1346 USA
313/761-4700 800/521-0600

MODEL VERIFICATION OF QUANTITATIVE PRECIPITATION FORECASTS OVER CALIFORNIA

A Thesis

Presented to

The Faculty of the Department of Meteorology

San Jose State University

In Partial Fulfillment

Of the Requirements for the Degree

Master of Science

By

Scott Archer

August 1998

APPROVED FOR THE DEPARTMENT OF METEOROLOY

Douglas M. Sinton

Prof. Douglas Sinton

Scot C.R Rafkin

Prof. Scot Rafkin

David W. Reynolds

Mr. David Reynolds

APPROVED FOR THE UNIVERSITY

William Fisher

ABSTRACT

MODEL VERIFICATION OF QUANTITATIVE PRECIPITATION FORECASTS OVER CALIFORNIA

By Scott Archer

The National Weather Service Forecast Office (NWSFO) in Monterey, California utilizes model data from the National Center for Environmental Prediction in producing quantitative precipitation forecasts (QPF). The Eta suite is utilized most frequently in making QPF's at the NWSFO in Monterey because of its relatively high resolution and decent microphysical package as compared to other operational models. This study addressed the question of whether increased horizontal resolution improves model QPF. Model precipitation bias were calculated for the winter 1996-1997 and the January 1997 flood.

Model precipitation bias show that increased horizontal resolution improved model QPF, with the 29 km mesoscale Eta showing less of a bias than the 48 km Eta. Both models under predicted precipitation at all thresholds considered. Precipitation bias increased with increased threshold, suggesting that models are not capable of accurately predicting heavier precipitation. Increased horizontal resolution improved the spatial distribution of precipitation over the complex topography of California.

ACKNOWLEDGMENTS

First off, I would like to thank David Reynolds for his guidance and dedication to this study, even after the big move to Maryland, he continued to support my work. He gave me the opportunity to improve my skills beyond anything I ever imagined. Now for Dr. Sinton, or should I say, Doug. His incredible knowledge on synoptic meteorology has given me the desire to learn as much as I can about the topic. If only I could learn more. Doug got the ball rolling for my National Weather Service "experience", and continued to support my efforts, not to mention reading my thesis drafts. If only I could have worked more with him.

I would also like to thank Dr. Scot Rafkin for taking the time to read my thesis and giving me excellent advice and correcting my horrible errors. He saved me some embarrassing moments should my thesis have been printed with those mistakes. Since this is the culmination of seven years at SJSU, I'd like to thank all of the staff and faculty in the Meteorology department for the knowledge they bestowed upon me and the help given to me. Without it, I could never have completed my thesis. Now for the staff at the NWS, thanks for putting up with me all those years. I learned a lot about operational forecasting in that time.

Lastly, I'd like to thank my father for his support and insisting that I continue my education and get a M.S. in meteorology.

TABLE OF CONTENTS

LIST OF TABLES

LIST OF FIGURES

I. INTRODUCTION

The National Weather Service Forecast Office (NWSFO) in Monterey California is interested in improving quantitative precipitation forecasting (QPF) over their area of responsibility - the Northern and Central California forecast area (FA). Complex topography in the Western United States, along with inadequate observations over the Eastern Pacific contribute to poor model initialization and poor precipitation forecasts over California. Currently, the Monterey NWSFO receives numerical guidance including QPF from several synoptic scale and mesoscale models running at the National Center for Environmental Prediction (NCEP), the Lawrence Livermore National Laboratory (LLNL), the United States Navy (USN), the Naval Postgraduate School (NPS) in Monterey, and the California/Nevada River Forecast Center (CNRFC). This research will address the operational QPF problem in the FA by evaluating the performance of various mesoscale models on both a statistical and case study basis. The primary emphasis will focus on the NCEP Eta suite resolution and it's effect on model QPF's.

The first goal of the proposed research is to describe the various model physics, including microphysics, convective parameterization, variations in spatial resolution, and topography. This will provide an understanding of how precipitation is produced by each model. Enhancement of precipitation through various microphysical processes, convection, topography, and mesoscale phenomena can then be related to model physics and resolution.

The second goal is to identify and describe several flood events that have occurred in California. In addition, a limited set of model predictors will be used for comparison purposes for future events. This will provide forecasters the opportunity to review rain totals and rain rates that historically produce flooding and flash flooding.

The third goal will be to determine the accuracy of synoptic-scale and mesoscale model precipitation forecasts at several California locations using bias statistics. Local NWS studies have shown that during major flood events, synoptic-scale models under predicted precipitation at favored orographic locations, whereas, the higher resolution mesoscale models over predicted precipitation. This study will examine the precipitation trends from NCEP's 29, and 48 km Eta models, which are identical except for resolution, and MM5 currently being run at the NPS in Monterey. Precipitation forecasts for the winter of 1996-1997 will be analyzed and compared to observations which will then determine if biases are associated with the 29 km and 48 km Eta.

Once the precipitation trends are determined on a statistical and case by case basis, a strategy for improving operational QPF based on interpretation and application of model products will be implemented. By addressing model weak points such as topography, frontal movement, moisture initialization, and convective parameterization, forecasters will better understand the model they are using as a forecast tool. With this knowledge forecasters at the NWSFO in

Monterey and all offices in Northern and Central California will be better prepared to utilize these model forecasts when preparing QPF's.

Past studies conducted at NCEP (Mesinger, 1998; Gartner, 1996) have shown that the Eta model has less of a precipitation bias than does the aviation (AVN), medium range forecast model (MRF), the nested grid model (NGM), and the regional spectral model (RSM). That is, the Eta tends to neither over or under predict precipitation as compared to other models run at NCEP. This study will expand on the regional bias idea by determining bias statistics for locations in California, including 144 locations in the Northern and Central California mountains, during the New Years Flood of 1997. First, the physical and microphysical processes involved in precipitation development will be reviewed.

2.0 Physical characteristic of California rains

A. Precipitation Processes

Knowledge about the processes that produce precipitation can enable forecasters to make a better forecast of precipitation intensities and amounts. This section will briefly describe some microphysical processes observed in cloud and precipitation formation. The material in this section is primarily drawn from a NWS training manual by Chappell.

Condensation of water vapor to form cloud droplets requires cloud condensation nuclei (CCN), or a small particle of dust or other aerosol. As CCN

and water vapor rise in the atmosphere, the parcel of air cools approximately at the adiabatic lapse rate and can result in a parcel becoming saturated with respect to water, at which point condensation begins on the most effective CCN. The droplet population that results depends on the spectrum of CCN which can vary greatly, especially from oceanic to continental locations. The CCN spectrum is important since it will influence the initiation and efficiency of droplet growth. Cloud droplets will grow through diffusional growth, or condensation. Diffusional growth by itself is very slow as compared to growth through collision and coalescence. This will be discussed later.

A necessary but not sufficient condition for heavy rainfall rates is the high production rate of condensate. The condensate supply rate is defined by:

$$C_r = -\int_{CB}^{CT} \varrho W \frac{\partial r_s}{\partial Z} \Delta Z \qquad (1)$$

where ρ = air density, W=updraft speed, r_s = saturation mixing ratio, ΔZ = cloud depth of layer, CT is cloud top, CB is cloud bottom, and C_r = rate of condensate production for a column of unit area. The rate at which condensate is produced in a column of air is directly proportional to air density, updraft speed, cloud thickness, and the vertical gradient of the saturation mixing ratio. The term ρW is the vertical mass flux term. That term combined with $\partial r_s/\partial z$

describes the vertical flux of moisture/condensate within the cloud, or the convergence/divergence of moisture/condensate. The density and vertical gradient of saturation mixing ratio terms act to limit the higher condensate supply rates to lower portions of the cloud, as density and mixing ratio decreases with height. The vertical motion will largely depend on large scale and orographic lifting and upright or slantwise convection. High condensate supply rates may be necessary for large rainfall rates, however, the condensate must be converted to precipitation sized particles through either collision/coalescence or ice processes, or a combination of the two.

Hess (1974) stated that orographic lift on the west slope of the Cascades and Sierra can contribute to droplet growth and broadening of the droplet spectrum for several hours. This can lead to the formation of coalescence type precipitation. In addition, low level clouds in the California central valley can exist for many hours, resulting in larger droplets. The typical residence time in a cloud would be between a one half to one hour, which will limit the droplet size and produce a relatively narrow droplet spectrum. On the west slope of the Sierra, residence times can be as long as several hours (Hess 1974).

The development of rain in clouds that contain no ice is known as collision and coalescence (warm rain process). Collision and coalescence depends to a large part on the droplet size spectrum. Collisions are rare for droplets smaller than 18 microns, but larger droplets can collide with droplets

either smaller or larger than 18 microns. The broader the droplet spectrum, the higher the collision efficiency. In order to form a rain drop, the cloud droplets must collide and coalesce, forming one drop. Drops may break up or bounce off upon collision. Should the cloud droplet size spectrum be narrow, most cloud droplets will have the same fall speeds and few collisions will occur, and precipitation formation will be slow. If the cloud droplet spectrum is wide, there will be many different fall speeds and the probability of collisions between cloud droplets will increase, and precipitation sized drops will form much faster. Some factors that influence the precipitation efficiency include variable fall speeds and the residence time in the cloud. Longer residence times in clouds allow for greater chances of collision and is related to updraft speed and cloud depth.

Rain drops seldom exceed a radius of 2.5 mm due to droplet break up. Since radar reflectivity is proportional to the sixth power of the drop diameter, drop breakup may cause the radar to underestimate precipitation intensity (Ray 1986). This is primarily due to the small drop radius, which results in lower reflectivity, but can result in continuous moderate rainfall if there are many drops. This has been observed in the Santa Cruz Mountains and the San Francisco Bay area in the past (Reynolds 1995).

In general, during winter precipitation, ice growth rates are comparable to the rate at which condensate is being produced in the cloud. Growth of ice crystals in a cloud at water saturation is rapid since the cloud will be highly

saturated with respect to ice. Ice crystals will grow at the expense of the cloud droplets, so if condensation does not sufficiently replace the cloud droplets being depleted by ice crystal growth, all cloud droplets may evaporate resulting in a glaciated cloud at ice saturation. In this case, ice particle growth will be near zero. The rate at which the mass of an ice crystal grows is given by equation 2.

$$\frac{dM}{dt} = 4\pi CGS \qquad (2)$$

Where C is the analog of electrostatic capacity, which is a function of crystal habit and size. G is the thermodynamic function which is a function of temperature and pressure and is a maximum at -15 °C. S is the supersaturation relative to a plane ice surface and is a maximum at -12 °C for a water saturated cloud. The growth of ice crystals also depends on the number of crystals per unit volume that are growing. Ice particle concentration is roughly 1-10 crystals/liter at -20 °C, and 10-100 crystals/liter at -25 °C. Additional increases in ice particle concentrations may result from fracturing of crystals and splintering when cloud droplets freeze (ice multiplication). At cloud top temperatures warmer than -5 °C, ice particle concentration is small enough so that snow does not usually occur. For cloud top temperatures between -5 °C and -25 °C, precipitation efficiencies within stratiform or orographic clouds will

vary from 0-100%, where precipitation efficiency is the percent of condensate that is used in the production of precipitation. At cloud top temperatures less than -25 °C all condensate will be used and precipitation efficiency will be high.

A phenomena called ice multiplication can occur if cloud top temperatures are near -5° C. Freezing of larger drops as they accrete onto existing ice can lead to ice splintering, increasing the number of ice crystals (Hallet and Massop 1974). These ice crystals can act as precipitation embryos which can grow rapidly by coalescence or aggregation, and result in heavy rain or snow. Thus, a combination of ice splintering/riming and coalescence growth can be a major mechanism for heavy precipitation.

Houze (1993) describes the seeder-feeder mechanism as a possibility of enhancing precipitation. Weak convective cells above nimbostratus produce about 20% of the mass of precipitation in the form of ice particles. The convective cell can act as the "seeder", which will precipitate into the lower clouds. The feeder zone consists of the orographic cloud layer, and contains 80% of the precipitation mass. Ice particles that fall through the warmer cloud can grow through deposition, or collision and coalescence if they melt.

Processes in heavy precipitation involve collision and coalescence growth, ice crystal multiplication processes, and seeding of the orographic cloud by ice crystals precipitating from higher, colder clouds. (Hess 1974). Hess noted

that clouds over higher mountains of continental areas will have minimal ice multiplication effects, whereas maritime clouds in lower elevations will be more likely to utilize ice multiplication. Another factor influencing orographic precipitation is the presence of convection, but is poorly documented. Along the west coast, higher clouds will over-run warm orographic cloud regions. Ice crystals formed at the colder temperatures can settle into the lower orographic clouds, increasing the ice particle concentrations within the orographic cloud. This results in increased precipitation efficiency and heavier precipitation (Hess 1974).

A typical heavy rain event in California is associated with a shallow layer of orographic clouds (3000 m deep), and a much deeper layer of cold clouds. Large-scale cyclonic storms are typically observed with a lower cloud deck containing the primary water supply, and an upper cloud deck containing ice crystals that precipitate into the lower clouds (Byers 1965). In some cases, due to the shallow nature of the orographic clouds that contain most of the liquid water, precipitation may not be seen by KMUX WSR-88D. A typical storm of subtropical/maritime origin will likely have a high liquid water content, deep moisture, relatively warm temperatures, and a deep surface low producing strong southwesterly winds. The combination of the warm rain process, ice multiplication, seeding from higher clouds, orographic enhancement, and strong

forcing associated with a powerful jet (deep surface low, large upward vertical velocities) combine to produce very heavy rainfall over mountainous regions of California.

One way of viewing the physical state of the atmosphere is through vertical soundings. From an observed or model forecast sounding one can determine the local stability, temperature, moisture, and wind profiles, and determine if heavy precipitation is possible. The next section will show observed and model soundings for major storms, which can be related to some microphysical processes.

B. Model and Observed Soundings

Model and observed soundings clearly show the nature of major precipitation events. Figures 1-4 are model soundings for the March 1995 flood, December 1995 storm, the January 1997 flood, and a storm from December 10 1996 over the Santa Cruz mountains that resulted in flash flooding. Similar characteristics are seen in all four soundings with strong south-southwesterly winds in the lower levels, the air mass is nearly saturated from the surface to the tropopause, with warm temperatures near 700 mb (T>0°C). Deep moisture seen in soundings combined with strong upward vertical velocities, high mixing ratios, and strong winds perpendicular to mountain ranges imply that high condensate supply rates exist. In addition, the soundings are nearly saturated up to -30 °C, implying the possibility of both warm and cold clouds that can result in a highly

efficient precipitation pattern.

C. Hydrological Factors

The next section discusses precipitation rates and synoptic characteristics typical of California floods. The floods of January 1982, February 1986, January 1995, March 1995, and January 1997 all show similar features.

The following section describes the hydrologic factors to consider in determining the possibility of flooding or flash flooding as a result of a major storm. The information comes from Barbato (1989).

Precipitation or QPF greater than the following rates should always be closely monitored for possible flooding/flash flooding:

a) 0.5 to 1.0 " per hour, sustained, anywhere.
b) 1.5 to 2.5 " in six hours over any high flash flood risk areas such as: areas with saturated soils, urban areas, headwater, lightly vegetated, steeply sloped, landslide-prone, low channel capacity areas.
c) over 3" in six hours in areas with less risk: dry soils, heavily vegetated, non-headwater, high channel capacity areas.

The areal extent, speed, and direction of movement of the precipitation with respect to the topography, drainage, basin orientation are important. The threat of flooding is usually increased when the storm is:

a) Of wide areal extent.
b) Slowly moving.
c) Continually tracking over the same area or same drainage basin.
d) Moving down the basin, or
e) In the downstream part of the basin (causing higher, quicker crests downstream).
f) Moving perpendicular to the orientation of mcuntain ranges (causing increased orographic effects).

Antecedent soil conditions and other physical conditions of the basin are also a necessary factor to include. The threat of flooding is usually increased when heavy precipitation is falling on:

a) saturated ground in any terrain.
b) Impervious surfaces such as rocky ground, urban areas or frozen ground.
c) Very small basins, especially in headwater areas.
d) Steep terrain; in or near mountainous or hilly areas.
e) Areas void of live vegetation, such as deserts and high mountains.

Generally, the smaller the creek and basin, the greater the flash flood potential because of the small streams inability to carry large amounts of water. Large rivers and streams generally do not flash flood because they are able to hold great amounts of water. Also, because of the large basin size, it takes water longer to collect into the rivers from smaller tributaries. Sustained widespread heavy rainfall and/or snow melt is generally what causes mainstem flooding, not localized heavy precipitation. Only low elevation shallow snow pack will contribute to runoff. For rainfall intensity return periods, see table 4.

Synoptic situations associated with previous floods and flash floods are described by Barbato (1989). Four meteorological factors that summarize the characteristics of winter season heavy precipitation events in northern and central California include:

a) A long, moist fetch of southwesterly flow (i.e. the "pineapple connection").
b) Tight surface pressure gradient resulting in flow perpendicular to the orientation of mountain ranges (causing increased orographic effects).

c) Slow southward movement of the frontal boundary.
d) Cyclogenesis on the front, prolonging the period of rain.

When viewing model output, forecasters should keep these criteria in mind.

A major portion of this research involved the collection of model and observed precipitation at the NWSFO in Monterey which is discussed next.

3.0 DATA COLLECTION, PROCESSING, AND RESOLUTION

The NWSFO in Monterey utilizes a Hewlett Packard (HP) 735 workstation that receives numerical model and weather products. The HP is running Unidata's Local Data Manager (LDM) which captures, processes, and distributes data. The system performs event-driven data processing. That is, when a product arrives it is immediately processed. The HP ingests both the Automation of Field Operations and Service (AFOS) products from the AFOS Protocol Translator (APT), and gridded Binary (GRIB) data from the Western Region Headquarters (WRH) server.

Nearly all AFOS products available in the United States are processed by the LDM on the HP 735. Surface and upper air observations are decoded and converted into the GEneral Meteorological PAcKage (GEMPAK) format. For this study, precipitation amounts were taken from the AFOS product SFORR4SAC to verify model QPF's.

The HP 735 receives model data in a GRIdded Binary (GRIB) format from the Western Region Headquarters. The LDM first captures the data, then

processes it via GEMPAK programs, and distributes it to the proper directories. Raw GRIB data is first written to disk (/usr1/nawips/metdat/raw/grib directory). The LDM then runs the GEMPAK program "nagrib" or "nagrib_nc" (low memory). Nagrib converts the raw GRIB files into gempak grid files. The LDM then runs the script make_meta.csh (/usr1/nawips/ldm) which reads the gempak grid files and creates "metafiles" that are viewed using NTRANS. The precipitation grids are created for all forecast times except the initial time. The 48 km Eta has six hour forecasts, while the Mesoscale Eta has a three hour forecast period. The conversion of precipitation from GRIB to text is discussed in appendix A.

The different resolution Eta models are each post-processed on different grids with different resolutions, as seen in Table 1. Discrepancies may arise from the fact that NCEP output for the Eta is on the staggered Arakawa E grid and eta vertical coordinate, which is then converted to the AWIPS grids and various vertical coordinates. For the purpose of this study it is convenient to verify the data on the grids that are viewed by the forecasters (AWIPS grids).

While the Eta suite is run at 48, 29, and 10 km, the fields that are viewed are actually interpolated from the 48 km to 80 km, 29 km to 40 km and 20 km grid, while the 10 km data is on a 10 km grid. This means that the data is interpolated to a non-native grid, which will introduce discrepancies between the true model and the data being viewed. This will have a profound impact on all

graphical displays and bias statistics that are determined at a "single" point.

The NWSFO in Monterey receives four sets of Eta model output at various grid spacing (48/29/20/10km). The final products viewed at the NWS are actually interpolated to a different grid than the original run, as seen in table 1. NCEP has created a 20 km output grid for the 29 km Eta, where the full computational resolution can be reproduced. The 20 km grid contains the same model output as the 40 km grid but is interpolated to a higher resolution. It also contains fewer output fields, some of which are: pressure, precipitation, 2 m temperature, 2 m RH, 10 m wind and boundary layer fields. By looking at model topography in figure 5, one can clearly see the difference in the final graphical resolution. In figure 5, the NGM and ETA output is on an 80 km grid, the 29 km Mesoscale Eta data is on a 40 km grid, and the 10 km Mesoscale Eta is on a 10 km grid. One would expect higher resolution models to produce better QPF's. Bias statistics in section six will prove this to be true for the Eta suite.

Bias scores for the 48 and 29 km Eta (discussed in section 6) show that improved resolution produces a better QPF. As resolution increases, the effective barrier height of mountains increases, increasing the vertical velocity and precipitation as a result. Figure 6a shows the graphical difference between model QPF's, with the higher resolution models resolving mountain and valley locations much better than the lower resolution models. However, graphical

smoothing for the 29 km Eta is only a product of the interpolation to the 20 km and 40 km grids. The 48 km Eta interpolated to 80 km produces a precipitation maxima that is spread out over both mountains and valleys which is not observed nor expected climatologically. However, given the models resolution, one would not expect model precipitation to represent climatology. The 29 km Eta and 12 km MM5 clearly show rain-shadowed valleys and precipitation maxima in the mountains. Figure 6b shows the climatological precipitation average for northern California, with maxima in mountainous regions and minima's in valleys. The Eta suite can only represent the topography that they resolve, therefore the need for improved resolution. Given a sufficient grid resolution, models should reproduce climatologically observed patterns during orographic events.

4.0 MODELS

This section will discuss some important model features that are necessary for understanding how models predict weather and precipitation. With some knowledge of microphysical processes involved in the formation of precipitation, we now want to see how numerical models either predict or paramaterize precipitation. With a better understanding of model parameterization and microphysics, forecasters can better understand the products they are using as guidance for QPF's. In addition, the MM5 and Rhea orographic model will briefly be summarized.

A. The Eta Suite

The current suite of "Eta" models were developed and run at NCEP's Environmental Modeling Center, Mesoscale Modeling Branch. The 80 km, 38 layer 'early' Eta, became operational and replaced the Limited-area Fine-mesh Model (LFM) in June 1993; this was later reduced to 48 km resolution. The 48 km Eta is called the 'Early' Eta because it is the first of the operational models to run after the 12z and 00z data assimilation. The 29 km/50 level Mesoscale Eta was tested in early 1996 and became operational in August 1996. Between January and August 1997, the 10 km/60 layer Eta was run once per day over the Western United States for test purposes. Currently, the same source code is used for both the Early and Mesoscale Eta Model systems, with the last major implementation on 18 Feb 97.

The 29/10 km Mesoscale Eta is a 50/60 layer hydrostatic model with its greatest vertical resolution near the mean height of the tropopause and near sea-level, with layer depths ranging from 20 meters at sea level to 2 km at 50 mb. In areas of higher terrain, the model will not utilize the higher resolution since the model coordinate will be under ground. The addition of 10 vertical levels to the 10 km domain mainly impacts grid points just cff the West Coast (Mittelstadt 1996) by improving the resolution of the boundary layer. The Mesoscale Eta forecast period is 33 hours which takes 35/105 (29/10 km) minutes to run on a CRAY at NCEP (Mittelstadt 1996). The 48 km 'early' Eta is

run twice daily at 12z and 00z. The 29 km Mesoscale Eta is also run twice a day, but at 03z and 15z. The 10 km Eta (no longer operational) was run only once a day at 03z.

The 29 km Mesoscale Eta is nested within, and receives its boundary conditions from the Aviation (AVN) run of the Global Spectral Model (GSM) which has a horizontal resolution of roughly 105 km. In early 1997, a 10 km Eta grid for the western United States was nested within the 29 km model. Thus, the 10 km Eta is triple nested with the outer, coarse grid being the 105 km AVN, the intermediate grid being the 29 km Eta, and the inner (fine) domain being 10 km resolution. All interactions with grids are one-way only (Mittelstadt, 1996). The Eta suite uses a semi-staggered Arakawa E-grid that staggers the mass and wind variables; this minimizes errors that can occur with horizontal grid domains associated with geostrophic adjustment and topographic forcing (Holton 1992). To reduce the number of calculations required per time step a split-explicit integration scheme is used. The time step for advective processes is 144 seconds and the fundamental time step for internal gravity waves is 72/24 seconds for the 29/10 km models (Swanson 1995).

The Eta model derives it's name from the Eta, or "step mountain" coordinate (figure 7) used in the model. This coordinate system is incorporated instead of the sigma coordinate for several reasons. The eta coordinate allows for the removal of large errors that can occur when computing the horizontal

pressure gradient force, advection, and horizontal diffusion near steeply sloped coordinate surfaces as seen in figure 8 (Swanson 1995). The coordinate also simplifies the solutions to those equations. The sigma surface can be steeply sloped, while the eta coordinate system makes the eta surfaces quasi-horizontal. Because of this feature the Eta model may perform better in areas of complex topography, at lower elevations. The Eta coordinate is defined by:

$$\eta = \frac{P - P_T}{P_{sfc} - P_T}\left[\frac{P_{ref}(z_{sfc}) - P_T}{P_{ref}(0) - P_T}\right] \qquad (4)$$

where sfc is the model's lower boundary, ref is a reference pressure state that is a function of distance above sea level, and T refers to the top of the domain (25 mb). One disadvantage of the eta coordinate is that the number of vertical levels is less over higher terrain, implying that the planetary boundary layer may not be well defined in higher terrain. This produces problems when incorporating sounding and observations into the model. Also, higher elevation locations will lack the detail and physics that are seen near the surface at coastal and low elevation sites.

The Eta Data Assimilation System (EDAS) was developed to produce the most accurate forecast possible by producing initial conditions that are consistent with the forecast model. By using the EDAS, the initial conditions will better

represent a regional model rather than a global model such as the AVN. In other words, rather than initializing with data from a 100 km domain, the EDAS produces an initialization for the exact resolution of the Eta model, thus satisfying mass conservation and producing greater detail.

For the 48 km Eta, a first guess is provided by the Global Data Assimilation System (GDAS) twelve hours prior to the actual start of the forecast. After the GDAS starts the assimilation, the EDAS is used to assimilate observations at 3 hour intervals throughout the 12-hour pre-forecast assimilation period. After a spectral to grid transformation, the GDAS forecast is interpolated to the Eta model vertical layers and grid points. The higher resolution EDAS is based on an Optimum Interpolation (OI) analysis update that is performed on the model domain, and in the model's Eta coordinate every three hours (Black 1994). The OI scheme incorporates high frequency wind profiler, ACARS, and ASOS data. By using the high resolution Eta model during the assimilation, the first guess is much better than that of GDAS. Studies have shown that this leads to reduced precipitation spin-up in the early part of the Eta forecast. Staudenmaier (1996, TA 96-30) states that the mesoscale Eta EDAS ignores most NWS surface observations (14% used) and the lowest levels in soundings over the western United States. This is due to the mismatch in elevation of the model topography to the actual stations, and is worse where steep mountain valley terrain exists such as Reno, Nevada. This implies that mesoscale

phenomena are often not initialized and the low level moisture and temperature profiles are in some cases completely lacking detail. It has not yet been determined that high resolution surface observations provide any useful information with respect to the final forecast product. However, as model resolution and topography improves, more surface observations will be incorporated into the analysis.

Moisture initialization is an important aspect in model QPF. The spatial and temporal variation of moisture will directly affect the model QPF. In 1995, the 29 km Eta used the EDAS OI to initialize moisture. However, the EDAS first guess is provided by the Global Data Assimilation System (GDAS) used by the AVN and MRF. GDAS relies on radiosonde and SSMI polar orbiting sounder data. The EDAS incorporates new data into the Mesoscale Eta's domain every three hours, thus enhancing the GDAS first guess. The EDAS provides fine scale moisture updates, while the GDAS gives the global scale representation of moisture at the initialization time. Due to the sparsity of radiosonde data (none over the ocean), both the EDAS and GDAS poorly represent moisture, especially over the Eastern Pacific. In this area, the EDAS and GDAS derive moisture and total precipitatable water products from satellite sounder data that lack good vertical resolution and cannot be used when cloud layers are present.

The Mesoscale Eta uses a modified Mellor-Yamada level 2.5 (prognostic

TKE) scheme for vertical turbulent exchanges. Exchange coefficients for the transfer of moisture, heat, and momentum between adjacent model layers is determined by changes in TKE due to vertical advection (Janjic 1994).

The radiation methods are nearly the same as the Medium Range Forecast Model (MRF) run at NCEP and developed at the Geophysical Fluid Dynamics Laboratory. The carbon dioxide and ozone profiles are taken from climatology and held constant while the surface albedo is initially taken from climatology and then is allowed to evolve over the forecast. (Swanson 1995).

In an attempt to improve large-scale cloud and precipitation forecasts, an explicit cloud prediction scheme has been incorporated into the Eta suite. This scheme explicitly predicts the cloud liquid water and cloud ice, using only one prognostic equation of cloud water/ice mixing ratio, with precipitation diagnostically calculated from the predicted cloud fields (Zhao 1997).

Model precipitation paramaterization will produce both stable/stratiform (resolvable) and convective (subgrid-scale) precipitation. Grid-scale precipitation is formed every two adjustment time steps while the convective precipitation is computed every four adjustment time steps. Grid scale or stable precipitation will occur in a level of the model if the relative humidity in a grid box exceeds 95%. If precipitation falls through a layer with the relative humidity less than 95%, then part or all of the precipitation may evaporate (Black 1994).

Liquid and ice clouds are produced from large-scale condensation/

sublimation, with both cloud fraction and cloud content (water/ice mixing ratio) calculated. Cloud fraction (equation 5) is a function of relative humidity, U. Condensation will occur if the critical relative humidity (U_∞) is greater than 75% over land and 85% over oceans. U_s=1.0 and is the relative humidity in a cloud region.

$$b = 1 - \left(\frac{U_S - U}{U_c - U_\infty}\right)^{1/2} \tag{5}$$

The water phase is determined by both the temperature at that level and the temperature at the cloud top (Tp). If T>0 °C then the cloud has no ice, while regions of T<-15 °C, no cloud water is allowed. If -15 °C < T < 0 °C then the phase of the hydrometeors is determined by the cloud top temperature. A cloud will consist of supercooled water if Tp > -15 °C, and ice particles if Tp < -15 °C (Zhao 1997). Evaporation of clouds will occur when there is no condensation, or the relative humidity is less than the critical relative humidity (75% over land and 85% over water) (Zhao 1997). There is no vertical advection of clouds in this scheme, since there is an approximate balance between the gravitational fall speed of cloud particles and the models large scale vertical motion (Zhao 1997).

Rain and snow (precipitation) is diagnostically calculated from the cloud/ice scheme and falls to the ground in one time step, which implies 100%

efficiency. There are six microphysical processes observed in clouds that are used in the parameterization of precipitation (see figure 9). Autoconversion of cloud water to rain (very slow), collection of cloud droplets by the falling rain drops (collision/coalescence), autoconversion of ice particles to snow (deposition), collection of ice particles by falling snow (aggregation), melting of snow below the freezing level, and evaporation (or sublimation) of precipitation below cloud bases. The melting of snow occurs gradually, allowing for a mix of rain and snow. Precipitation is calculated from the top level down, and can fall through a dry layer (evaporate) and still reach the ground.

The current version of the Eta suite does not allow for the interaction of convection with the explicit cloud prediction scheme.

Convection must be parameterized in order to duplicate the vertical structure of both temperature and moisture observed in the atmosphere, assuming the model can not resolve the convection. Cumulus convection is not resolved by spatial grids in the Mesoscale Eta, so it is parameterized using the Betts-Miller (Betts 1986; Betts and Miller 1986) convective adjustment scheme discussed below. The parameterization/adjustment is performed in order to remove instability (CAPE) from the atmosphere.

The Mesoscale Eta uses the Betts-Miller cumulus parameterization scheme which was modified by Janjic (1994), hereafter the BMJ scheme. The Kain-Fritsch scheme is currently being tested. The BMJ scheme used in the

model will relax the moisture and temperature profiles at a given grid point toward a profile typical of the atmosphere. It is important to note that this scheme was designed for the topics. By relaxing the moisture and temperature profiles at a grid point, the model attempts to retain a realistic vertical structure when convection is present (Staudenmaier 1996, TA 96-29). The model first looks for deep convection, then shallow convection.

The BMJ shallow convective parameterization scheme uses a mixing line approach to modify soundings so that they reflect a moist mixing process between the sub-cloud layer and the drier air aloft. The mixing line is a linear approximation between those two layers and it is the point where a parcel becomes saturated after lifting. This scheme does not modify the upper troposphere above 450 mb, thus, cloud tops are forced to be below that level. The most unstable parcel at each grid point determines the lifted condensation level (LCL), or the cloud base. The cloud top is determined by lifting the parcel to, or just below, the equilibrium level (EL), or the level where the parcel becomes cooler than the surrounding environment. The criteria for shallow convection are met if 1) the cloud is greater than 10 mb deep and less than 290 mb deep, 2) at least two model layers deep at that grid point. The mixing line is further defined as the line connecting the saturation point of the cloud base with the saturation point of the cloud top (see figure 10).

Moisture is transported vertically with drying (of water vapor) near the

cloud base and moistening (of water vapor) near the cloud top. This process is meant to duplicate the warming and drying due to condensation at the cloud base and the cooling/moistening at the cloud top caused by evaporation. In other words, condensation of water vapor will warm the cloud base and downdrafts will decrease the amount of water vapor. Near the cloud top evaporation and detrainment of liquid water cools the air and increases the amount of water vapor.

Janjic (1994) stated that the deep convective parameterization scheme is derived from the observation that deep convection is a thermodynamically driven process that results in precipitation and transports heat and moisture upward in order to remove or reduce conditional instability. It is assumed that deep convection will produce precipitation in this model. The deep convection scheme will look at all the parcels within the lowest 130 mb of the model surface and find the most unstable parcel at each grid point and calculate the LCL. The cloud base is assigned to the layer below the LCL and must be one layer above the lowest model layer and/or at least 25 mb above the middle of the lowest layer. The cloud top is defined as the level at, or just below the EL. If the cloud depth is greater than 290 mb then the deep convection parameterization scheme will be satisfied and the vertical profile will be modified (Zhao 1997). Figure 11 shows the first guess temperature reference profile for deep convection. The temperature profile is modified to be 90% of the slope of the moist adiabat from

the cloud base to the ambient (environmental) freezing level (Betts 1986, pp 677-691). From the ambient freezing level to the cloud top a straight line is drawn to connect the points.

The amount of latent heat produced by a modified sounding is converted into precipitation. If no precipitation is produced or if the entropy of the grid point decreases then the deep convection parameterization is aborted and the shallow convective parameterization is used. To reproduce the effects of convection, the moisture profile must become drier and the modified temperature profile must become warmer. Model warming is produced by latent heat release through condensation from which precipitation forms, while condensation produces drying by removing water vapor from the atmosphere. With an understanding of cumulus parameterization one might ask, "how important is it"? The horizontal space scale of deep cumulus clouds are two or more orders of magnitude smaller than those of synoptic weather systems, with similar vertical scales. In general, an individual, stratiform cloud within the model should not influence the synoptic pattern, but an organized area of convection can have significant effects on the large-scale system via the transfer of heat, momentum, moisture, and non linear interactions (Holton 1992). Therefore, smaller systems could be greatly influenced by convection that may normally go unnoticed by models. Convection in some storms can also contribute to excessive rainfall amounts and are thus important to the model QPF. However, convection is not

as important in the western United States cold season.

Swanson (1995), has shown that the convective schemes perform poorly over the Western United States, especially in areas of higher topography. Convective precipitation is primarily limited to locations below 4000 feet due to the limitations of the BMJ deep convection scheme, i.e. cloud depth must be greater than 290 mb. The BMJ scheme was developed for tropical regions with deep moisture, however, the Western U.S. typically has dry low levels and marginal instability (during the summer). This may not affect convection during major West Coast precipitation events since the air mass originates from the sub-tropical regions and is quite moist. Still, model convection is lacking in higher terrain of California even during these events (figure 20).

The Eta suite physical/microphysical package has shown improvements in precipitation forecasts (Zhao 1997). The data assimilation process is still in a research and development mode and can use many improvements, which would reduce precipitation spin-up time, and initialize and resolve mesoscale phenomena.

B. Rhea Orographic Model

The Rhea orographic model (Rhea 1978) was developed in order to quickly simulate the process of orographic rainfall in the mountainous west. Rhea noted that precipitation in mountainous terrain varied markedly over

distances as small as 2 to 5 km (Rhea 1978). Considering the time scale of snow crystal (and rain) growth and typical wind speeds, the lower horizontal scale limit of the orographic precipitation process should be about 10-20 km. Flow interaction with the complex terrain of California reduces the horizontal scale, requiring the need to reduce model resolution further.

The Rhea orographic model is a steady-state, multi-layer model with 5 km grid spacing that was developed for hydrometeorological and climatological use (Rhea 1978). It was developed to run with a grid mesh as small as 2.5 km. The Rhea model utilizes no dynamics, explicit microphysics, or convective parameterization. Instead, it keeps track of condensation, evaporation, and fractional precipitation layer by layer as the parcels move over the topography from one grid point to the next along the direction of the 700 mb flow. Any amount of condensate that does not precipitate out becomes imported condensate for the next grid interval downstream. The total precipitation from all model layers are calculated at each grid point and then summed and averaged for each desired basin. Because of the model's strong dependence on the 700 mb wind direction, there are different topographic grids used for each of the 10 degrees of wind direction (180,190,200...340...) which supplies an effective cross-sectional area for each direction.

National Weather Service forecast offices generate QPF's using the Mountain Mapper (MM) (Henkel and Peterson 1996, Appendix B) software,

which utilizes the Rhea orographic model that is run at the CNRFC. Model QPF's from the Rhea model are derived based on the repeatability of 700 mb wind direction-dependent orographic precipitation patterns over a basin. Precipitation magnitudes are scaled by wind speed, moisture depth, and temperature from a comparison of predicted soundings to a reference sounding which is used to derive reference tables of orographic model precipitation (Rhea 1978). Model grid point input from NCEP's Eta, NGM, AVN, MRF, and the U.S. Navy NOGAPS model are produced at the NWSFO in Monterey and sent to the CNRFC as input for the Rhea model.

One method for determining the accuracy of model QPF's is to find the error as related to areal/spatial coverage of model rainfall. This is a difficult process because of the sparsity of observations in mountainous terrain. In addition, the smoothing of terrain by the model does not adequately represent point values of precipitation at specific sites (Rhea 1996). This error can be particularly bad in areas where valley observations are surrounded by mountains. In this case, the model has mountainous terrain where a valley existed, due to the smoothing of terrain, or the valley exists but is too high.

Studies by Rhea have found that: 1) Large QPF errors can occur due to serious deficiency of vertical resolution in predicted profiles of humidity for mountain precipitation forecast purposes. 2) There was sufficient error in the Limited Fine Mesh model (LFM) wind speed component to frequently give a QPF

error of at least +- 60%.

The Rhea model is currently used as the backbone to produce QPF's for several Western Region offices, and should thus be more closely monitored to see any bias associated with that model.

C. The Fifth-Generation NCAR / Penn State Mesoscale Model (MM5)

The NWSFO in Monterey receives MM5 data from the NPS in the form of GEMPAK grid files. While MM5 was not available during the winter of 1996/1997, it was during the 1997/1998 winter. MM5 will offer the Monterey NWSFO a more detailed view of weather phenomena in California.

The PSU/NCAR mesoscale model is a limited-area, nonhydrostatic, sigma-coordinate model designed to simulate or predict mesoscale and regional-scale atmospheric circulation (Grell et. al. 1994).

For this study, only the MM5 run of 31 December 1996 (supplied by the NPS) was used since it was not available during the entire winter period. The model was run with one-way nesting, with a coarse grid resolution of 36 km (57 x 61 grid points) and a fine grid resolution of 12 km (91 x 91 grid points), see figure 12 for the domain. There were 30 vertical sigma levels. All model output is viewed on the native 12 km grid. The model was initialized from the NCEP 29 km mesoscale Eta 9 hour forecast (961231/03z run), and blended with standard NWS surface and upper air observations using 2D multiquadric univariate interpolation. The outer domain boundary conditions come from the NCEP

Mesoscale Eta 9 hour forecasts (961231/15z, 970101/03z, and 970101/15z runs), updated every 12 hours, assuming a linear change in time at the boundaries (relaxation boundary conditions). There is an upper radiative boundary condition used to minimize reflections off the model top (100 mb).

The Kain-Fritsch cumulus parameterization scheme was used in both domains. The simple ice scheme of Dudhia, and the Dudhia longwave and shortwave scheme, and the Blackadar PBL model was used.

5.0 PAST FLOOD EVENTS

In order to recognize the potential for flooding or flash flooding, one should first know the trends of past flood events. This section will describe the basic synoptic setting and precipitation amounts seen during past floods in California. Some of the rainfall amounts were gathered from an unknown NWS report, while others are from Goodridge (1987). There appears to be two major types of synoptic patterns that develop into flood events. One type is the cold storms originating in the Gulf of Alaska that produce local basin flooding, while the major, wide spread flood events tend to be of subtropical nature.

A. January 2-5 1982 Flood

The January 1982 flood primarily affected the Santa Cruz mountains and the Bay Area in Central California and occurred over a relatively short period (30 hours). Prior to the heavy rain event a Rex block in the mid Pacific and upper low near 35N 160W developed a strong northwesterly jet stream that extended

from the gulf of Alaska to central California. This pattern produced very cold conditions over California, with snow levels down to only a few hundred feet in the Bay Area. The leading edge of the cold air associated with this storm extended to just south of San Francisco. Strong westerly zonal flow developed in the lower latitudes (under the Rex block) over the Pacific from near Hawaii northeastward toward central California. In addition, a deep surface low northeast of Hawaii enhanced low level flow over California, providing orographic lift over the coastal terrain.

Rainfall totals ranged from 15 " in portions of Marin County to 25" in the Santa Cruz Mountains during a 30 hour period. Rainfall rates were 1/2 to 1 inch per hour in the mountains and lasted for nearly 30 hours. Ben Lomond received 15.2" in one day. Additional 2-day totals include; Alpine Dam 13.60", San Francisco AP 6.31", Ben Lomond 16.10", and Scotts Valley 24.75".

B. February 1986 Flood

Heavy rain fell across northern and central California for 1 1/2 weeks (Feb 11-22). A series of extratropical cyclones embedded in southwest flow produced between 8-16" of rain in lower elevations, 24-35" in the coast range, and as much as 55.72" of liquid precipitation at Bucks Lake in the northern Sierra Nevada. Table 2 shows storm totals from 2/12/86-2/21/86 and some select 24-hour totals.

Prior to the storm the western Pacific was characterized by a significant

influx of cold air from Asia that strengthened and displaced a very strong zonal jet to between 30N and 40N. During the period of the flood the strong jet axis was at 30N. There was a blocking high in the gulf of Alaska, with a ridge extending southward to central California. During the flood period the blocking ridge shifted north to 60N, with a strong westerly jet cutting underneath (30-40N). West-southwesterly flow prevailed over California with moisture surges organizing into frontal bands. Subtropical air from near Hawaii became entrained in the strong south-westerly flow, increasing the amount of moisture heading toward California. The increased source of moisture at all levels suggests the combination of warm rain and ice processes could combine to produce heavy rain. The flood event ended with the northward push of rainfall due to ridging off the west coast.

Other floods in California were noted on 23 January 1943, 17-27 December 1955, 11-13 October 1962, and 19-24 December 1964. The 1955 flood resulted in 1000 year return rates in the San Francisco Bay Area. The greatest 24 hour rainfall was 15.34" at Lakeshore in the Shasta drainage, and an eight day total of 49.20" at Honeydew in Humboldt county. The 1962 flood dropped 14.1" of rain at Ben Lomond in one day. With the introduction of workstations, model and satellite data were available for more recent floods such as January, March, and December of 1995, and January of 1997, which is discussed below.

C. Synoptic Description of the January 1997 "New Years" Flood

During late December 1996 and early January 1997 a series of storms dropped heavy rain over portions of northern and central California resulting in major flooding of rivers and streams. These storms were similar to those observed in February 1986. Model output from NCEP failed to predict the excessive amounts of rain over mountainous regions, as expected, due to the lack of resolution. Satellite imagery shows the moisture moving along the subtropical jet between 20 and 30 north (figure 13). Medium range forecast models (MRF, figure 14) predicted a strong west-southwesterly flow at 500 mb at least 144 hours prior to the heaviest rainfall.

One characteristic of this storm was the persistence of "flat" zonal flow over northern California and southern Oregon. There was very little vorticity advection during the period and persistent, strong warm air advection ahead of the main surface lows kept 500 mb heights relatively high along the coast (figure 15), with the heaviest rainfall coincident with the 570-573 dm height contour.

Three distinct surface lows moved northeast well off the Oregon and Washington coast. Strong south-southwesterly on-shore flow advected warm, moist air northward into northern California (figure 16). Orographic lift and latent heat release enhanced vertical motions and produced widespread light rain in valleys and persistent heavy rain over orographically favored locations.

GOES-9 4 km visible imagery for Dec 31 (figure 17) clearly shows the deep surface low off the Washington coast and its trailing cold front. Waves propagating along the cold front are evidence of the 180 knot jet maxima at 250 mb.

At 250 mb a strong 120-160 knot west and southwesterly jet persisted through the period off the California coast and over the Pacific Northwest (figure 18). By January 1st a 180 knot jet pushed inland over northern California and southern Oregon, and on the 2nd another 160 knot jet max moved over California. Even with a lack of cyclonic curvature, direct and indirect circulations associated with the well defined jet entrance and exit regions provided the necessary upper-level forcing to enhance vertical motions.

Model forecast precipitation indicated heavy rainfall (4-10 inches) would occur over mountainous regions of northern California, as seen in figure 19. Notice the broad distribution of precipitation for the low resolution models, while the mesoscale Eta depicts more detail, with maxima on the western mountains and valley rain shadows. Convective precipitation was also expected to be heavy over the same period (figure 20). Model QPF verification is discussed later.

Model and observed soundings (figures 21-23) indicated that a major rainfall event would occur over the entire period. Soundings show that 700 mb temperatures would be near 0 °C, 700 mb winds of 45-60 knots out of the south

and southwest were observed on the Oakland sounding, and the soundings were nearly saturated from the surface to 300 mb, implying the possibility of mixed phase precipitation processes.

Isentropic analyses on the 300 °K surface (figure 24) shows that strong isentropic lift was occurring. On the 300 °K surface, 40-70 knot winds were blowing perpendicular to isobars, indicating rising motion that could lead to precipitation formation. In addition, very high precipitable water was observed in both soundings and model forecasts. Precipitable water values approached 1.75" over the San Francisco Bay Area.

Model analyses show that a series of jet maxima moved inland over the west coast. As a result, three deep surface lows tracked northeast into British Columbia. Warm air advection ahead of these surface lows enhanced vertical motions over northern California, resulting in widespread rain. Moisture advection from the subtropics increased the potential for heavy rain. The main 500 mb and surface lows remained well off the coast, keeping most of the vorticity advection and strongest winds away from California. Model precipitation forecasts indicated that between 4 and 10 inches of rain would fall in a 33 hour period. The QPF forecasts, as discussed in another section, under-predicted rainfall amounts over the northern Sierra and Shasta drainage, but over predicted amounts in the Sacramento and San Joaquin Valleys, as is expected given the model resolution. Model soundings show that this event was clearly of

a warm nature (i.e. 700 mb T>0°C), favoring both orographic and mixed phases processes. The floods of February 1986, and several other floods show similar characteristics. Due to the zonal nature of the flow, there was a lack of strong vorticity advection such as occurs when a sharp (curved) trough passes through the state. Only strong warm advection and orographics played a role in the production of precipitation, with rainfall amounts as much as 5 times higher on windward slopes of the northern Sierra versus the upwind valleys.

In an attempt to determine how well numerical models predict precipitation during seasonal and flood events, bias statistics where calculated and are discussed in the next section.

6.0 BIAS STATISTICS

Due to mountainous terrain and the lack of observations, calculating precipitation scores over a basin, or deriving an areal error, is too difficult at this time. Therefore a bias was calculated for eight locations (table 2) used by the Rhea orographic model run at the CNRFC from November 1996 to March 1997. The bias is defined by:

$$B = \frac{F}{O} \qquad (6)$$

Where B is the bias, F is the number of grid forecasts greater than a threshold (T), and O is the number of observations at that grid point greater than T.

Threshold values of 0.1, 0.25, 0.5, 0.75, 1.00, 1.25, 1.50, 1.75, 2.00, 2.25, 2.50, 2.75, and 3.00 inches where used. If B>1 (B<1) then the model over-predicted (under-predicted) precipitation at that point.

The bias score is used not to verify the accuracy of precipitation forecasts at a location, but states the ratio of the total amount of precipitation produced by the model to that which was observed (Black 1994). This can tell us whether the total amount of water from the model is too wet or dry as compared to observations. Another problem associated with verifying at a single point on a domain is the interpolation to that point from the model domain. Precipitation is determined in a column, and therefore will be "dumped" into a box region. The location of the single point will then be interpolated from within this box, thus representing a smoothed value that may not represent the actual model. Precipitation amounts can vary greatly over a distance of 2 km due to complex topography, while the 29 km model can only resolve 58 km or 116 km wide mountains. In addition, precipitation data is interpolated to even coarser grids, introducing further error in comparing a single point observation to a model point. The comparison of a model grid box to a single point is like comparing a basin average to a single location, and thus is not fair to the model. This must be kept in mind when viewing the bias statistics.

In an attempt to determine whether resolution improves QPF, bias statistics were calculated for both the 48 km and 29 km Eta models. It is

important to remember that the 29 km Eta model output is interpolated to both a 40 km and 20 km grid, and the 48 km Eta output is interpolated to an 80 km grid. It is expected that the 29 km Eta should represent rainfall over complex terrain better than the 48 km Eta due to improved resolution.

A. Winter Bias

Seasonal bias scores for the 48 and 29 km Eta at the eight locations listed in table 2 are seen in Figure 25. Both the 48 km Eta and the 29 km Mesoscale Eta under-predicted precipitation at the eight points for the study period. As expected, the 48 km Eta had the lowest bias scores, or the largest tendency to under-predict precipitation. Both models performed reasonably well for a threshold of 0.1 inches (B~0.9) with the 48 km Eta actually doing better (since it smooths out the precipitation). As the threshold increases, the bias scores for both models decrease to about 0.23 for the 29 km mesoscale Eta, and 0.1 for the Eta at T=3.00". Clearly, the 29 km Mesoscale Eta, with it's higher resolution (topography) performed better than the coarser 48 km Eta.

It is worth noting that for the higher thresholds, the number of samples decrease significantly, indicating that the bias scores for those thresholds may not be statistically significant. Figure 25b shows the number of observations vs. threshold for both the Eta and mesoscale Eta for the winter season. Notice that the sample size diminishes with increased threshold.

The bias scores varied between different locations according to elevation and latitude (see figures 26-33). The 29 km Mesoscale Eta performed better than the 48 km Eta in mountainous locations, while at locations on the north coast and the coastal mountains north of San Francisco, both models performed poorly with the 29 km Mesoscale Eta showing only slight improvements. At Chews Ridge (figure 31), both models performed poorly with B~ 0.65-0.75 for T=0.1 and B=0 at T=1.25" for the Eta and B=0 at T=1.75" for the Mesoscale Eta. The poor performance in the south may be associated with poor sampling due to a lack of rainfall. Also, Chews Ridge is in the coastal range south of Monterey and the model topography does not accurately depict the area, and thus neglects orographic effects.

Winter bias statistics were determined for eight locations in California (see table 2) and shown in figures 26-33. It is clear from these figures that the 29 km mesoscale Eta outperformed the 48 km Eta at all locations. For the lower thresholds, the 29 km and 48 km models were similar, showing the trend of decreased skill with increased threshold. At nearly all locations, as the threshold increased the 29 km Eta tended to show more skill in QPF than the 48 km Eta. That is, the spread in the bias increased with increased threshold. At some locations like Venado and Chews ridge, the 48 km Eta shows no skill in forecasting amounts greater than 2.25 and 1.25 inches. The bias at Miranda

(figure 33) is nearly the same for both models since the actual model topography is similar. The 48 km Eta topography on the north coast is fairly steep and acts as a major barrier to winds, thus resulting in increased vertical velocities.

Figure 34 shows the winter 29 km bias divided by the 48 km bias for 144 locations in California. For any points above 1, the 29 km Eta forecast more rainfall than the 48 km Eta, and for any point below 1, the 48 km Eta forecast more rainfall than the 29 km Eta. This figure shows that the general trend is for the 29 km Eta to forecast more rainfall than the 48 km Eta at most of the 144 locations, as expected.

Figures 35-40 show the spatial distribution of the bias for the eight winter locations at the thresholds of 0.1", 1.5", and 3" for both the 48 km and 29 km Eta. While the bias are similar at the lowest threshold, they begin to diverge for the 1.5" threshold, with nearly a complete lack of skill in the 48 km Eta for the 3" threshold.

B. Bias Score for January 1997 "New Years Flood"

Twenty-four hour precipitation bias scores were calculated for the 961231/12z 48 km Eta on an 80 km grid, the 961231/15z run of the 29 km Eta on both a 20 km and 40 km grid, and the 961231/12z MM5 on a 12 km grid (figure 6). The biases were determined for the period 970101/00z to 970102/00z, or the 9-33 hour forecast period for the Mesoscale Eta, and 12-36 hour forecast period for MM5 and the 48 km Eta. 144 locations were used to verify rainfall

amounts. This time period was chosen because of the excessive rainfall rates that occurred in the Sierra. Figure 41 shows the spatial distribution of the 24 hour bias for the MM5 run. The bias in the northern Sierra and Shasta region show several locations with a bias under 0.85, with some in the Shasta area as low as 0.43. In addition, there is a major under prediction of precipitation in the Santa Lucia Range near Big Sur.

Figure 42 shows the bias scores at all 144 locations summed, for the 48/29/20 km Eta and the 12 km MM5. For thresholds below 1.75" all three models did relatively well with a bias near 1, or no bias at all. The MM5 model consistently predicted more rainfall than the Eta suite. Bias scores for the threshold of 2-3 inches ranged from near 1.05 to 1.2; this implies that all four models over predicted rainfall for those thresholds. Once again, MM5 over predicted more often than the Eta. For thresholds greater than 3", scores for the Eta suite dropped rapidly from near 1 to 0.4; this shows the major under prediction of rainfall over most basins for this period. The bias scores for MM5 dropped to near 0.8 and actually rose to over 1.2 for the 6" threshold. This was due to the fact that MM5 moved the system south faster than the other models, producing heavy rainfall amounts in the Southern Sierra before the actual front arrived. The dip near T=4.5" is due to the under prediction of rainfall over the northern Sierra. Due to the large over prediction of precipitation over the central and southern Sierra the bias scores did not fall as low as the Eta suite.

From these figures it is clear that, on a seasonal average, the Eta suite under-predicts precipitation at the eight locations studied. The January 1997 case shows that heavy precipitation events are also under-predicted over nearly all northern and central California mountainous locations. The results suggest that the higher resolution mesoscale Eta has less of a precipitation bias than does the 48 km Eta. Further studies, including seasonal bias for all San Francisco Bay Area rain gauges could further determine if model QPF is an adequate guidance in producing a QPF.

C. Precipitation volume

Another way of viewing the amount of precipitation (water) over an area is to calculate the volume of water that falls onto an area. By doing this, the total volume for the Eta suite can be compared. Four areas where selected that represent a cross section through central and northern California. These areas include a large plot of the west coast (Area 1), a smaller rectangle centered on central California (Area 2), and two smaller rectangles within that one (Areas 3 and 4). The smaller areas were selected because of their position in the central valley and the Sierra. Figure 43 shows the 24 hour total volume for areas 2-4 for the 48 km Eta and the 29 km Eta on a 40 km and 20 km grid. The 48 km Eta actually "dumps" more precipitation on all three areas than the 29 km Eta. This suggests that the partitioning of precipitation is different between the two resolutions as would be expected due to topography. Figures 44-46 show the

six hour volume for the Eta suite at areas 2-4. These figures show that the Eta prediction would imply an increase in precipitation through the period, while the 29 km Eta suggests a peak in intensity around the 12Z time period, and a decrease in intensity afterwards. Figures 44-46 also show how the 48 km Eta has a larger volume for the eastern area as compared to the coastal sections. This is due to the 48 km Eta's topography sloping slowly towards the east, producing the greatest lift in the eastern section, while the 29 km Eta resolves the coast range and dumps more precipitation there. In addition, the areal extent of precipitation appears to decrease with the higher resolution models as topographical features are better resolved. This can be seen by the topography and precipitation plots in figures 5 and 6. By plotting the total volume over the state, meteorologists and hydrologists can see the total volume of liquid water that will affect creeks and rivers, and determine whether a storm is strengthening, maintaining a steady state, or weakening.

7.0 CONCLUSION/FINDINGS

This study was conducted in an attempt to answer the question of "how does improved model resolution/topography effect California QPF's". It is clear that at the eight locations studied for the winter QPF bias, that the higher resolution 29 km Eta model had improved QPF's. In this case, the 29 km Eta under predicted precipitation less often that the 48 km Eta at all thresholds (0.1-3.0"). Where terrain resolution is poor for both models, such as the central

California coast, both models performed poorly, with the 29 km and 48 km showing nearly the same bias.

The effects of highly orographic precipitation events are clearly seen for the January 1997 flood event in northern and central California. In this case, all models (Eta interpolated to 20, 40, 80 km, the 12 km MM5, and the Rhea orographic model) under predicted rainfall in most mountainous locations that favor orographic enhancement. For the Eta suite this was likely due to the poor resolution of topography, since the precipitation fell over complex terrain above 1800 m. The MM5 model performed relatively well, except for the placement and timing of precipitation.

It is important to note that in areas of complex terrain, vertical velocities can exceed 1 m/sec, while vertical velocities in the models rarely exceed 0.25 m/sec due to resolution restrictions. Zhao (1997) states that the microphysical packages available are improving rainfall predictions. Given they can resolve topography and vertical motions forced by topography, even more improvement is expected. Most west coast heavy precipitation events are non-convective, therefore convection contributes little to the overall precipitation totals.

Although model initialization was not considered in the study, it is clear that much of the QPF error seen in models is due to the poor placement and timing of fronts. The January 1997 case shows how the southerly displacement of the front from the MM5 model leads to over prediction of rainfall over the

southern Sierra Nevada, and the under prediction of rainfall over the Northern and Central Sierra Nevada. With improved initialization, models should be able to forecast the placement, intensity, and timing of fronts over California, thus improving QPF's.

From this study, it can be assumed that increased model resolution so that dx,dy $\leq$ 10 km is needed to capture the very heavy rainfall totals observed during flood events in California. With California's complex topography, including coastal mountains/valleys, the Sierra Nevada, and the Shasta/Siskiyous, increased model resolution is needed to properly model the location and amount of precipitation. In addition, the current suite of models is not capable of modeling the intense and narrow cold fronts, that are operationally observed at the NWSFO Monterey, moving southeast over California (although the 12 km MM5 has shown hope). These cold fronts are capable of producing very heavy rainfall in a short period of time, resulting in flooding.

One would expect that with an increase in model resolution (i.e. decreased horizontal grid spacing and improved topography) that model grid scale/stable QPF would improve. This study compared the QPF for the 29 km mesoscale Eta and the 48 km Eta model, which are the same model except for improved resolution and the running time of 03/15Z vs. 00/12Z. Bias statistics were determined for the winter of 1996-1997 (November through January) at

eight locations around northern and central California. The bias statistics are capable of showing whether a model over or under predicted precipitation at a single location. Model data is interpolated from the nearest grid point to the latitude/longitude of a station. In addition to the bias for a three month period, statistics were determined for the flood of early January 1997.

Based on data collected from this study, the 29 km mesoscale Eta clearly produces an improved QPF over the 48 km Eta model during the three month winter period. Bias scores for seven of the eight locations clearly show that the 48 km Eta under predicted rainfall more often and to a larger degree than did the 29 km Eta. The degree of error was reduced over the northern coastal areas of California and the Santa Lucia range of Big Sur. The largest errors were seen in the orographically favored locations of the northern and central Sierra, where typical rainfall amounts are 2-3 times greater than valley locations.

Recent studies at NCEP (Gartner et. al. 1996) show that both the 48 km Eta and 29 km Mesoscale Eta have a tendency to under-predict precipitation. Model bias in this study were found to be similar to those of Gartner et. al.

The main purpose of this study was to determine if improved model resolution can improve model QPF's. From the simple bias statistics determined over much of Northern and Central California, it was determined that improved model resolution leads to improved model QPF. Therefore, forecasters should

utilize the higher resolution Eta products such as QPF products from the 29 km Mesoscale Eta, rather than those of the 48 km Eta.

APPENDIX A CONVERSION OF GEMPAK GRID FILE TO TEXT

Model data goes through a series of conversions before it can be used as verification. Model GRIB data is converted into GEMPAK format. From that, grid points must be extracted from the GEMPAK grid file into a text format.

Once the model output is in the GEMPAK grid file a program developed by Ron Miller (SOO Spokane) interpolates the grid point precipitation value to the latitude/longitude location that is being verified. Two versions of this program are run for various models, resulting in QPF's for the desired grid points. Model output appears in the following formats:

Model Precip for 97032003 at GAS

DATE/TIME	10 KM	29 KM
970320/0300V000		
970320/0600V003	0.18	0.10
970320/0900V006	0.14	0.06
970320/1200V009	0.15	0.07
970320/1500V012	0.05	0.03
970320/1800V015	0.00	0.00
970320/2100V018	0.00	0.00
970321/0000V021	0.00	0.00
970321/0300V024	0.00	0.00
970321/0600V027	0.00	0.00
970321/0900V030	0.00	0.00
970321/1200V033	0.00	0.00

SHEF format:

```
.B CNRFC 0320 DC 032012
.B1      /DH18 /PPQFN/DRH+06/PPQFN/DRH+12/PPQFN/DRH+18/PP QFN
.B2      /DRH+24/PPQFN/DRH+30/PPQFN/DRH+36/PPQFN/DRH+42/PPQFN
.B3      /DRH+66/PPQFZ
GASC1  .02/ .00/ .00/ .00/   .00/ .00/ .00/ .00/   0.00
```

```
EKA   .06/ .00/ .00/ .00/  .00/ .00/ .00/ .00/  0.00
MRNC1 .09/ .01/ .00/ .00/  .00/ .00/ .00/ .00/  0.00
WILC1 .03/ .01/ .00/ .00/  .00/ .00/ .00/ .00/  0.00
VNOC1 .00/ .00/ .00/ .00/  .00/ .00/ .00/ .00/  0.00
ACMC1 .00/ .00/ .00/ .00/  .00/ .00/ .00/ .00/  0.00
BDRC1 .00/ .00/ .00/ .00/  .00/ .00/ .00/ .00/  0.00
CHWC1 .00/ .00/ .00/ .00/  .00/ .00/ .00/ .00/  0.00
SMRC1 .00/ .00/ .00/ .00/  .00/ .00/ .00/ .00/  0.00
GRDC1 .10/ .02/ .00/ .00/  .00/ .00/ .00/ .00/  0.00
SHDC1 .07/ .03/ .00/ .00/  .00/ .00/ .00/ .00/  0.00
RBL   .03/ .02/ .00/ .00/  .00/ .00/ .00/ .00/  0.00
BRRC1 .00/ .00/ .00/ .00/  .00/ .00/ .00/ .00/  0.00
BLUC1 .00/ .00/ .00/ .00/  .00/ .00/ .00/ .00/  0.00
PCHC1 .00/ .00/ .00/ .01/  .00/ .00/ .00/ .00/  0.00
SAC   .00/ .00/ .00/ .00/  .00/ .00/ .00/ .00/  0.00
BLSC1 .00/ .00/ .00/ .01/  .00/ .00/ .00/ .00/  0.00
HNTC1 .00/ .00/ .00/ .00/  .00/ .00/ .00/ .00/  0.00
GNF   .00/ .00/ .00/ .00/  .00/ .00/ .00/ .00/  0.00
FAT   .00/ .00/ .00/ .00/  .00/ .00/ .00/ .00/  0.00
```

Finally, several fortran programs read the desired values, which are then compared to the observed amounts from SFORR4SAC. This can be done for all 144 locations in the SFORR4SAC product.

APPENDIX B Mountain Mapper

Mountain Mapper (MM) is a collection of programs used to process predicted and observed precipitation in the mountainous west. it is a diagnostic tool used in conjunction with the Rhea orographic model. MM assumes that the average monthly precipitation pattern (climatology) will determine the pattern of a single precipitation event. Mountain mapper consists of three separate programs run at the NWSFO and the CNRFC. The programs are: 1) specify QPF, 2) quality control of observed precipitation (used only at the CNRFC), and

3) verification of QPF against observed values. Display features include Mean Areal Precipitation (MAP) on a six hourly and daily time step, as well as HRAP (define) grids. The process of mapping isolated points to HRAP grids is accomplished by producing a ratio of normal monthly accumulations, then weighing them with the inverse of the distance of separation squared (Henkel and Peterson 1996). The accumulation of grids into MAP areas is done by integrating around digitized basin boundaries and separating by area elevational divides.

In summary, Mountain Mapper provides a means of integrating rainfall and QPF data from single data point values into an areal precipitation distribution based on PRISM monthly normals.

REFERENCES

Baldwin, M.E., and T.L. Black, 1996: Precipitation forecasting experiments in the western U.S. with NCEP's mesoscale Eta model. Preprints, *11th Conf. on Num. Wea. Pred.*, AMS, Norfolk, VA. Aug, 1996.

Barbato, Gary, 1989: QPF in Northern and Central California by the National Weather Service. Unpublished report.

Betts, A.K., 1986: A new convective adjustment scheme. Part I: Observational and theoretical basis. *Quart. J. Meteor. Soc.*, 112, 677-691.

_____, and M.J. Miller, 1986: A new convective adjustment scheme. Part II: Single column tests using GATE wave, BOMEX and Arctic air-mass data sets. *Quart. J. Roy. Meteor. Soc..*, 112, 693-709.

Black, T.L., 1994: The new NMC mesoscale Eta model: Description and Forecast Examples. *Wea. Forecasting*, 9, 265-278.

Byers, Horace R., 1965: Elements of cloud physics. University of Chicago Press, Chicago.

Chappell, Charlie (no date): Condensation-precipitation processes and precipitation efficiency, UCAR/COMET document.

Gartner, W.E., M.E. Baldwin, and N.W. Junker, 1996: Regional analysis of quantitative precipitation forecasts from NCEP's early Eta and Mesoscale-Eta models. Preprints, *15th Conf. on Weather Analysis and Forecasting*, AMS, Norfolk, VA. Aug, 1996.

Goodridge, Jim, 1987: Precipitation study: A comparison of eight large storms in California. Workshop on county hydrology manuals, October 1987.

Grell, Georg A., J. Dudhia, D.R. Stauffer, 1994: A description of the fifth-generation Penn State/NCAR Mesoscale Model (MM5). NCAR Tech. Note #398, June 1994.

Hallet, J., and S. Massop, 1974: Production of secondary ice particles during the riming process. *Nature*, 249, 26-28.

Henkel, Arthur, and Craig Peterson, 1996. Can Deterministic quantitative precipitation forecasts in mountainous regions be specified in a rapid, climatologically-consistent, and RFC-compatible manner with Mountain Mapper functioning as the tool for mechanical specification, quality control, and verification?. *5th Nat. Heavy Precip. Workshop*, State College, PA.

Hess, Wilmot N., 1974: Weather and climate modification. John Wiley and Suns Inc.

Holton, James R., 1992: An introduction to dynamic meteorology. Academic Press Inc., San Diego.

Houze, Robert A. Jr., 1993: Cloud dynamics. Academic Press Inc., San Diego.

Janjic, Z. I., 1994: The stop-mountain eta coordinate model: Further developments of the convection, viscus sublayer, and turbulence closure schemes. *Mon. wea. Rev.*, **122**, 927-945.

Mesinger, Fedor, 1998: Comparison of Quantitative Precipitation Forecasts by the 48- and by the 29-km Eta model: An update and possible implications. *16th Conf. on Weather Analysis and Forecasting*, Amer. Meteor. Soc., Bostona, Ma. J106-107.

Mittelstadt, Jon, 1996: A brief comparison of 29km and 10km Eta model simulations of a spring snow event. WR-Technical Attachment 96-13.

NOAA, 1994: An Initial forecast comparison of the Eta model to the Limited-area Fine-mesh model. Technical Procedures Bulletin No. 413.

NOAA, 1995: Changes to the operational Eta model analysis/forecast system. Technical Procedures Bulletin No. 423.

Ray, Peter S., 1986: Mesoscale meteorology and forecasting. AMS, Boston.

Reynolds, David W., 1995: The warm rain process and WSR-88D. WR-Techincal Attachment 95-08.

Rhea, J.O., 1978: Orographic precipitation model for hydrometeorological use. Colorado St. Univ., Dept. of Atmospheric Science, Atmospheric Science

Paper No. 287, 221p.

Rhea, J.O., 1996: An objective orographically-based QPF aid for California. WR-Technical Attachment 96-02.

Schneider, R.S., N.W. Junker, M.T. Eckert, and T.M. Considine, 1996: The performance of the 29 km Mesoscale Eta model in support of forecasting at the Hydrometeorological Prediction Center. Preprints, *15th Conf. on Weather Analysis and Forecasting*, AMS, Norfolk, VA. Aug, 1996.

Staudenmaier, M.J., 1996: A descrition of the Mesoscalee Eta model. WR-Technical Attachment 96-06.

Staudenmaier, M.J., 1996: Precipitation verification statistics from the NCEP operational model suite. WR-Technical Attachment 96-28.

Staudenmaier, M.J., 1996: The explicit cloud prediction scheme in the Mesoscale Eta model. WR-Technical Attachment 96-29.

Staudenmaier, M.J., 1996: The initialization prpocedure in the meso eta model. WR-Technical Attachment 96-30.

Staudenmaier, M.J., 1996: A western region guide to the Eta-29 model. NOAH Technical Memorandum NWS WR-246.

Staudenmaier, M.J., J. Mittelstadt, 1997: Results of the Western Region evaluation of the Eta-10 model. WR-Technical Attachment 97-18.

Swanson, R.R., 1995: Evaluation of the mesoscale Eta model over the western United States. Masters Thesis, University of Utah, 113pp.

Zavisa I. Janjie, 1996: The step-mountain Eta coordinate model: Further developments of the turbulence closure scheme. UCAR, 44 pp.

Zhao, Qingyun, T.L. Black, M.E. Baldwin, 1997. Implementation of the cloud prediction scheme in the Eta model at NCEP. *Weather and Forecasting*, **Vol 12**, No 3.

Table 1. Model resolution and output resolution.

Model(Eta) Resolution	AWIPS GRIB GRID #	Post Process Grid Resolution
48 km	211	Regional CONUS (80km)
29 km	212	Regional CONUS Double Resolution (40 km)
29 km	215	Regional Conus Quadruple Resolution (20 km)
10 km	218	(10 km)

Table 2. February 12-21 1986 precipitation totals.

Location	Storm total(")	Location	1-hr maximum rain rates (")
Shasta Dam	19.70	Bucks Lake	1.12
Sacramento	9.62	Four Trees	1.12 (day=17.60")
Blue Canyon	34.25	Brush Creek	1.47
Bucks Lake	55.72	Honeydew	0.60
Four Trees	52.68	St. Helena	0.70
Strawberry Vly	35.64	Strawberry	0.80
Oroville Dam	11.24	Venado	0.70
Yosemite NP	21.72	Santa Margarita Boost	1.00
Venado	39.28		
Calastoga	29.61		
Kentfield	25.48		
Felton	18.00		
Ben Lomond	22.49		
Mining Ridge	29.33		
Honeydew	25.50		

Table 3

Locations used in determining precipitation bias statistics for winter case.

LOCATION/ID	LAT	LON	ELEVATION
Blue Canyon (BLU)	39.28	120.7	5280
Brush Creek RS (BRR)	39.68	121.33	3560
Girard (GRD)	41.13	122.28	4800
Shasta Dam (SHD)	40.72	122.42	1075
Willits RS (WIL)	39.35	123.32	1925
Venado (VNO)	38.62	123.02	1260
Miranda (MRN)	40.18	123.78	263
Chews Ridge (CHW)	36.32	121.57	5040

Table 4. 2-year and 100-year precipitation return periods.

Location	2-year return period			100-year return period		
	1-hr	6-hr	24-hr	1-hr	6-hr	24-hr
N. Mountains	0.7	3.5	6.5	1.80	7.35	14.30
Central Coast	0.6	1.5	3.5	1.20	3.00	7.00
E. Mountains	0.6	2.0	3.0	1.25	4.20	6.60
S. Mountains	0.7	3.0	6.0	1.40	5.70	11.40

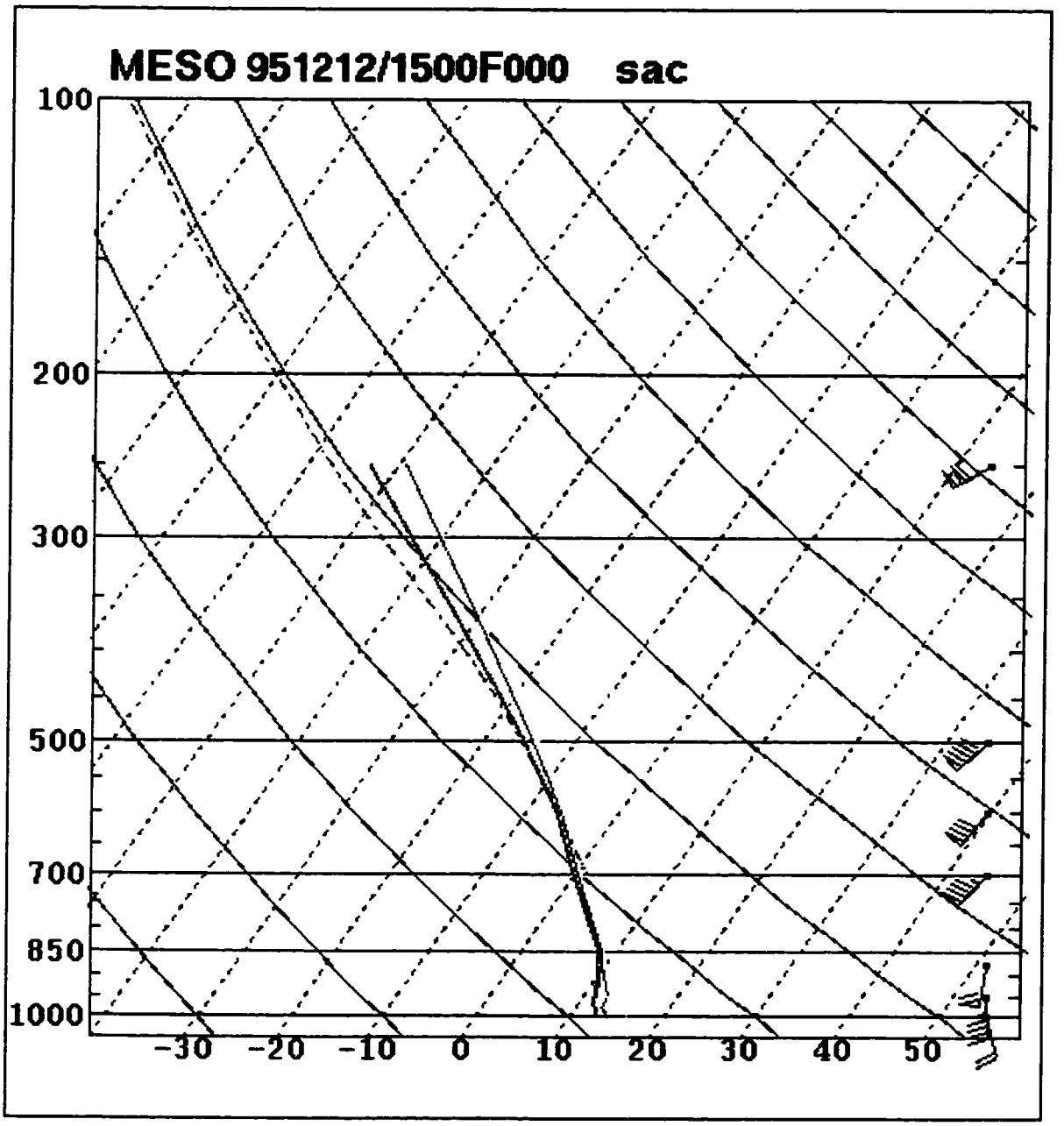

Figure 1 12 December 1995 12Z Mesoscale Eta model sounding for Sacramento.

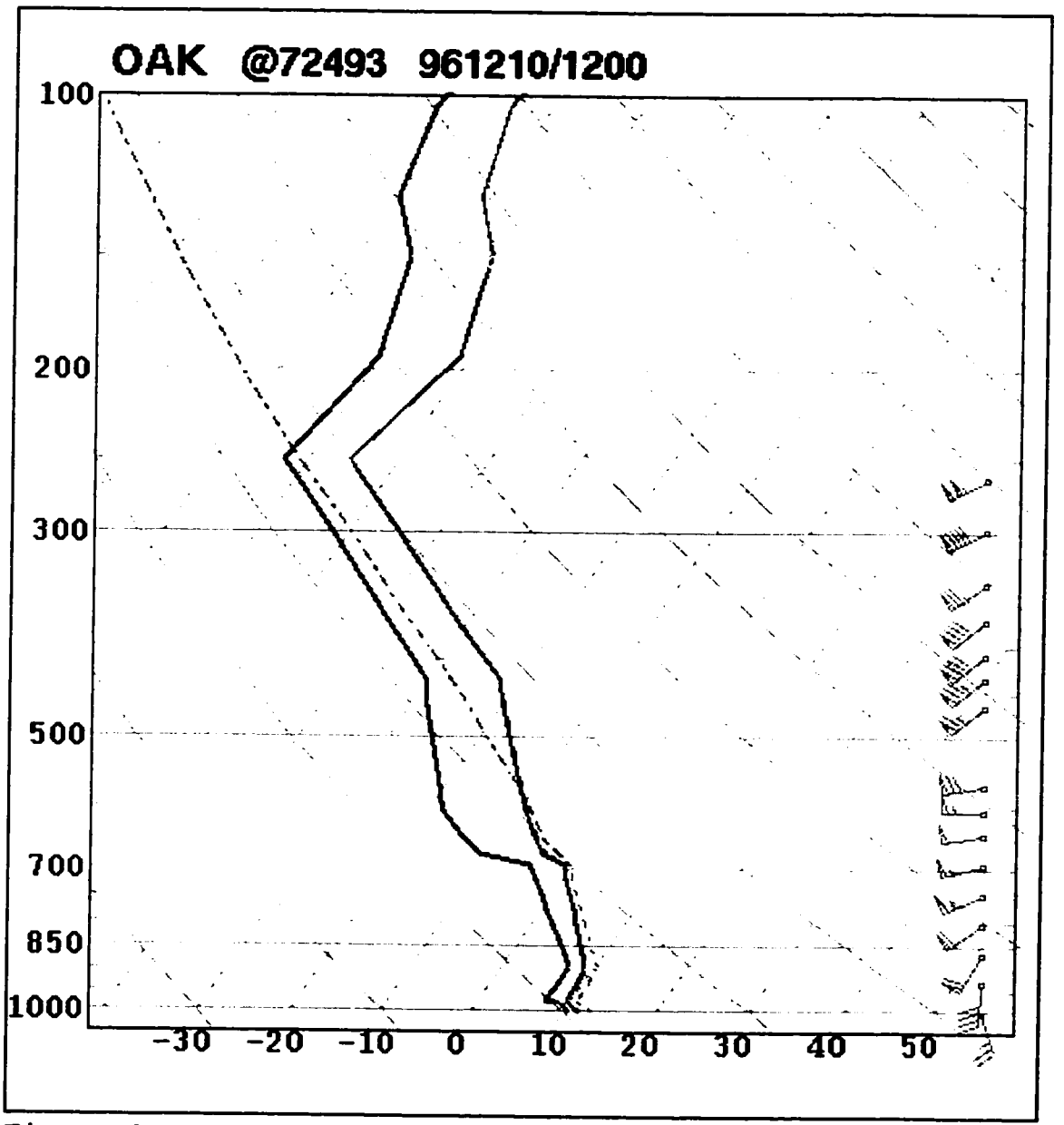

Figure 2 12 December 1996 12Z Oakland sounding.

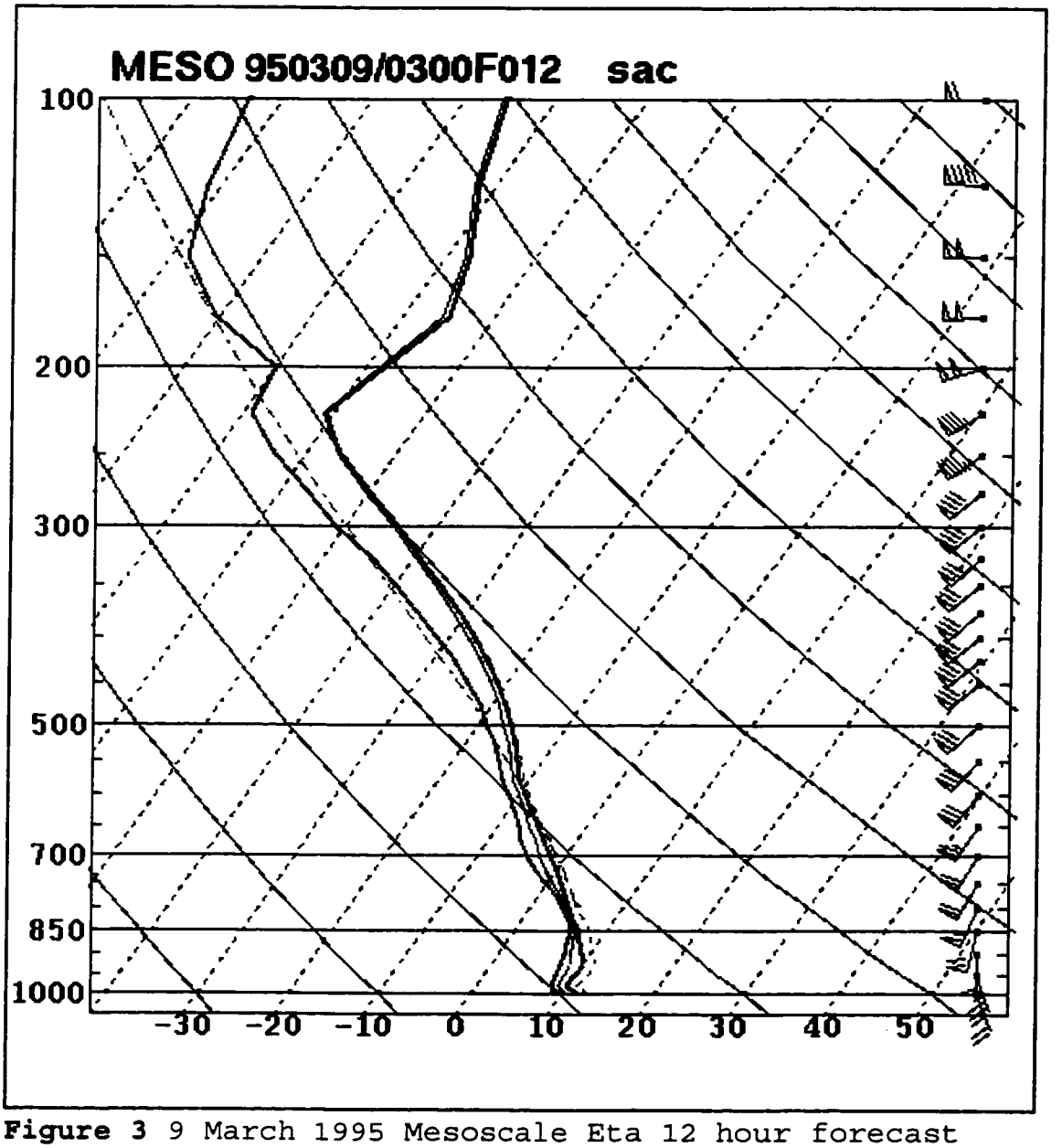

Figure 3 9 March 1995 Mesoscale Eta 12 hour forecast sounding for Sacramento.

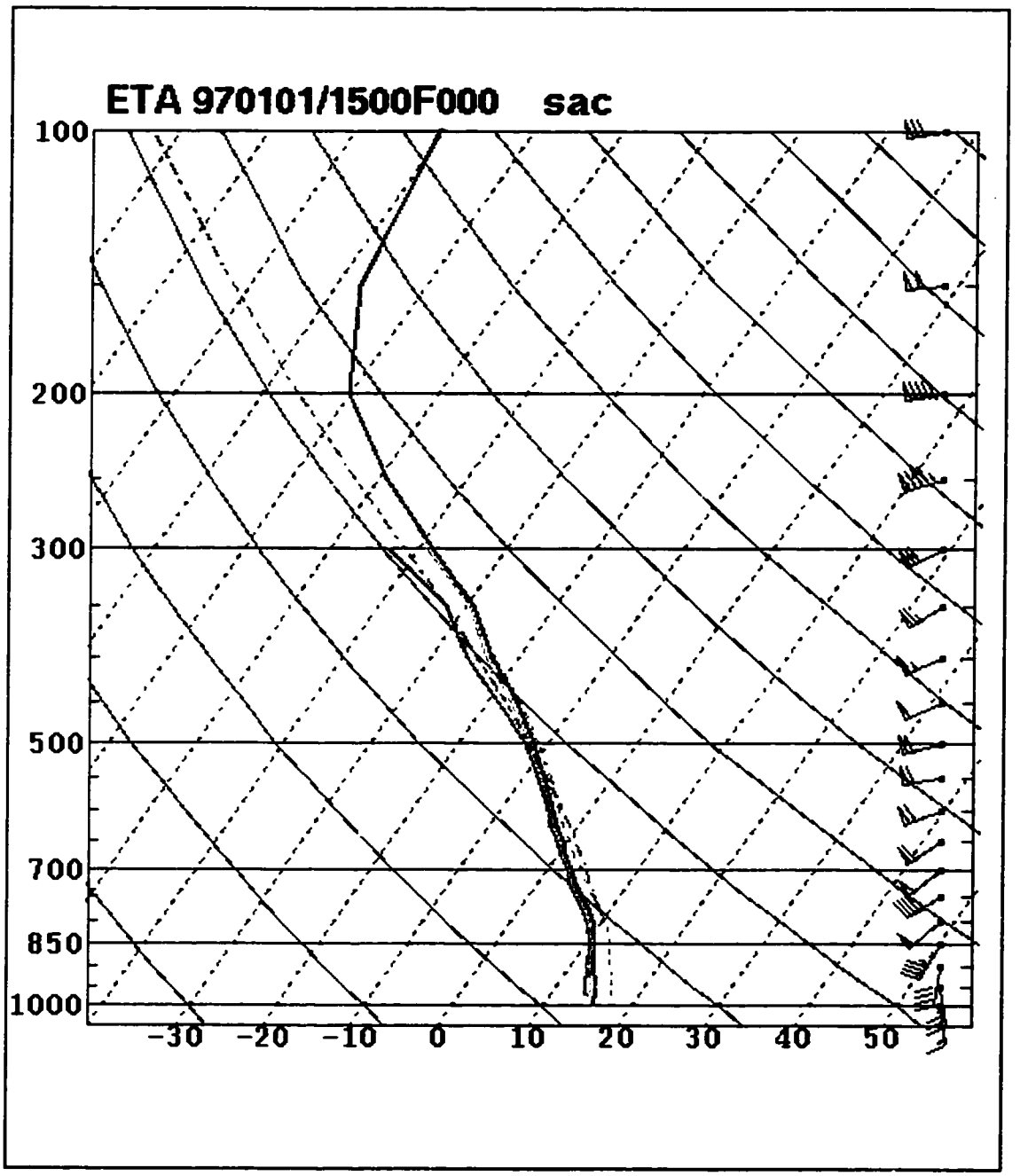

Figure 4 1 January 1997 Mesoscale Eta 15Z sounding

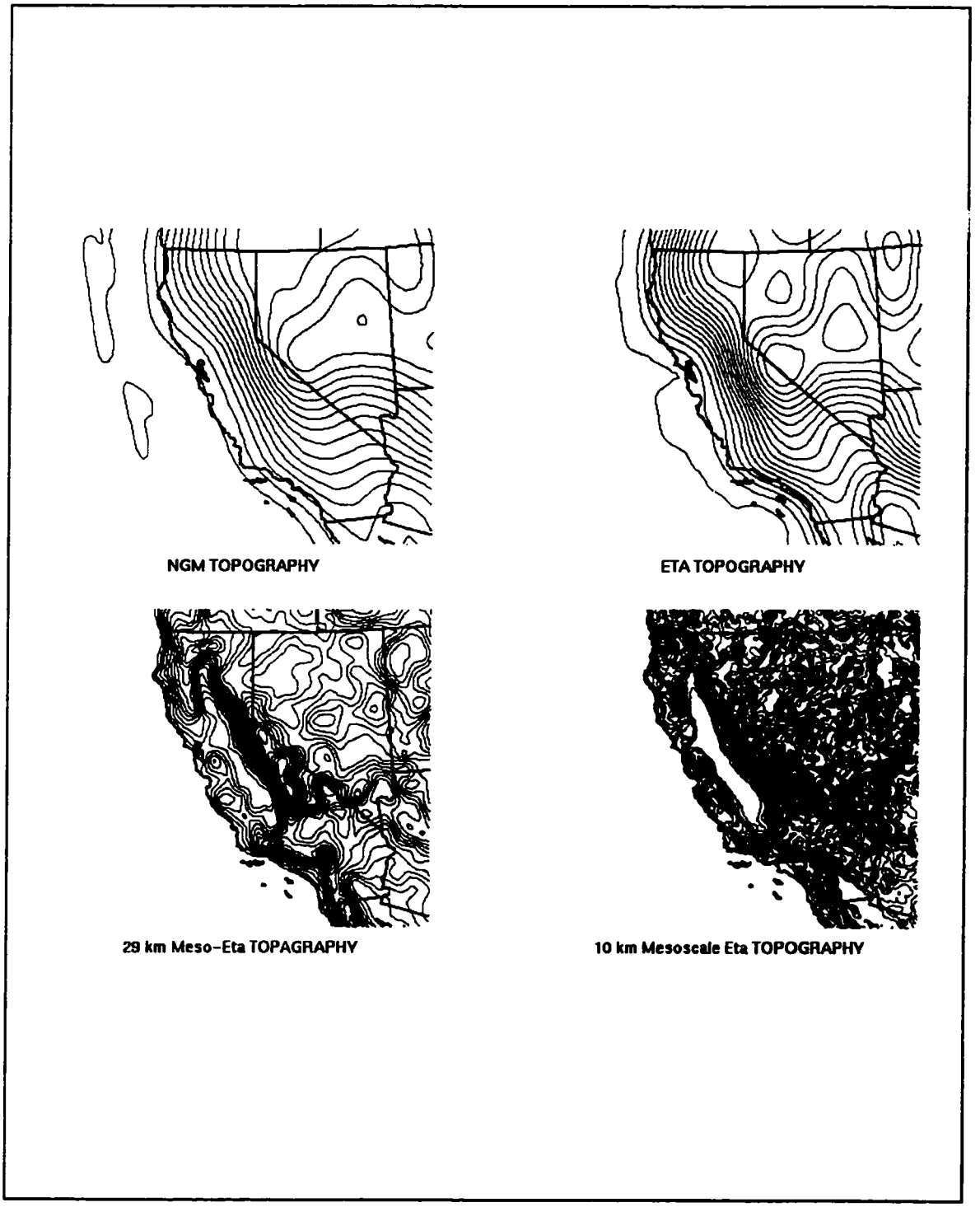

Figure 5 Model topography for the NGM, 48 km Eta interpolated to 80 km, 29 km Eta interpolated to 40 km, and 10 km Eta at 10 km.

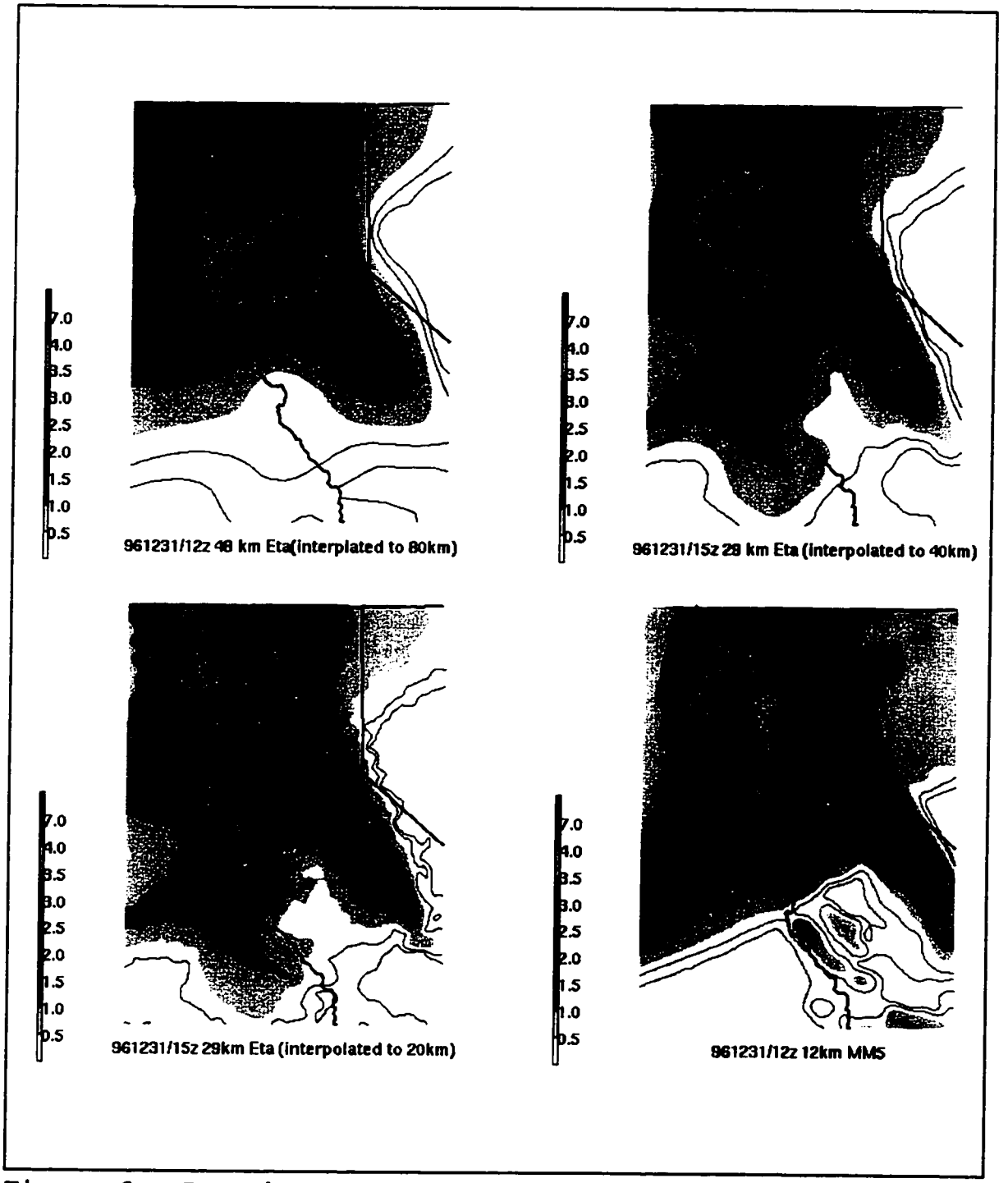

Figure 6a December 31st model QPF for the 48/80 km Eta, 29/40 km Eta, the 29/20 km Eta, and the 12 km MM5. Higher resolution models resolve topography and thus the spatial distribution of precipitation.

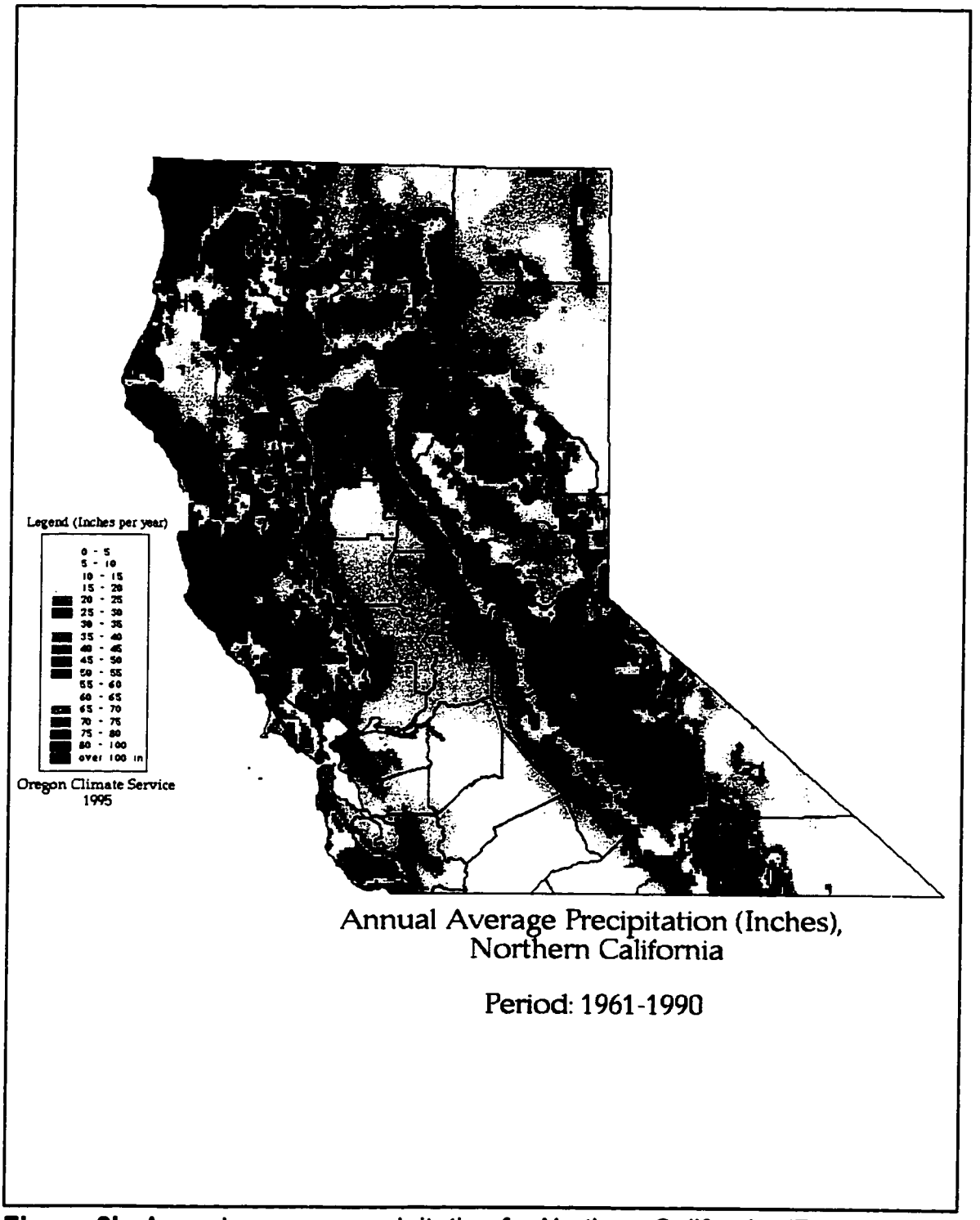

Figure 6b Annual average precipitation for Northern California. (From PRISM data).

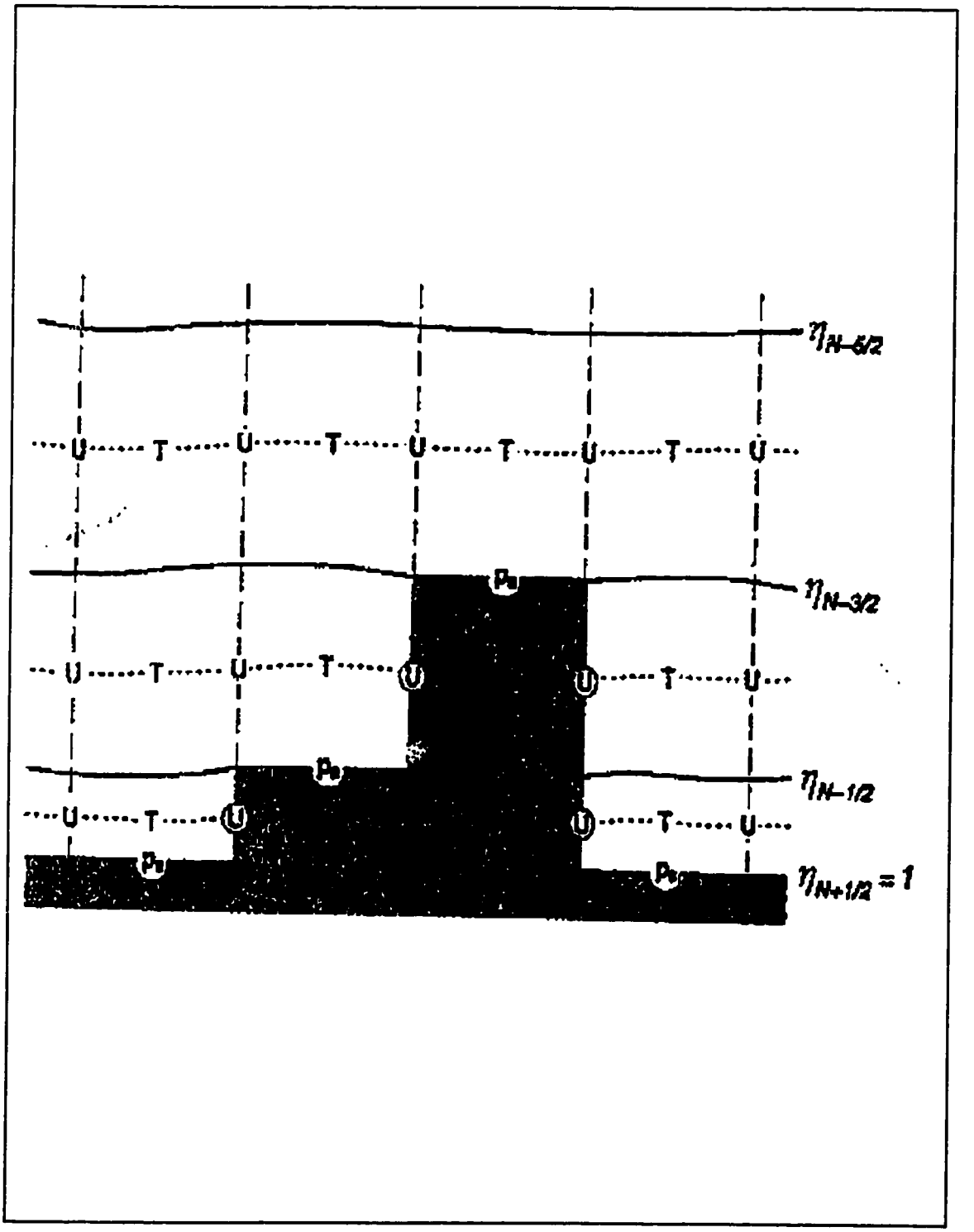

Figure 7 Eta step mountain topography from Black (1994) Where T is a "mass" variable, u represents both horizontal wind components.

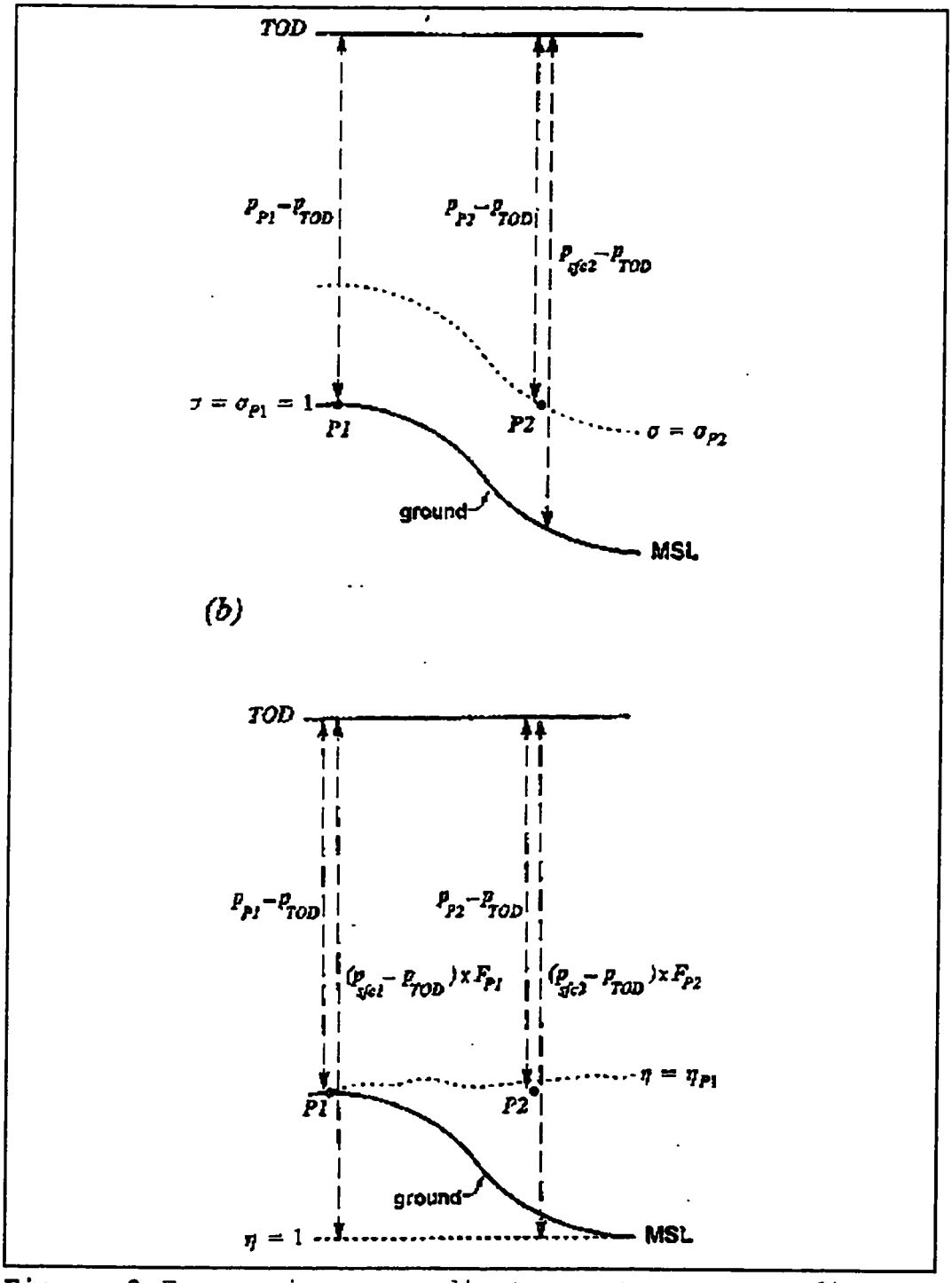

Figure 8 For a sigma coordinate system, a coordinate surface (thin dashed line) must slope steeply following the terrain (a). In an eta coordinate system, a coordinate surface is relatively horizontal regardless of the terrain. (From Black, 1994)

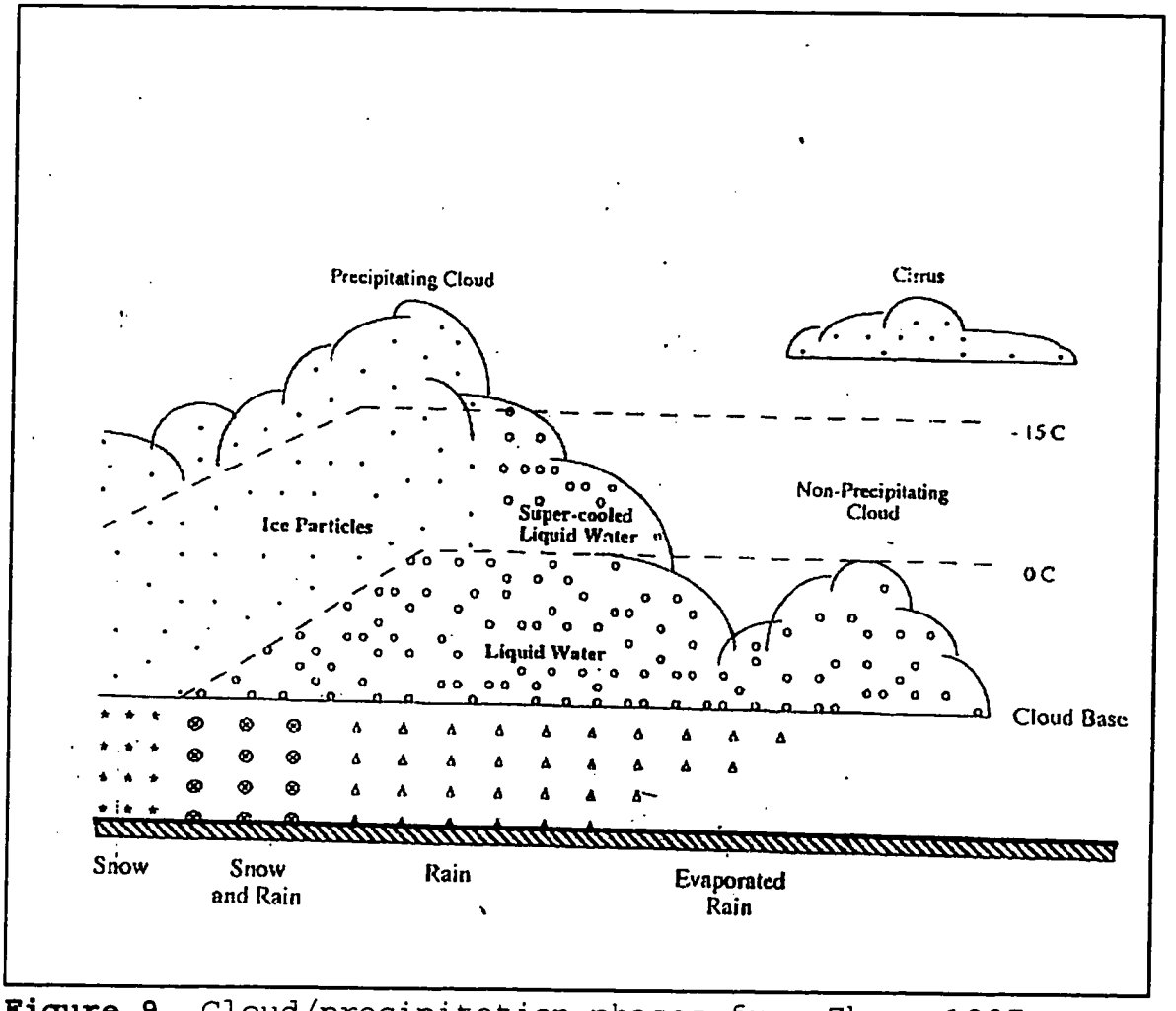

Figure 9 Cloud/precipitation phases from Zhao, 1997.

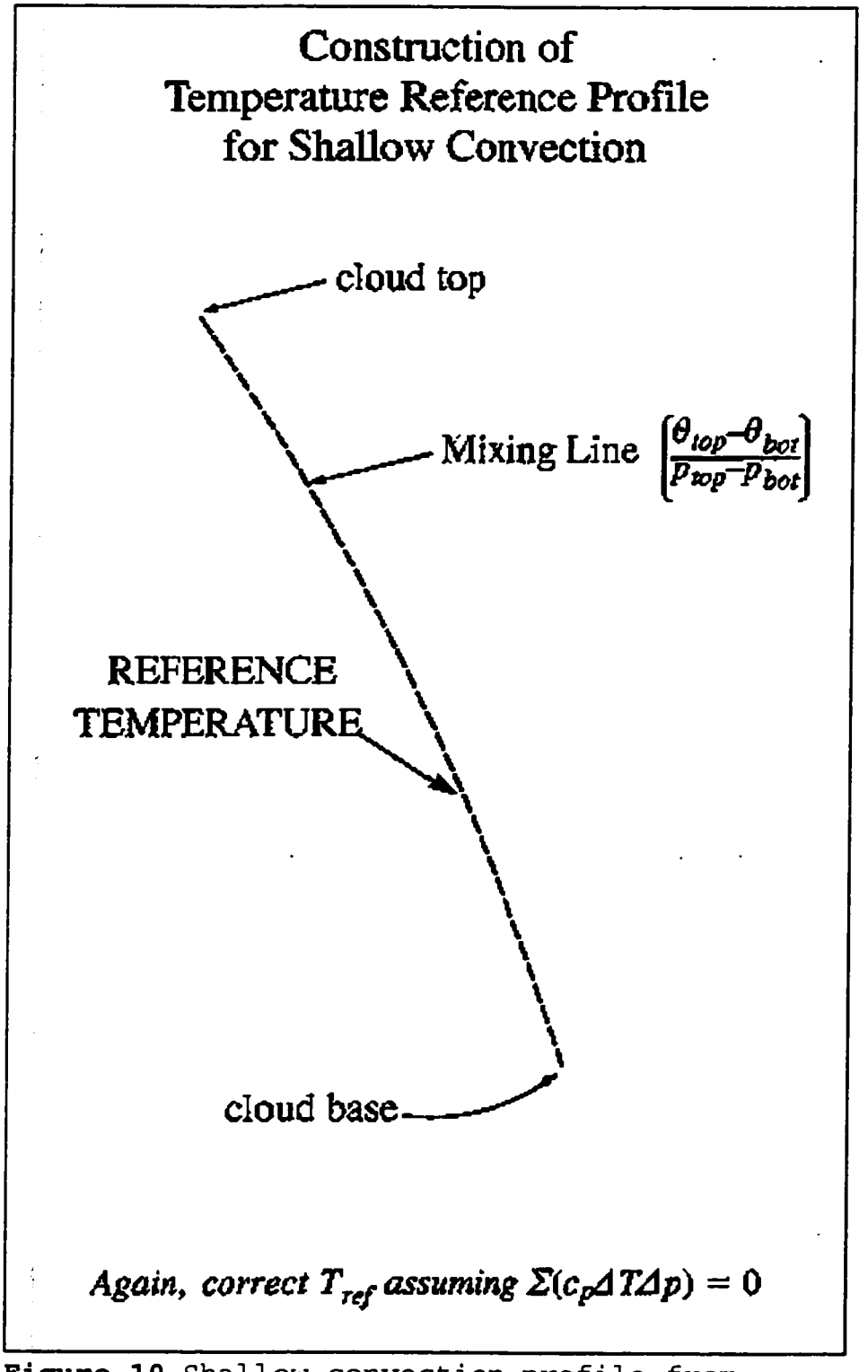

Figure 10 Shallow convection profile from Staudenmaier, Sept. 1996.

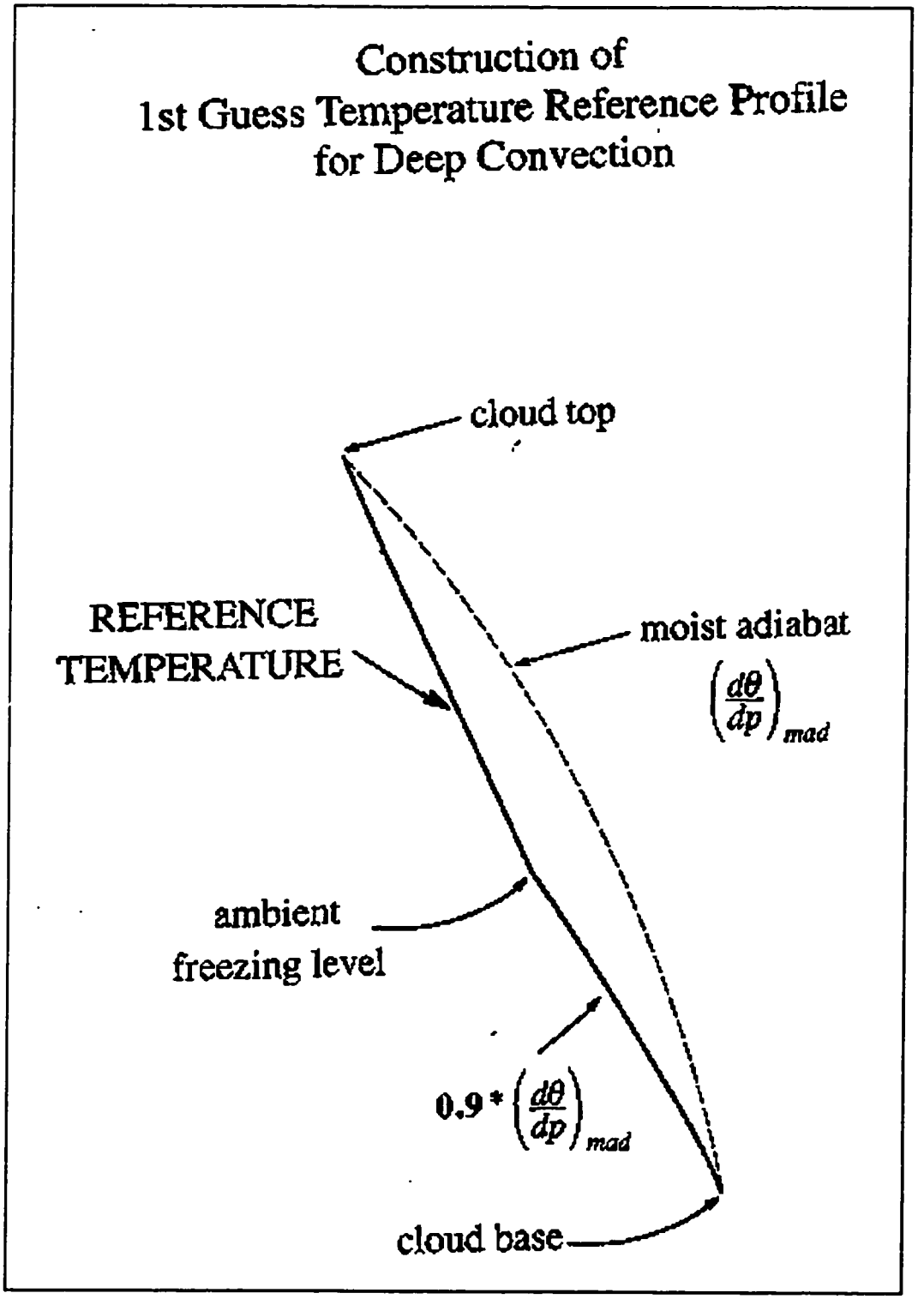

Figure 11 Deep convection profile from from Staudenmaier, Sept. 1996.

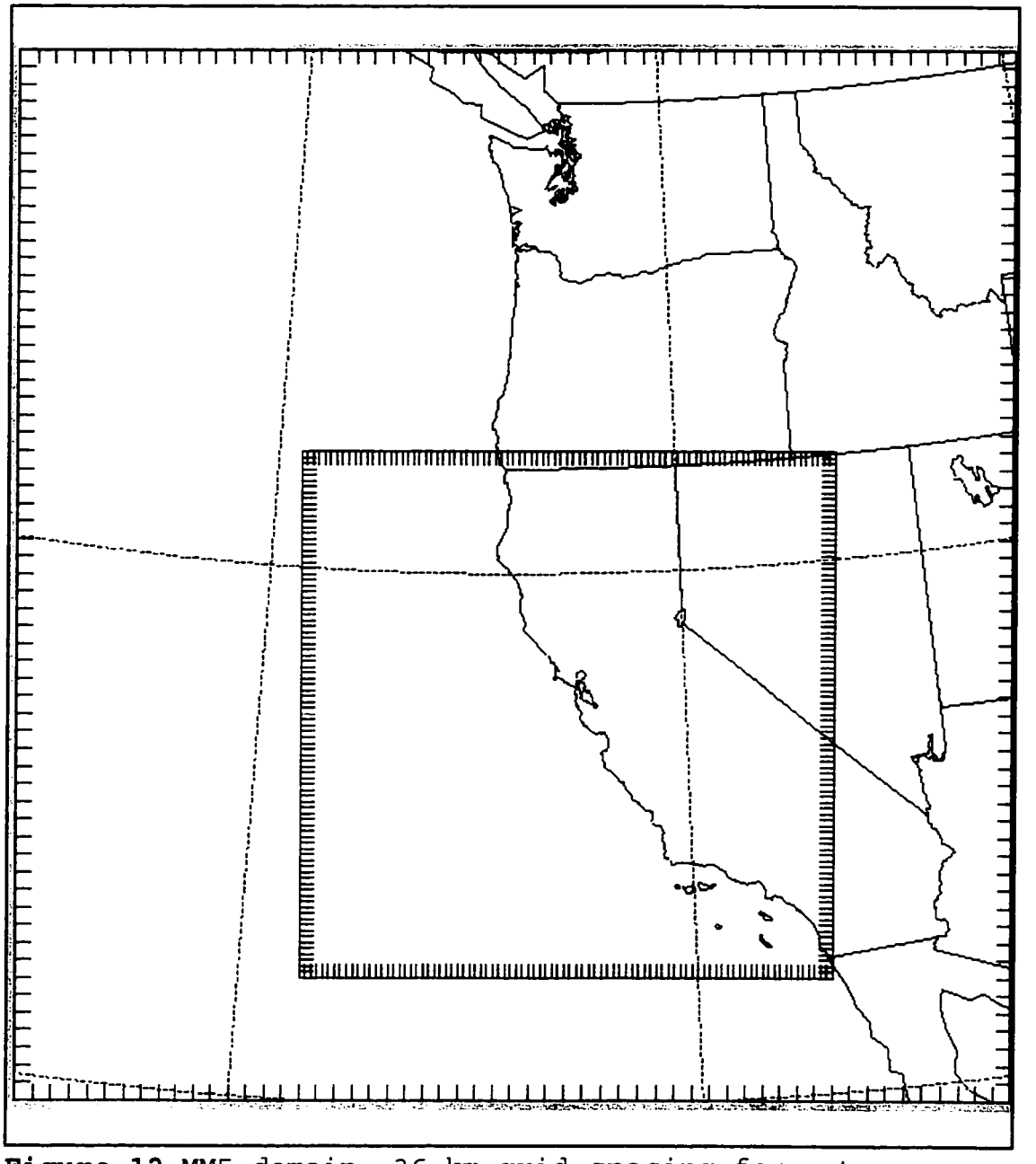

Figure 12 MM5 domain, 36 km grid spacing for outer domain and 12 km grid spacing for 12 km domain.

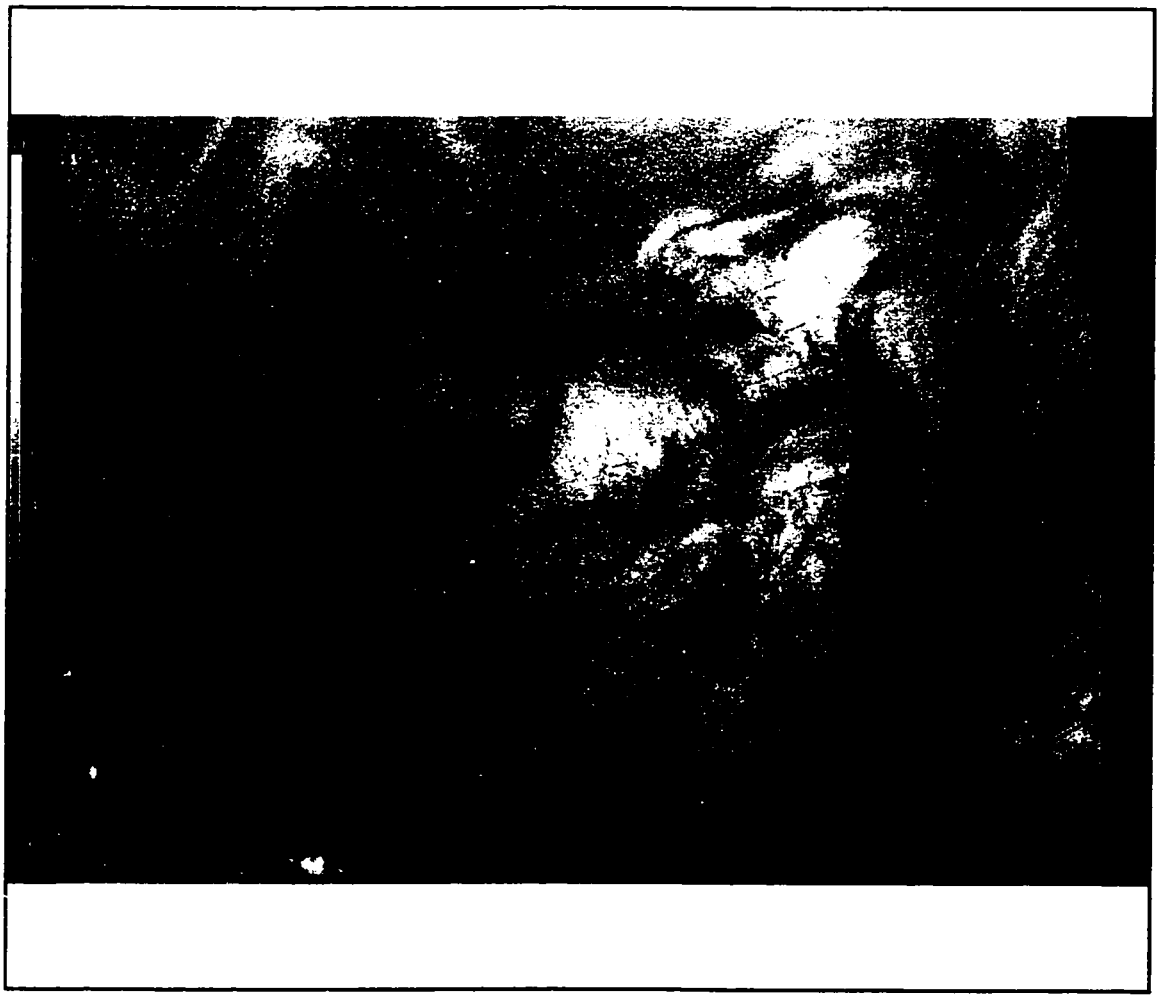

Figure 13 16 km water vapor imagery at 12Z, 31 December 1996.

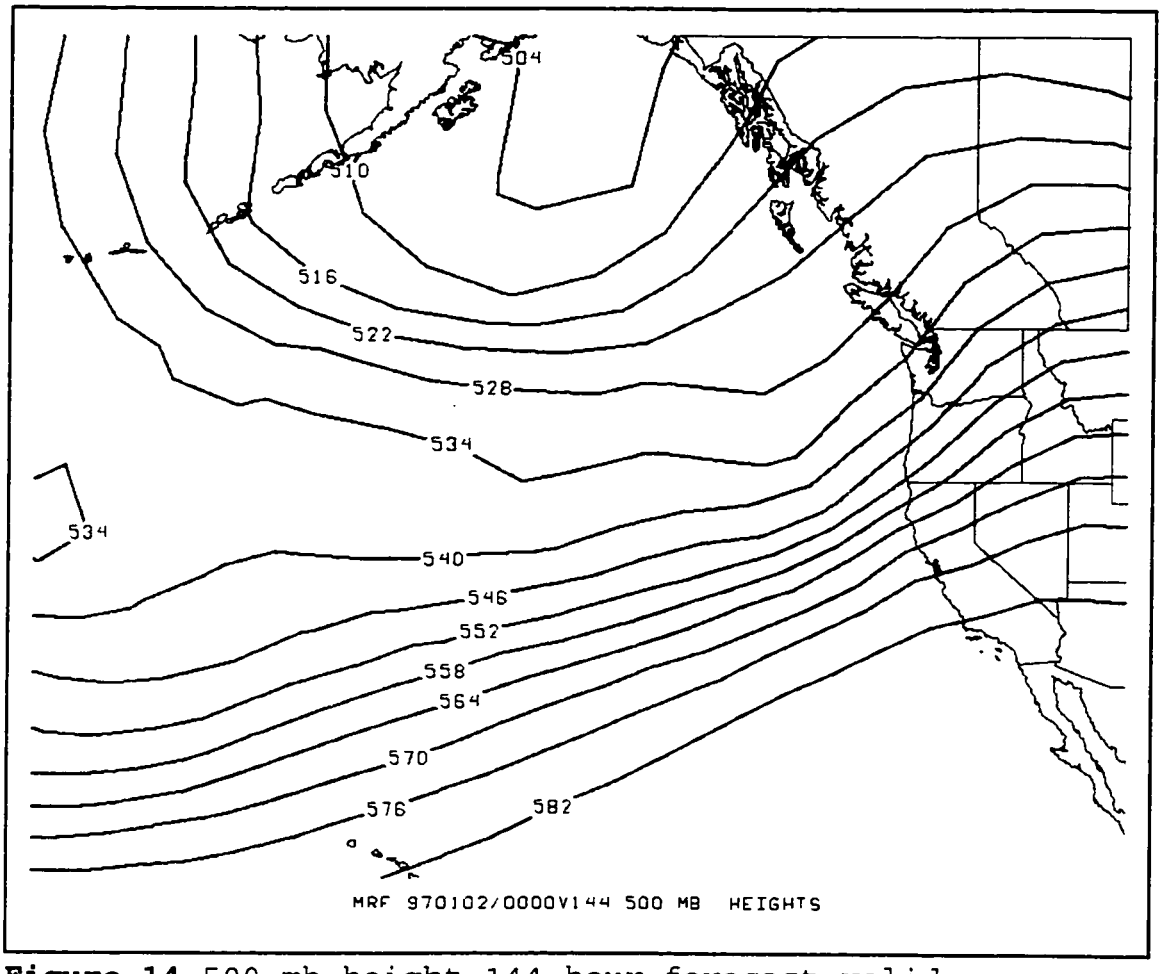

Figure 14 500 mb height 144 hour forecast valid 970102/00z.

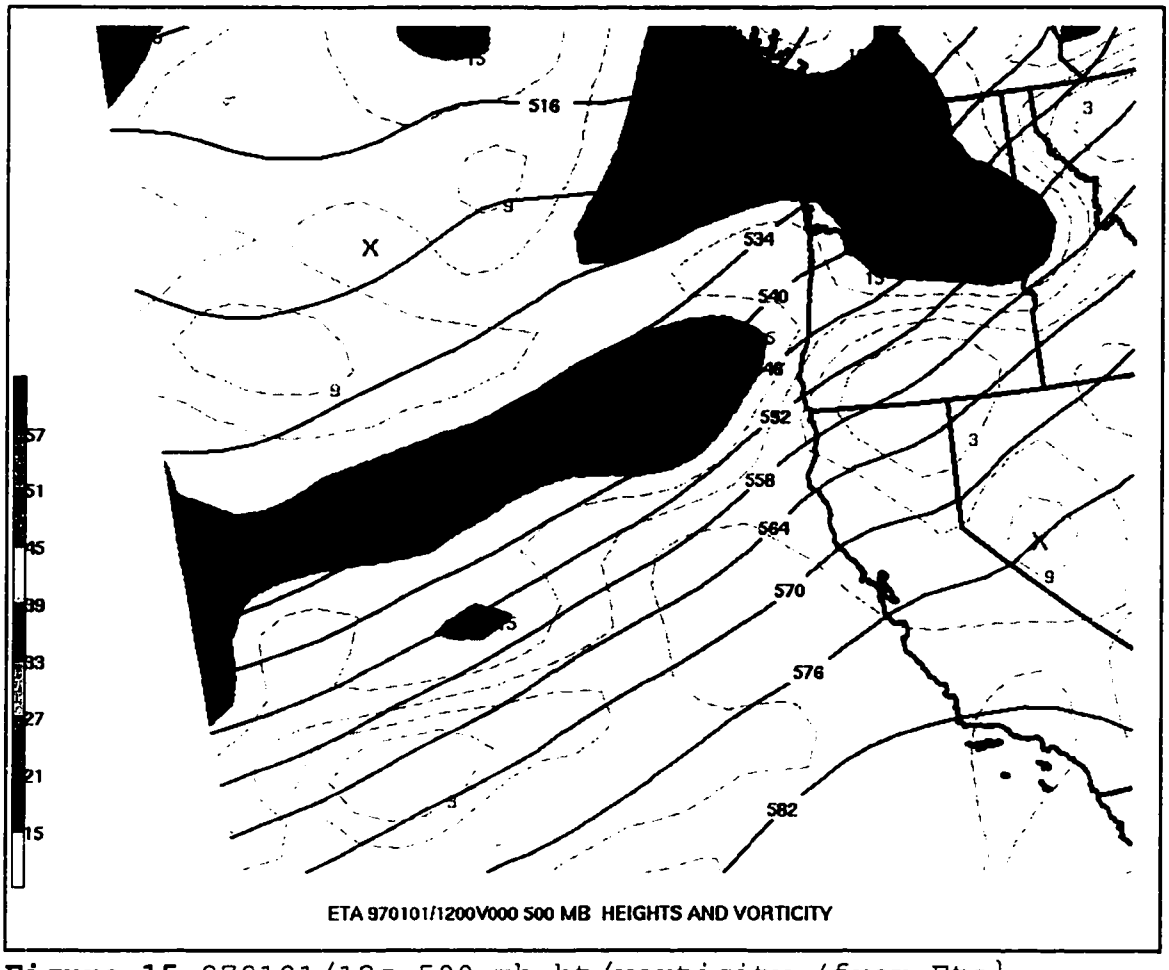

Figure 15 970101/12z 500 mb ht/vorticity (from Eta).

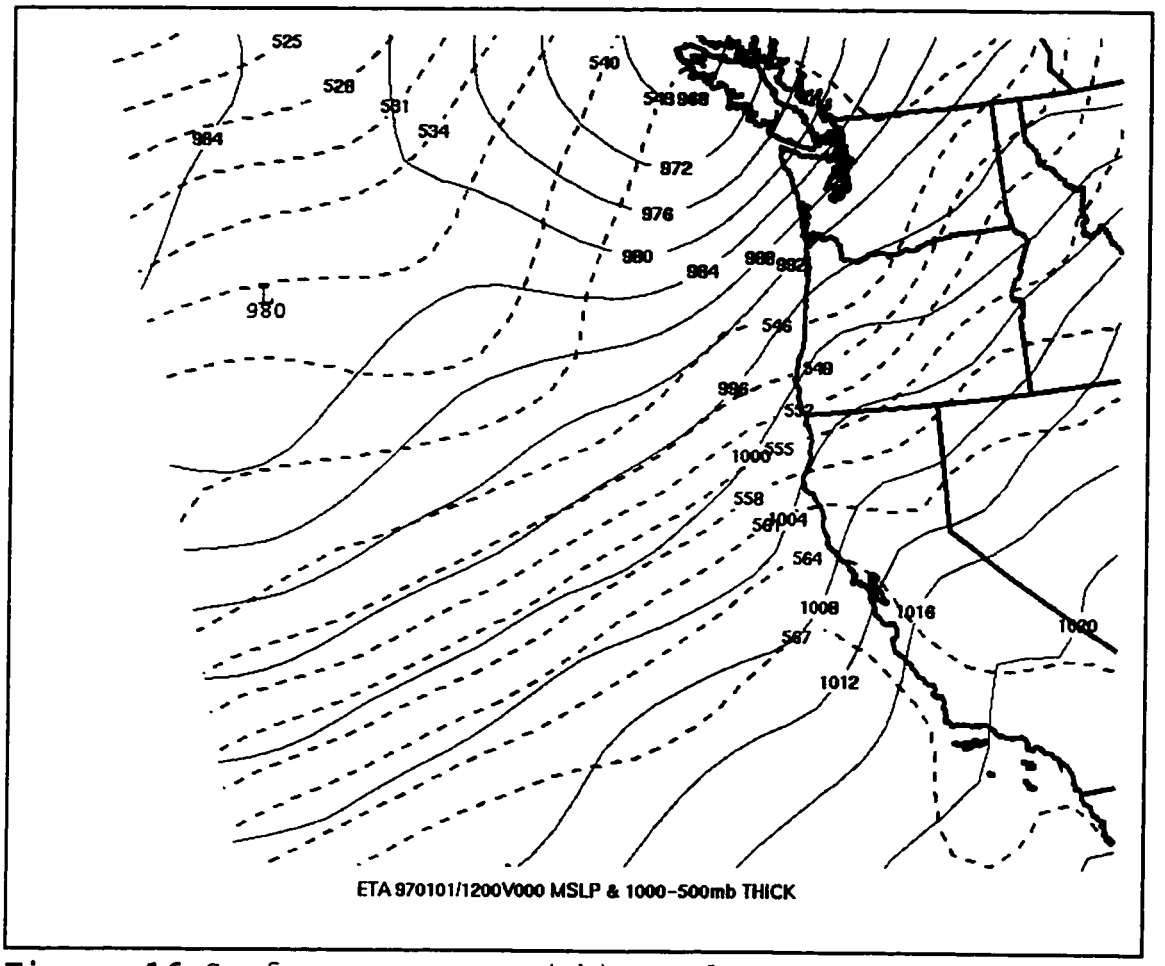

Figure 16 Surface pressure (mb), and 1000-500 mb Thickness (dm) for 970101/12z.

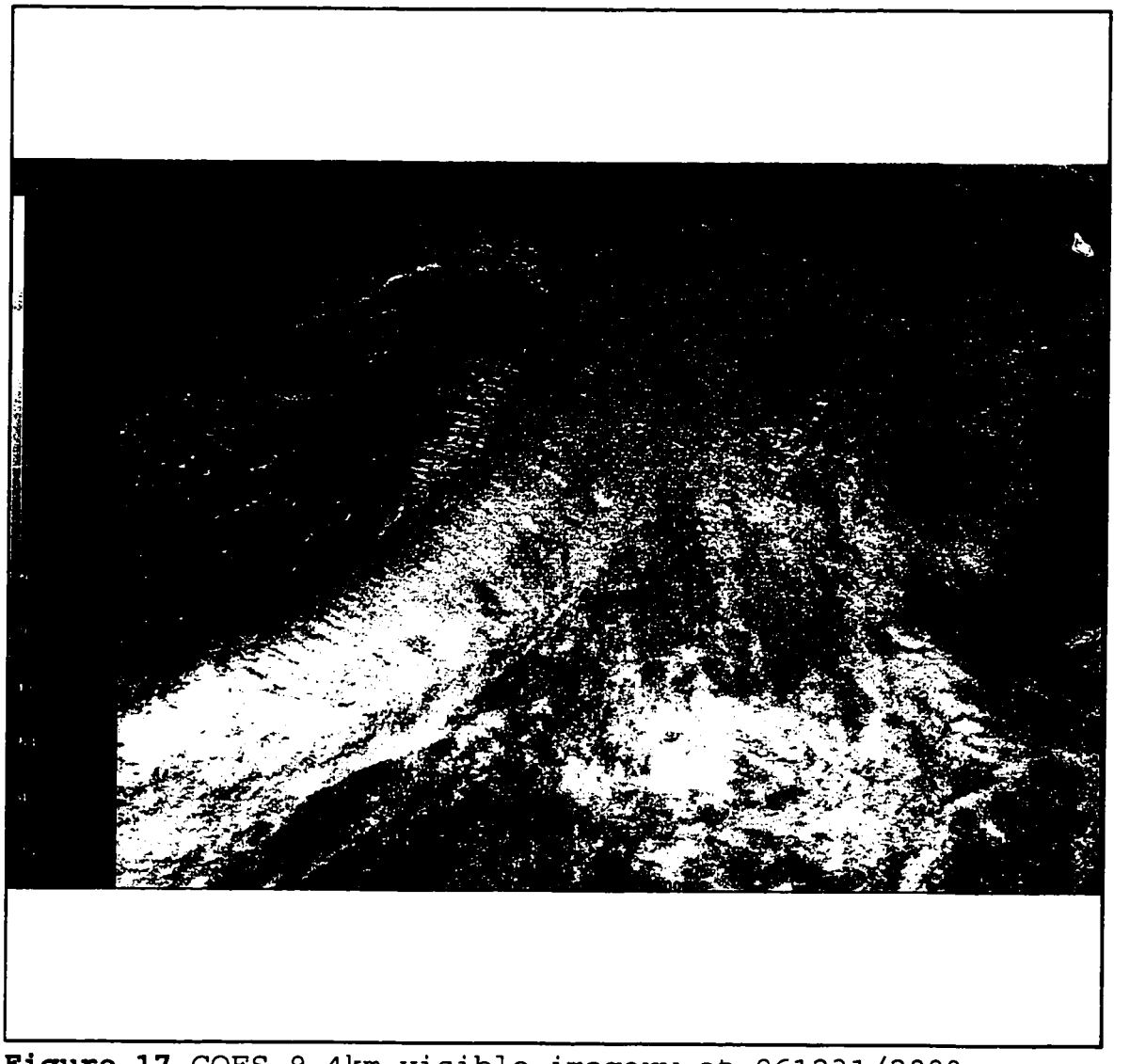

Figure 17 GOES-9 4km visible imagery at 961231/2000z.

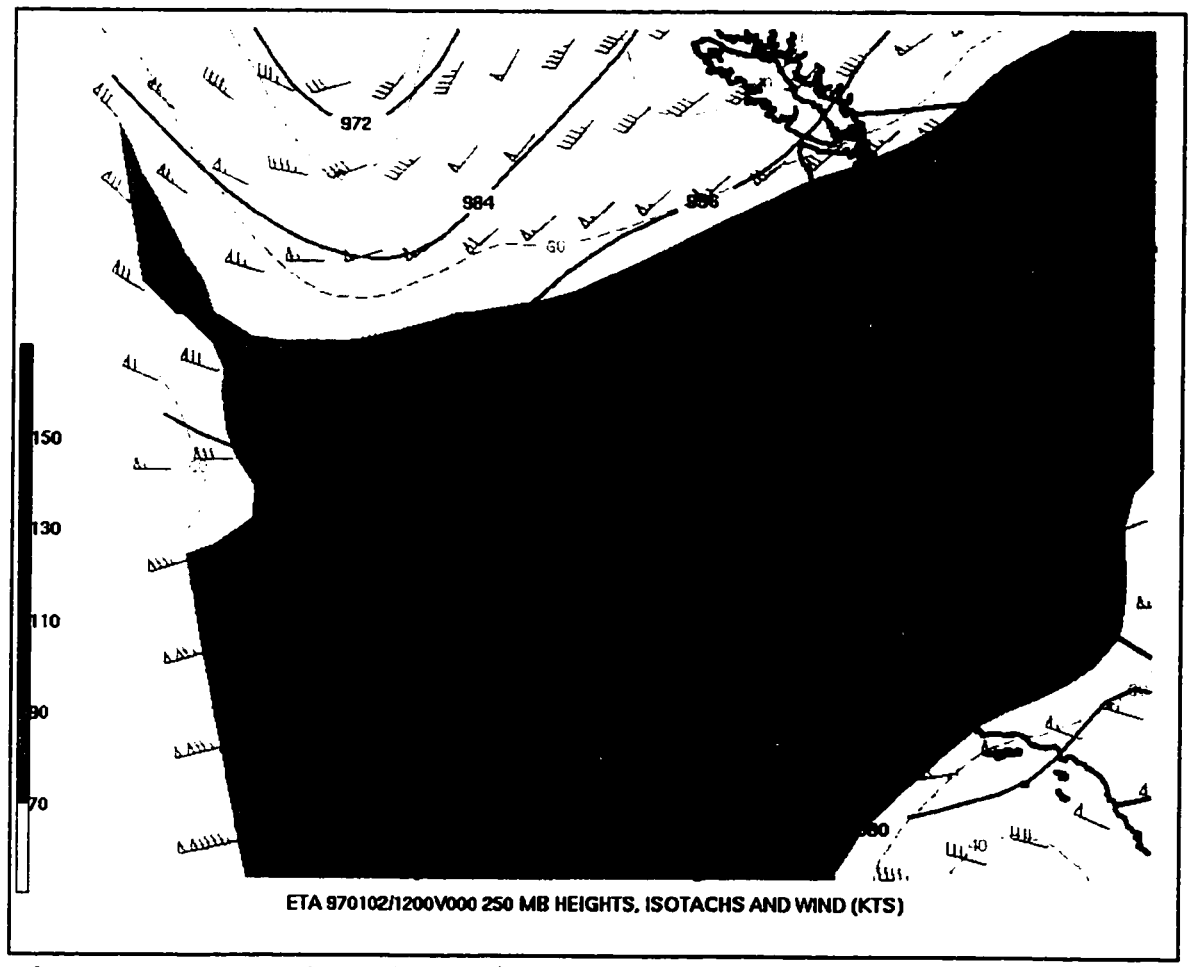

Figure 18 250 mb heights/wind (knt) for 961231/12z.

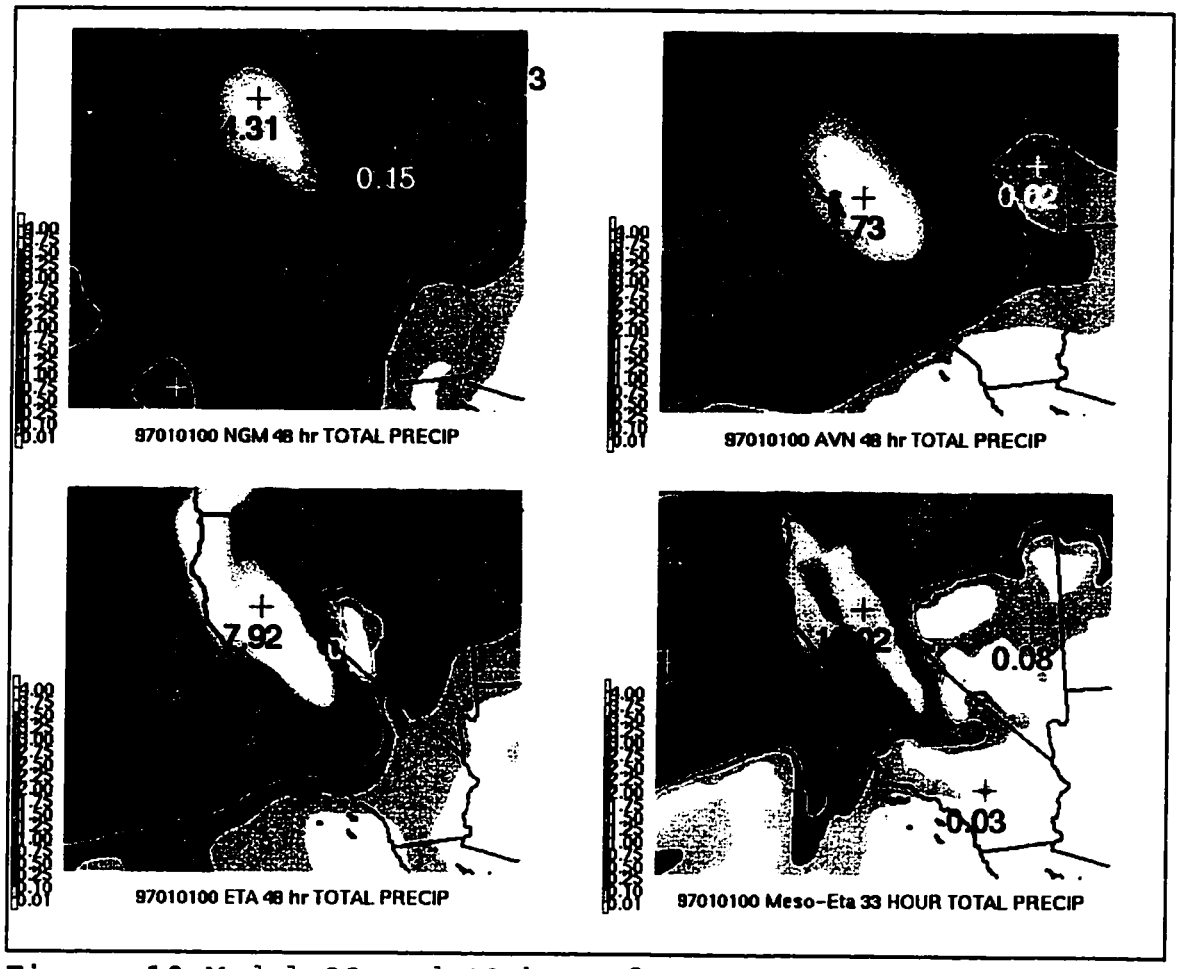

Figure 19 Model 33 and 48 hour forecast precipitation valid 970101/00z for the NGM, AVN, 48 km Eta, and 29 km Eta (33 hour forecast).

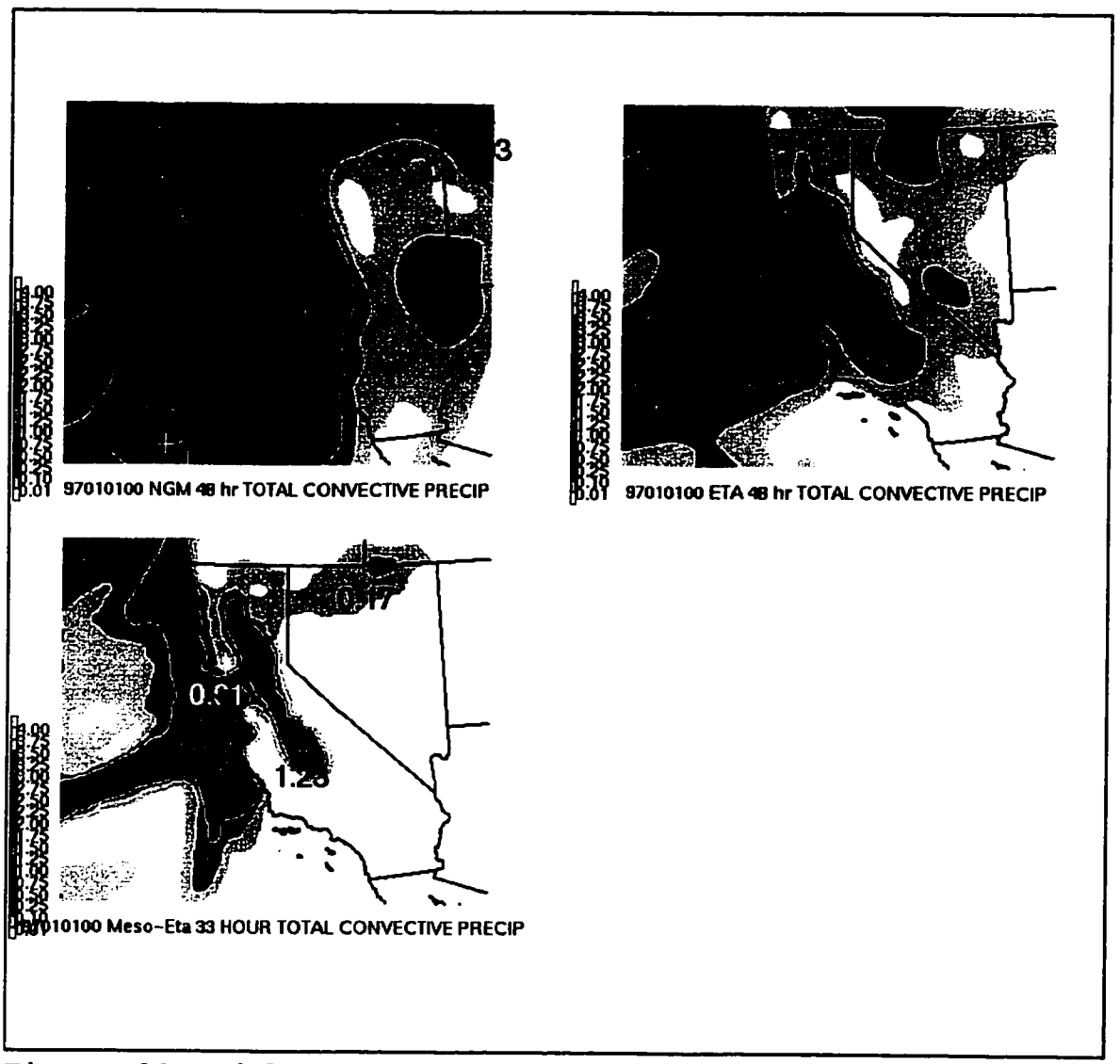

Figure 20 Model convective 33 and 48 hour precipitation valid 970101/00z for the NGM, 48 km Eta, and 29 km Eta (33 hour forecast).

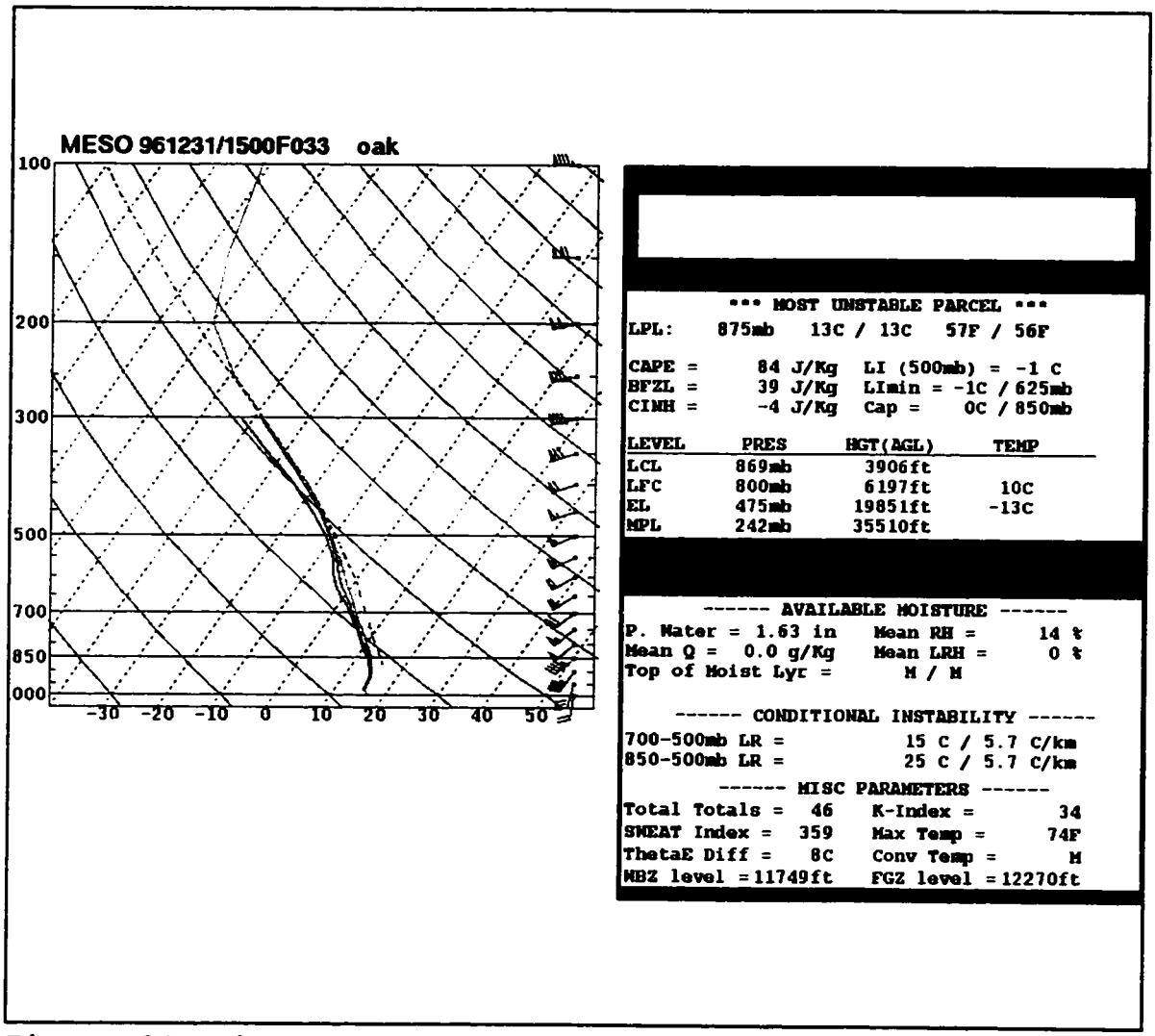

Figure 21 29km mesoscale Eta forecast sounding valid 970102/00z for Oakland.

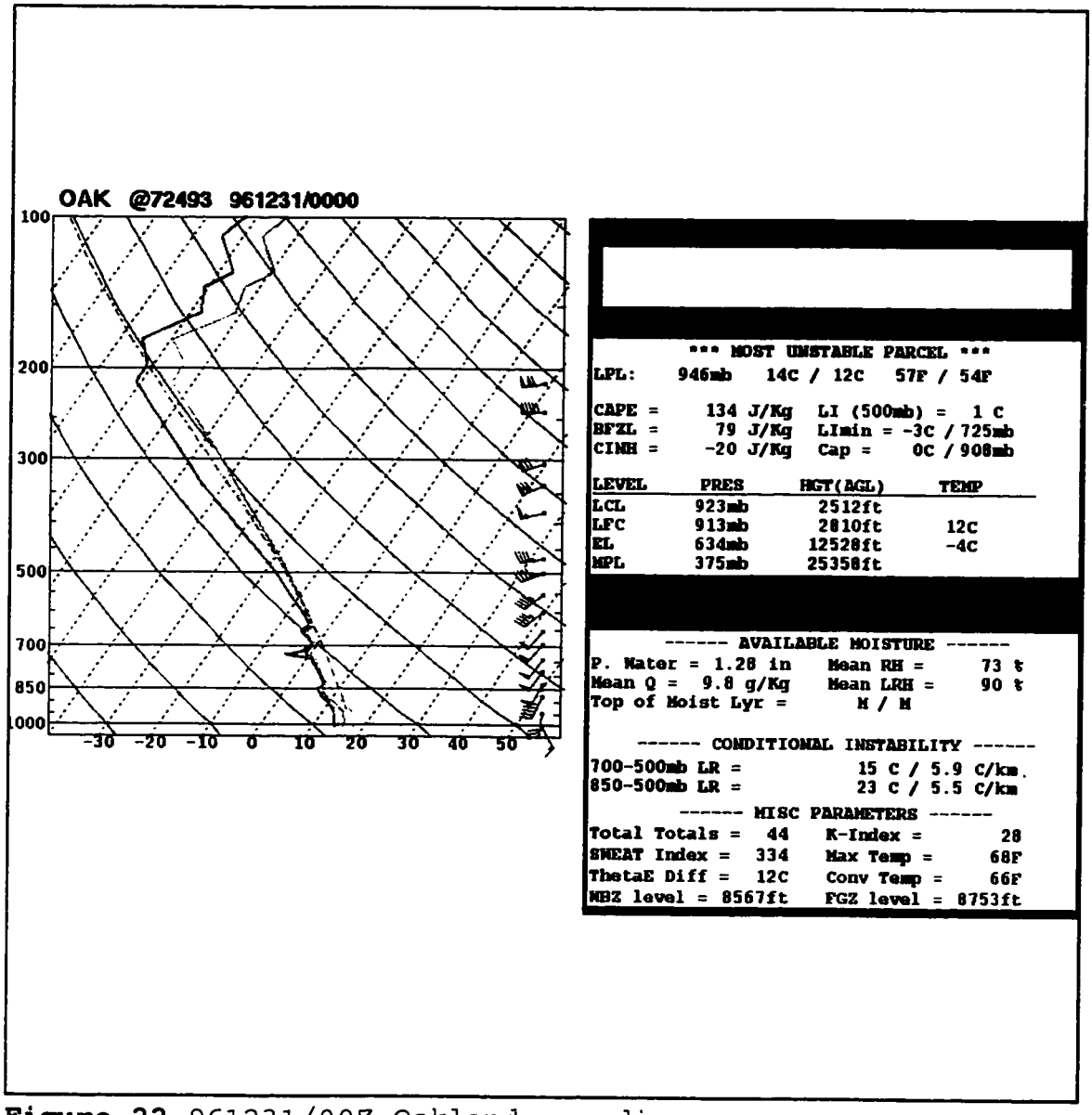

Figure 22 961231/00Z Oakland sounding.

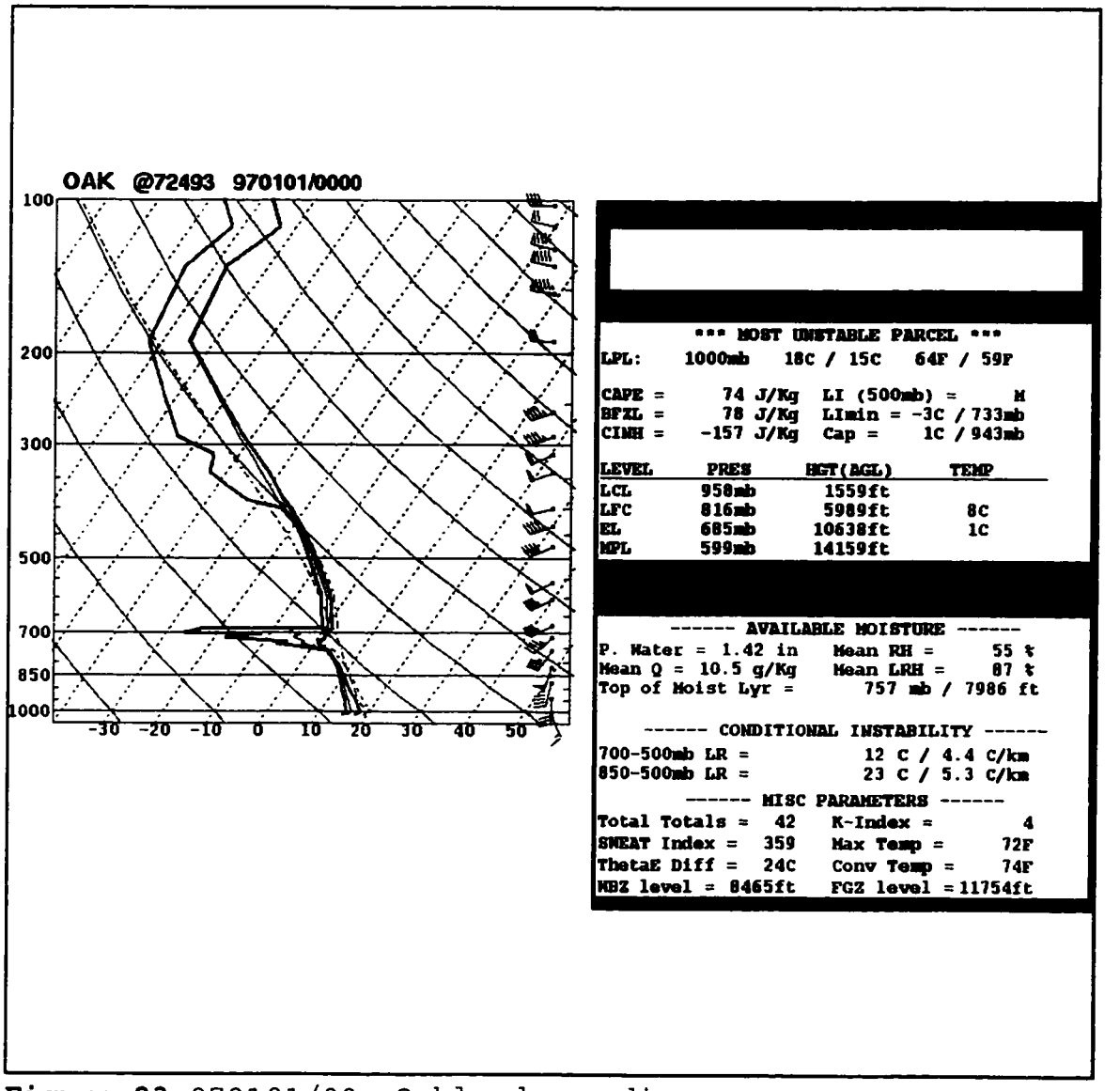

Figure 23 970101/00z Oakland sounding.

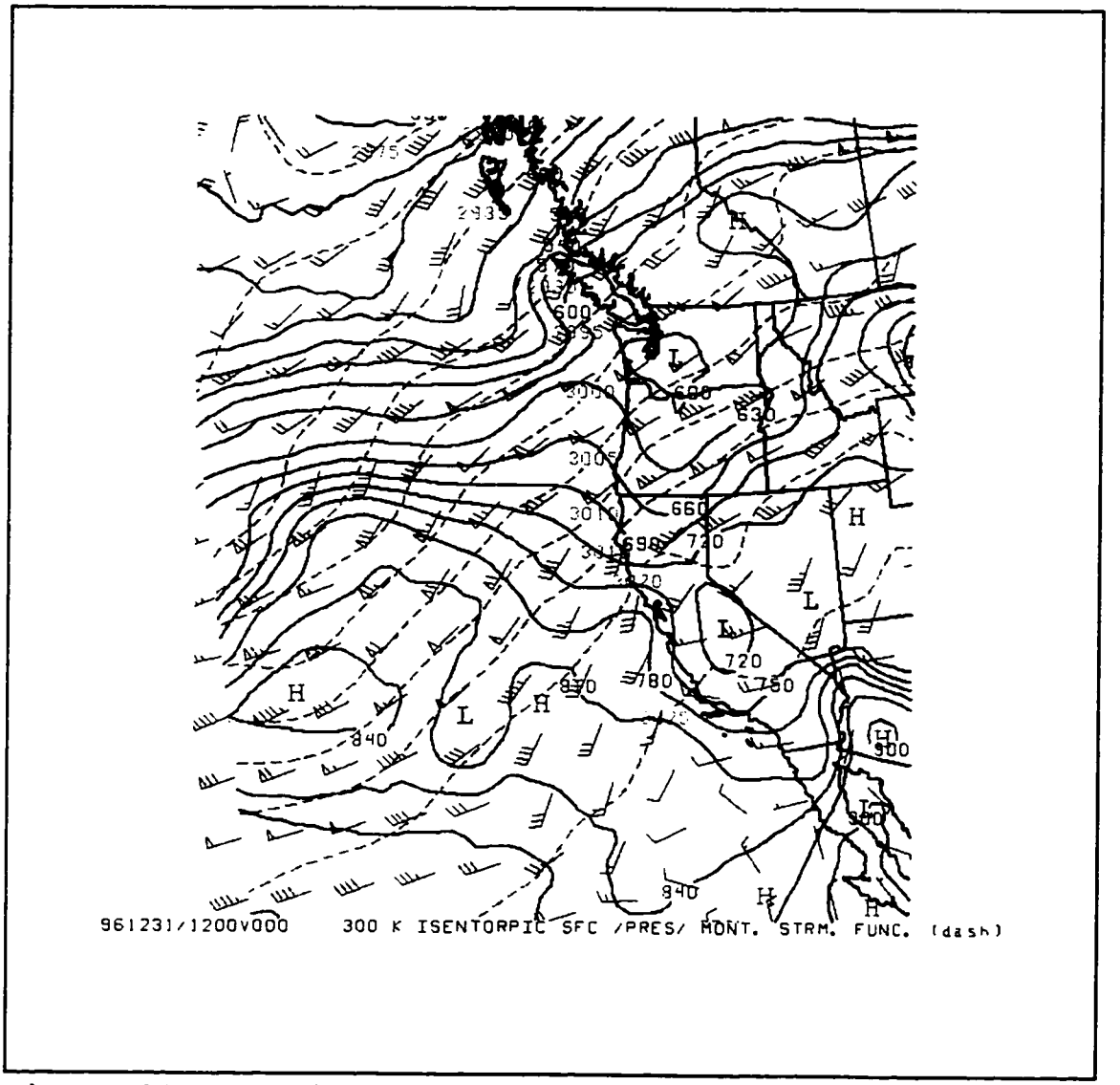

Figure 24 300 K isentropic analysis valid 961231/12z. solid lines=pressure surfaces, dash=montgomery stream function, wind barbs in knots.

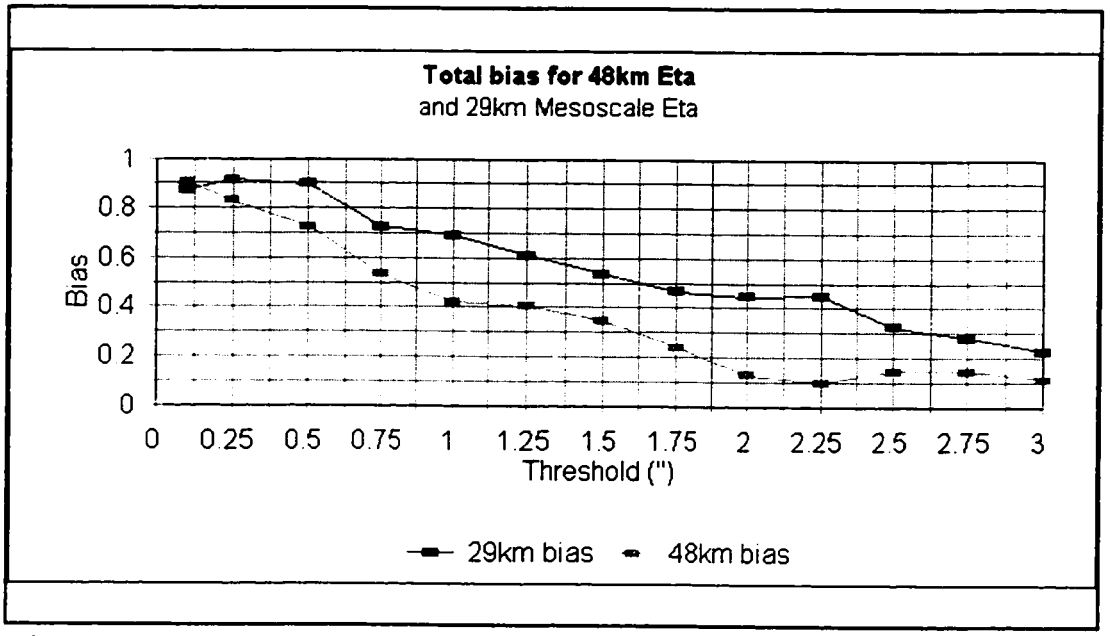

Fig 25 Winter Bias for 48 and 29 km Eta models

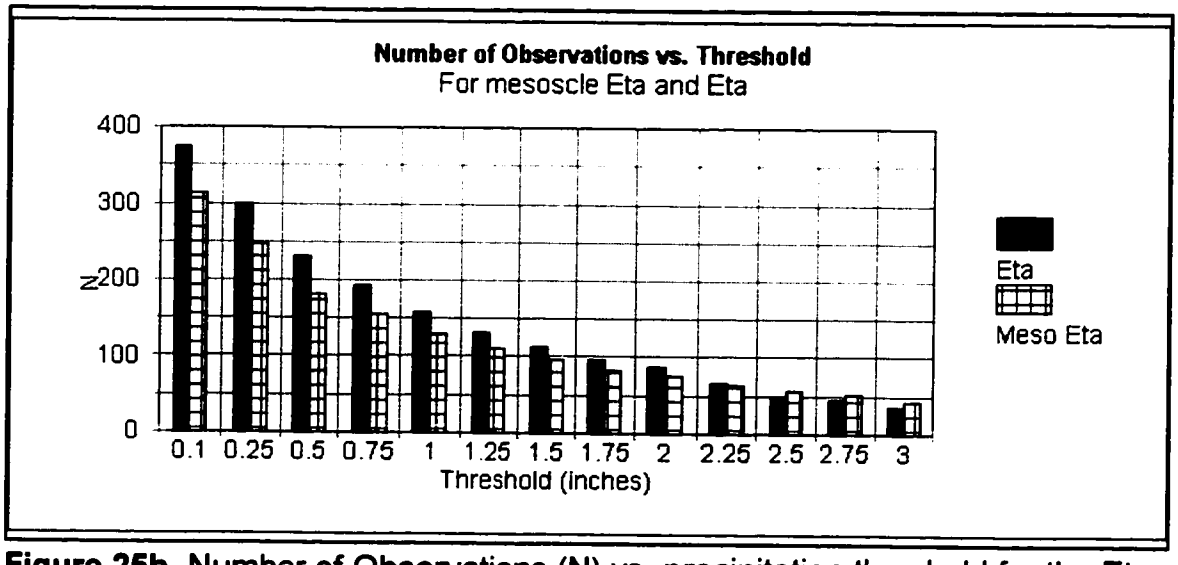

Figure 25b Number of Observations (N) vs. precipitation threshold for the Eta and Mesoscale Eta for the winter season statistics.

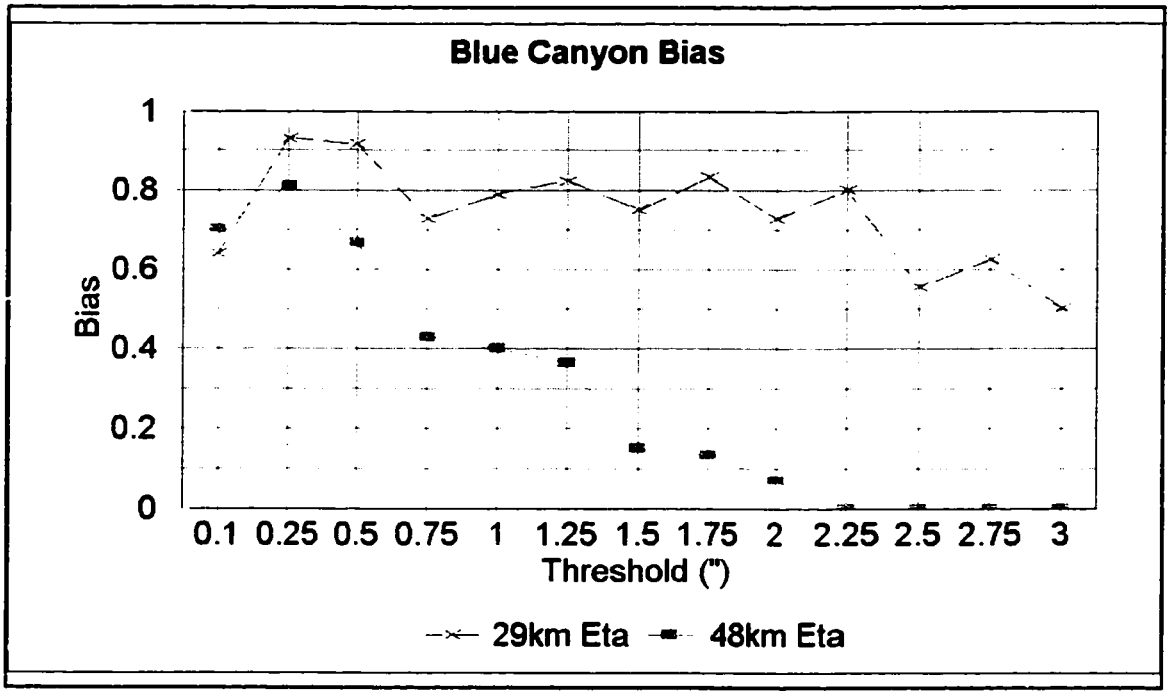

Figure 26 Model bias for Blue Canyon.

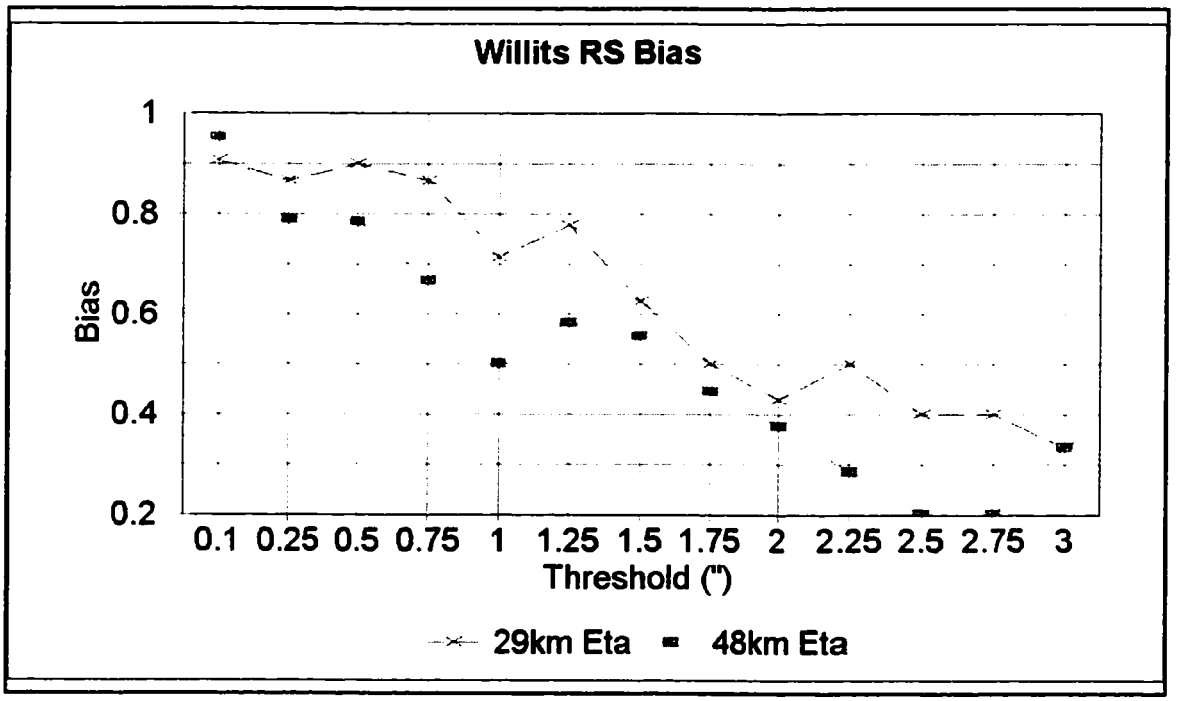

Figure 27 Model bias for Willits Ranger Station.

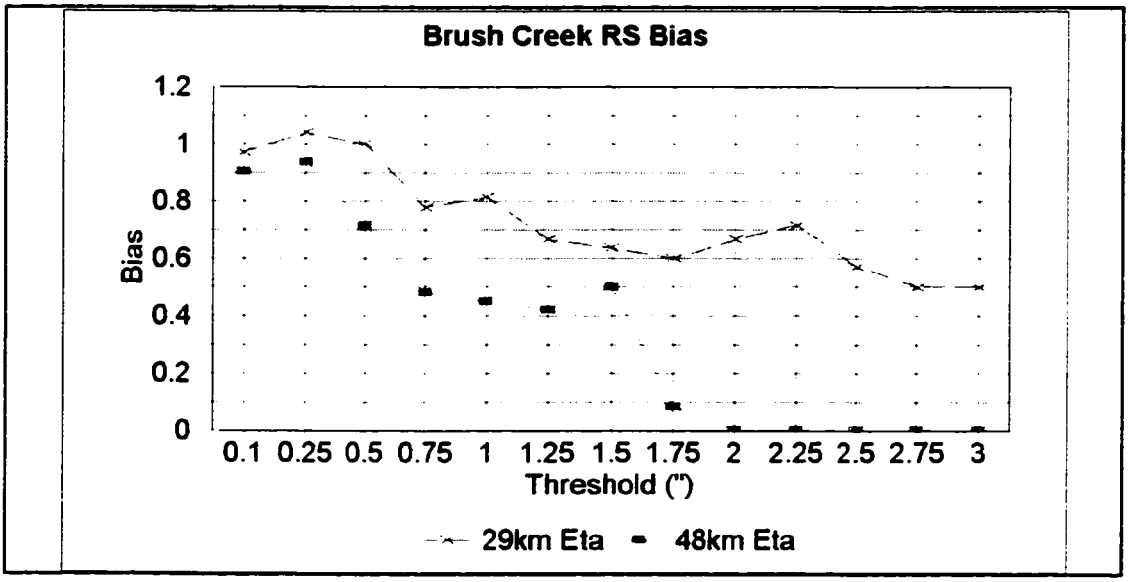

Figure 28 Model bias for Brush Creek Ranger Station.

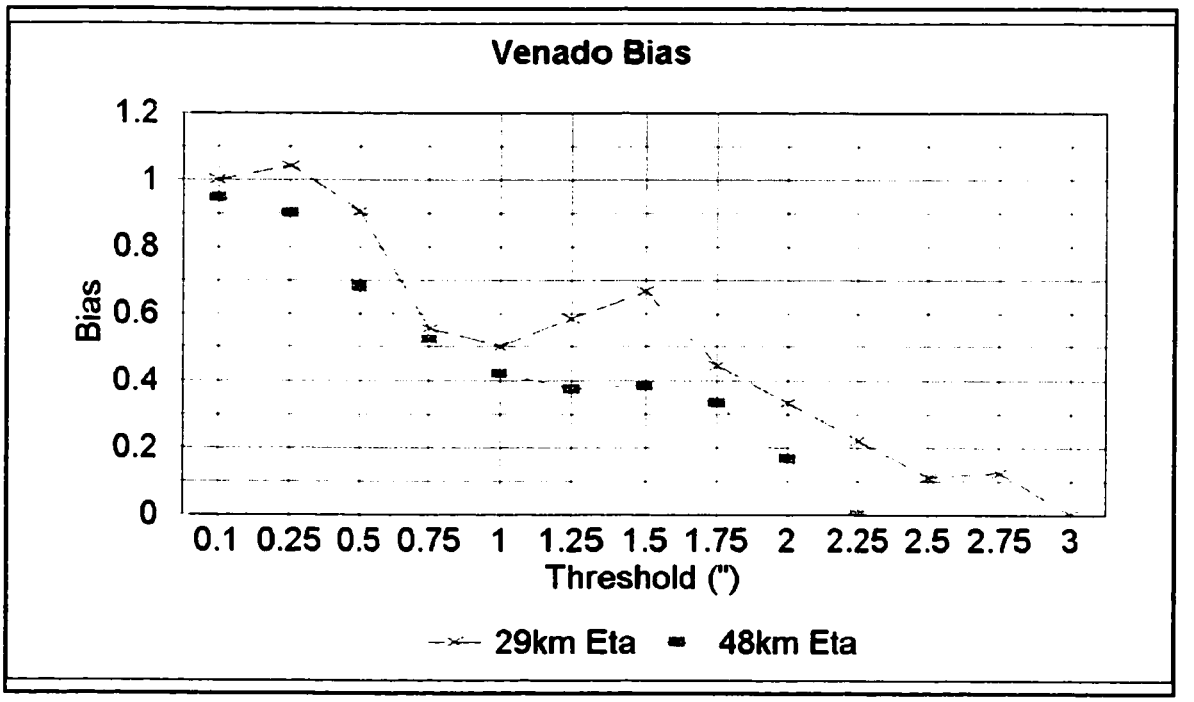

Figure 29 Model bias for Venado.

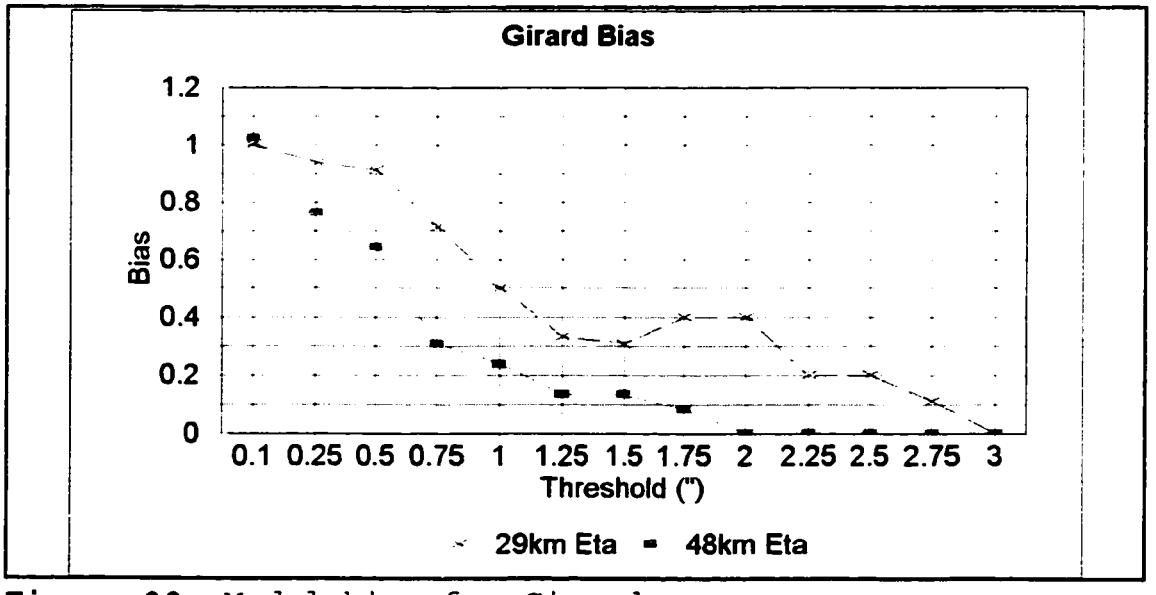

Figure 30 Model bias for Girard.

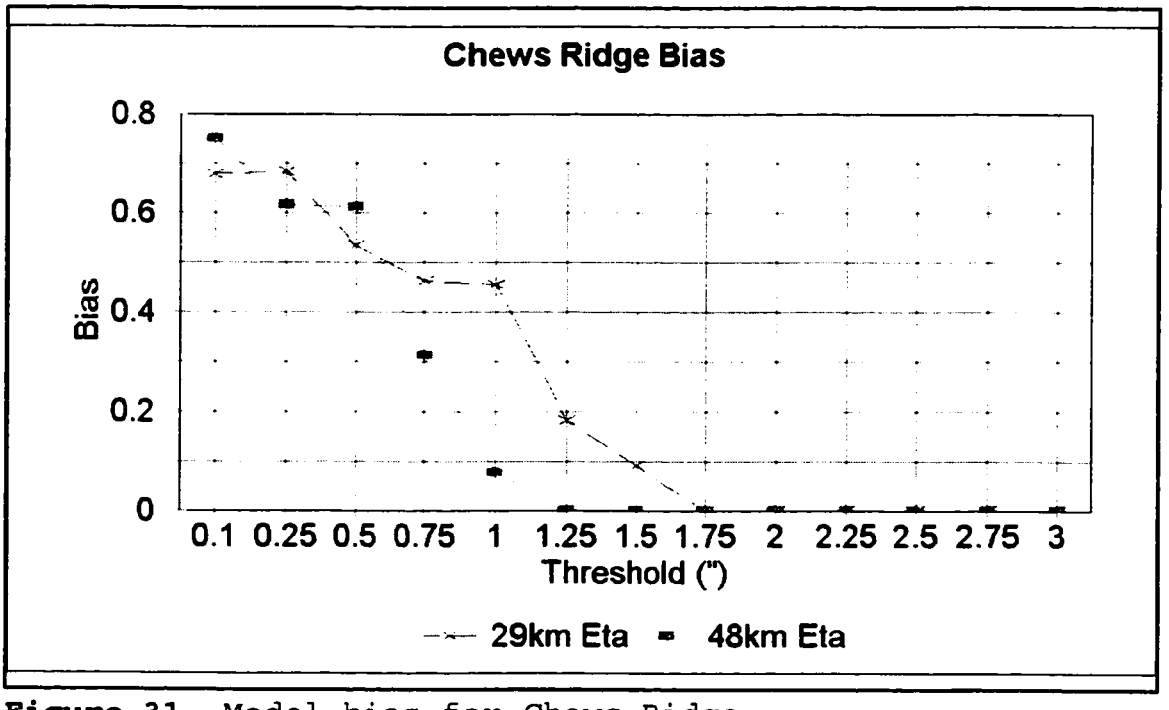

Figure 31 Model bias for Chews Ridge.

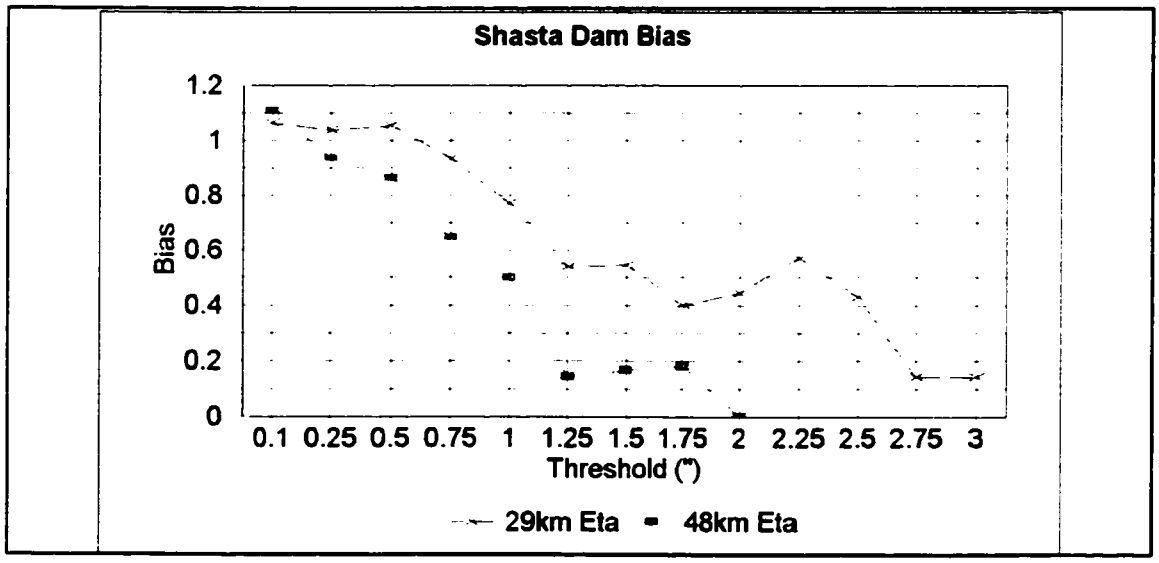

Figure 32 Model bias for Shasta Dam.

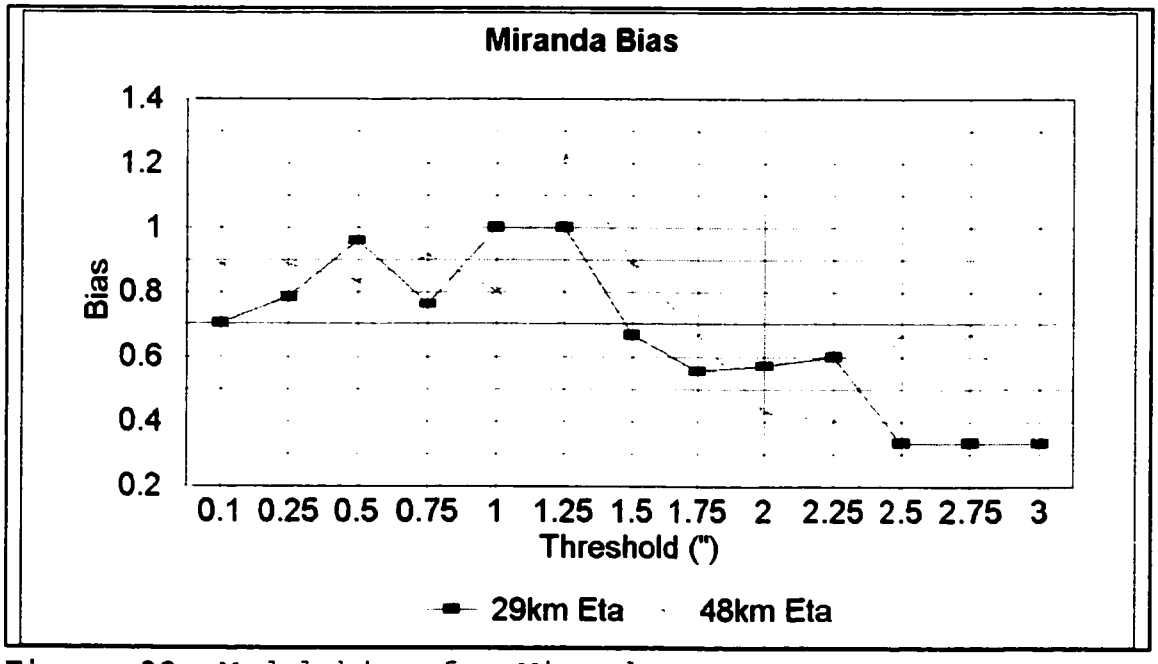

Figure 33 Model bias for Miranda.

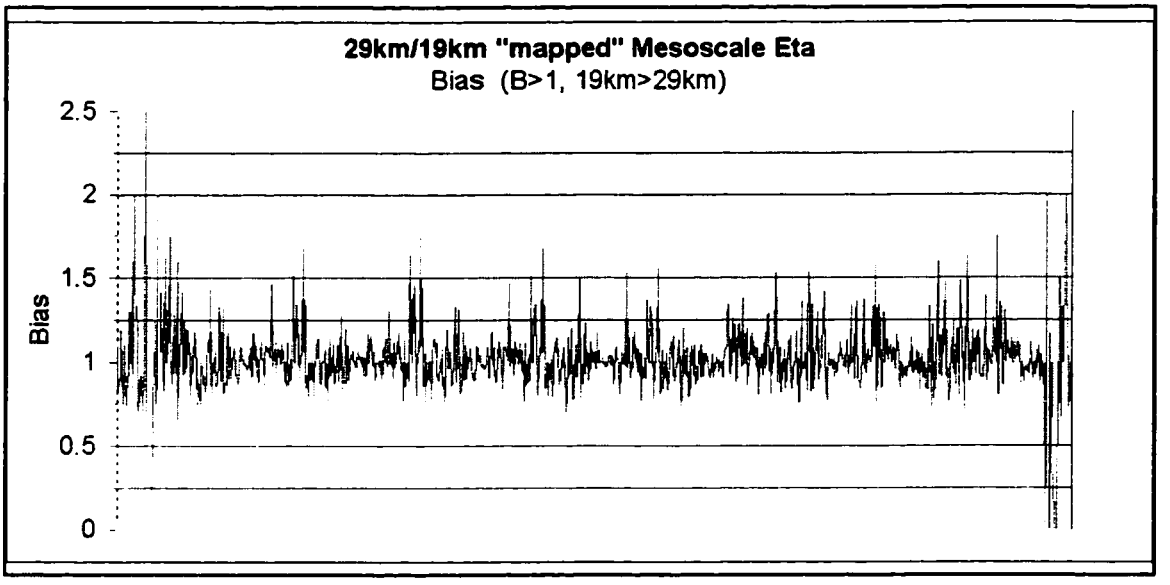

Figure 34 29 km Eta interpolated to 40 km / 20 km. For a bias>1, 20 km QPF > 40 km QPF.

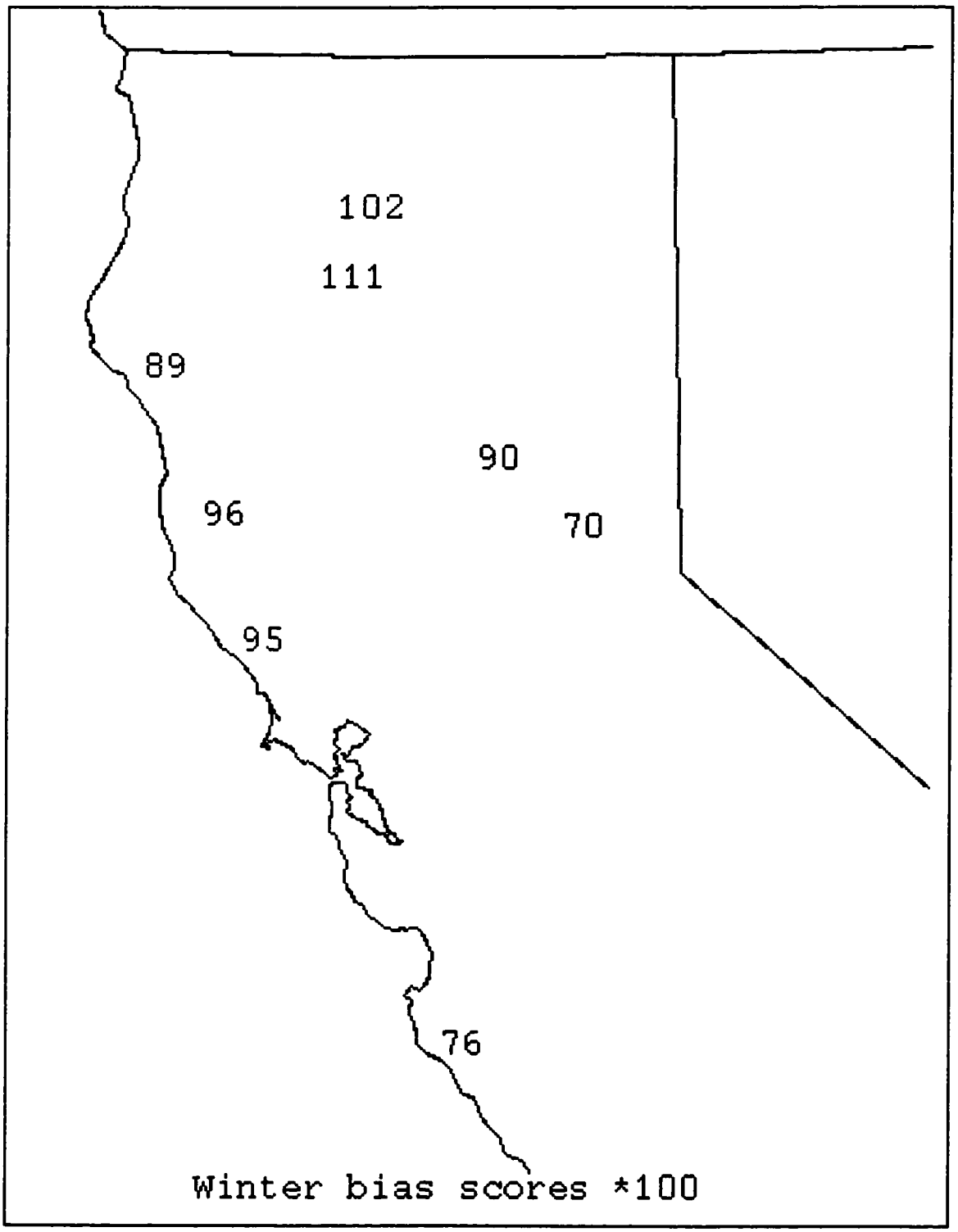

Figure 35 48 km Eta winter bias for 0.1" threshold.

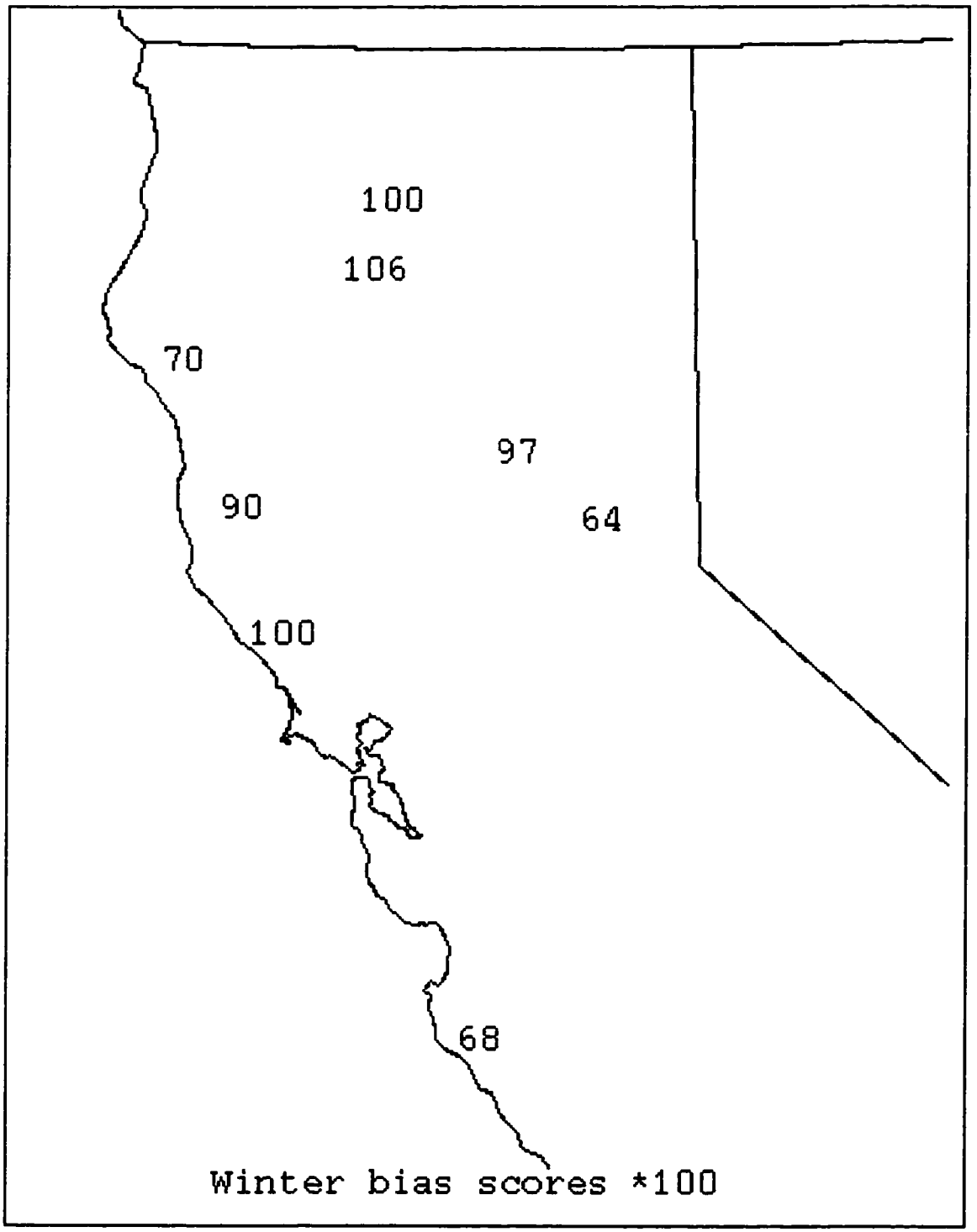

Figure 36 29 km Eta winter bias for 0.1" threshold.

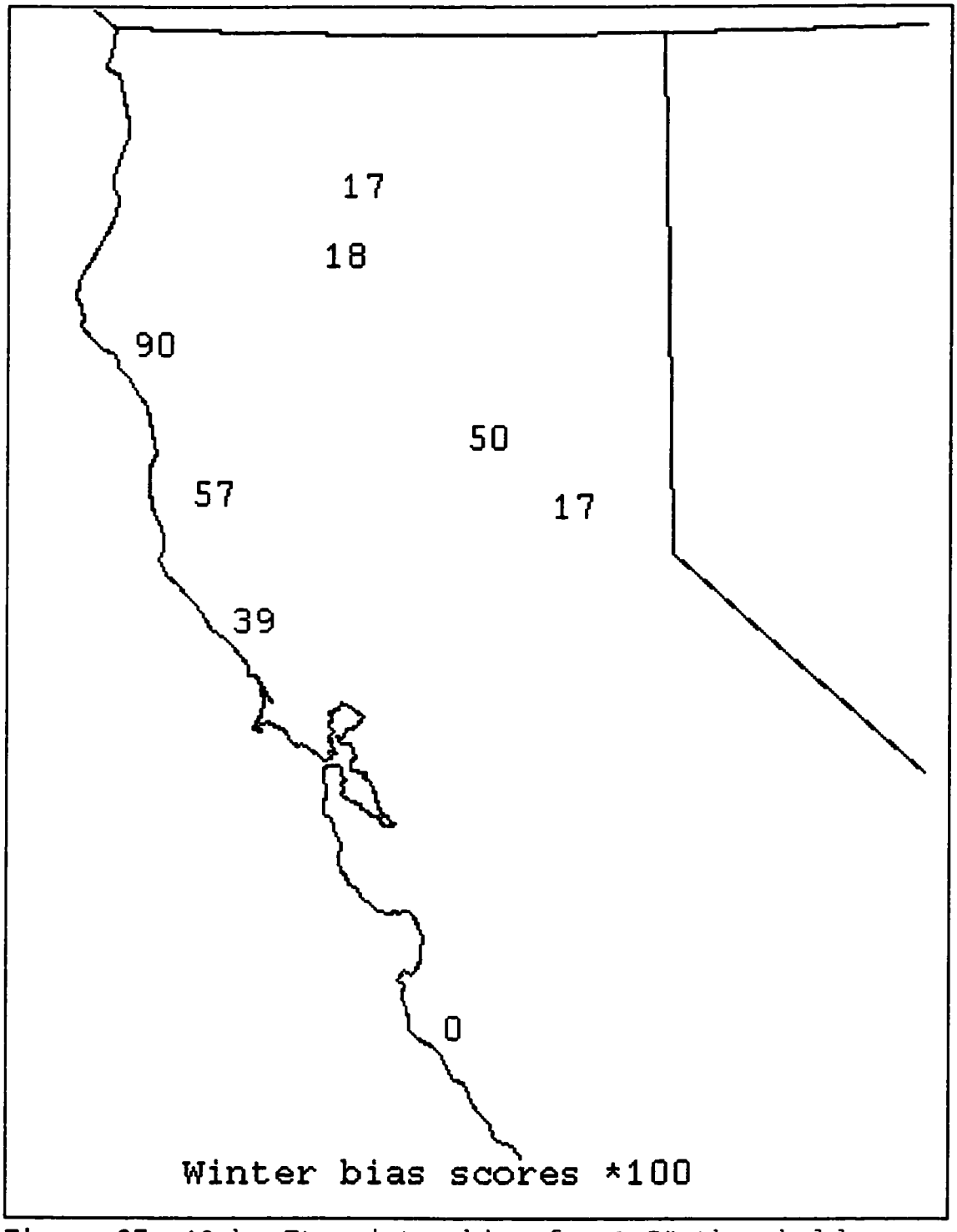

Figure 37 48 km Eta winter bias for 1.5" threshold.

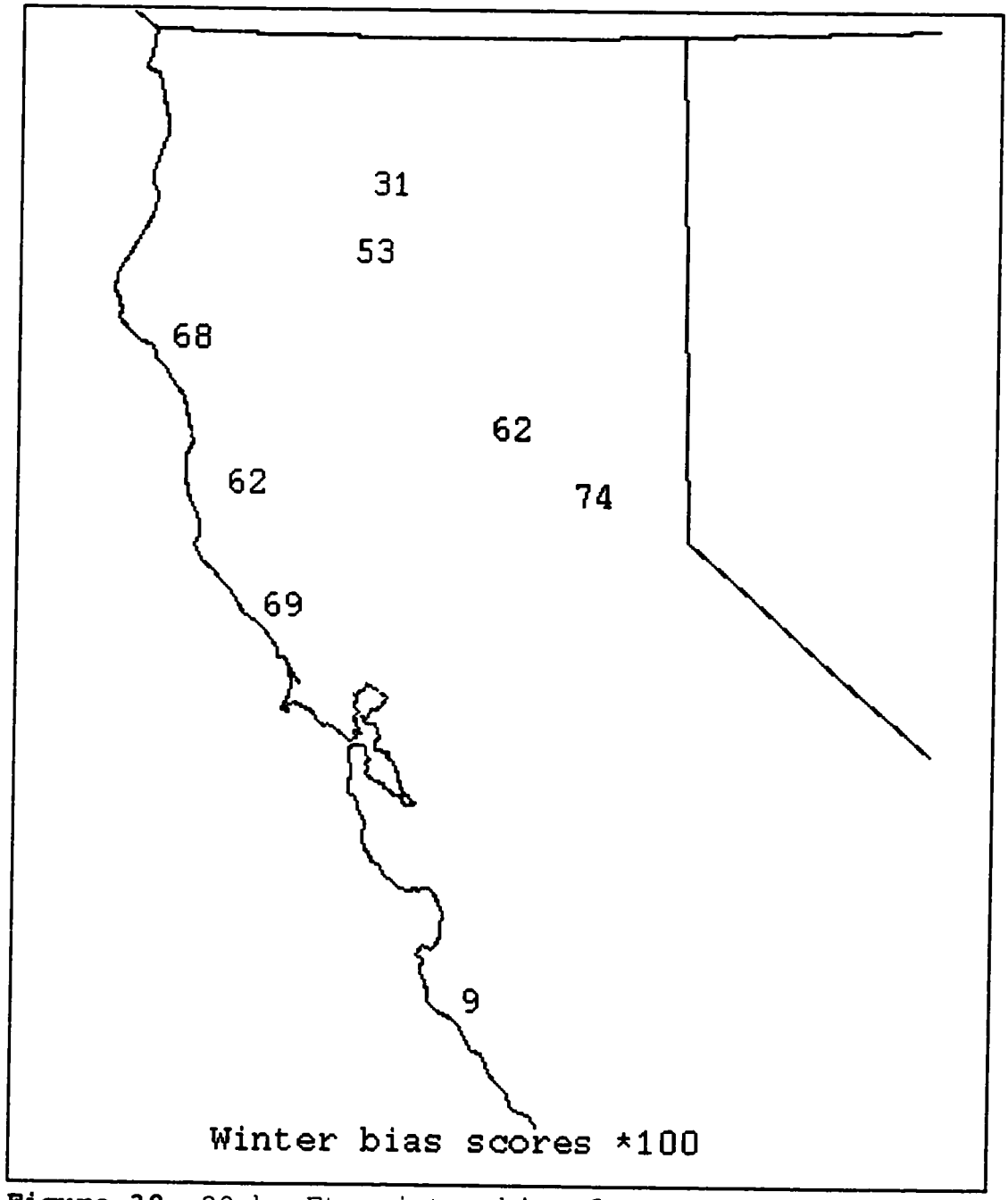

Figure 38 29 km Eta winter bias for 1.5" threshold.

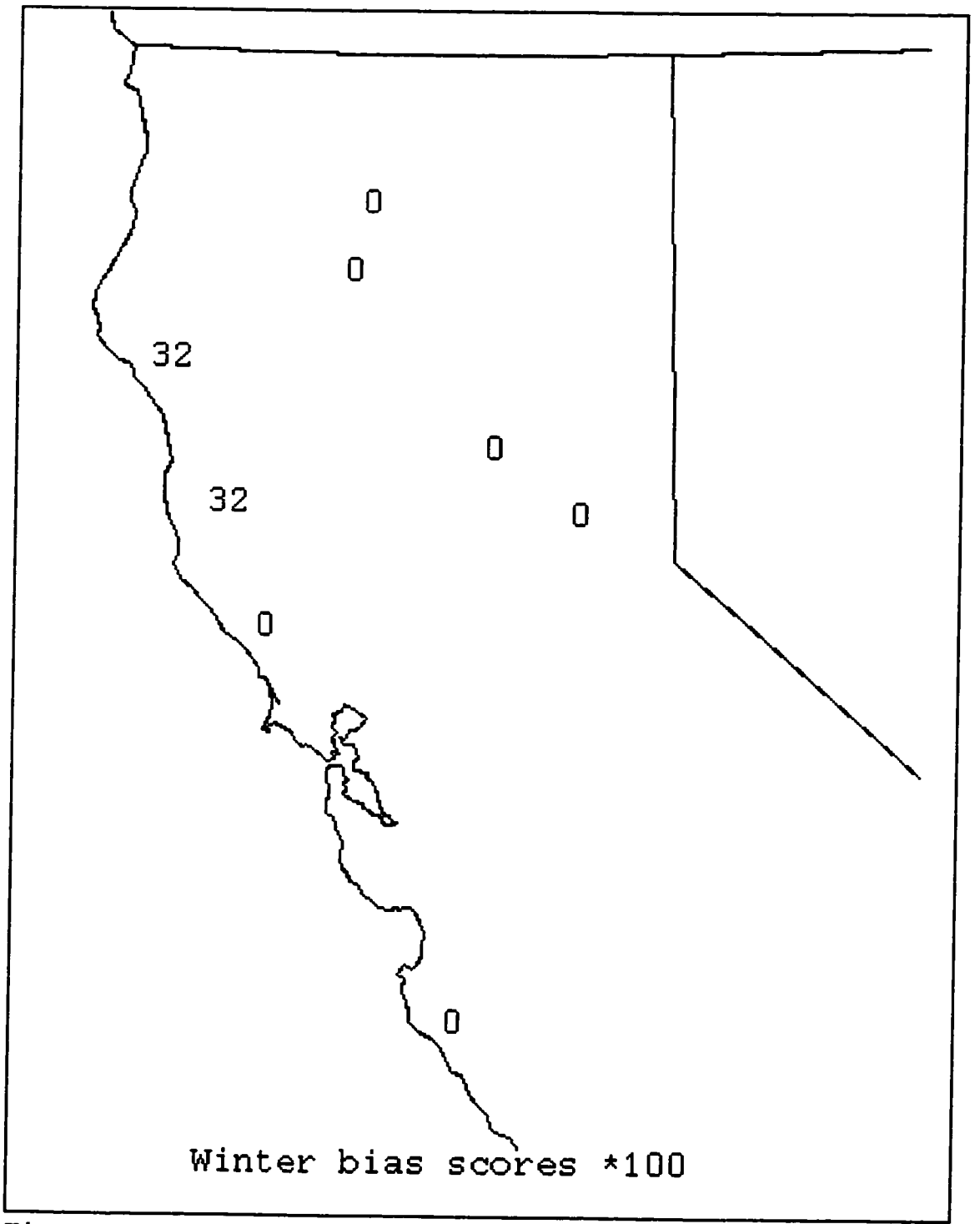

Figure 39 48 km Eta winter bias for 3.0" threshold.

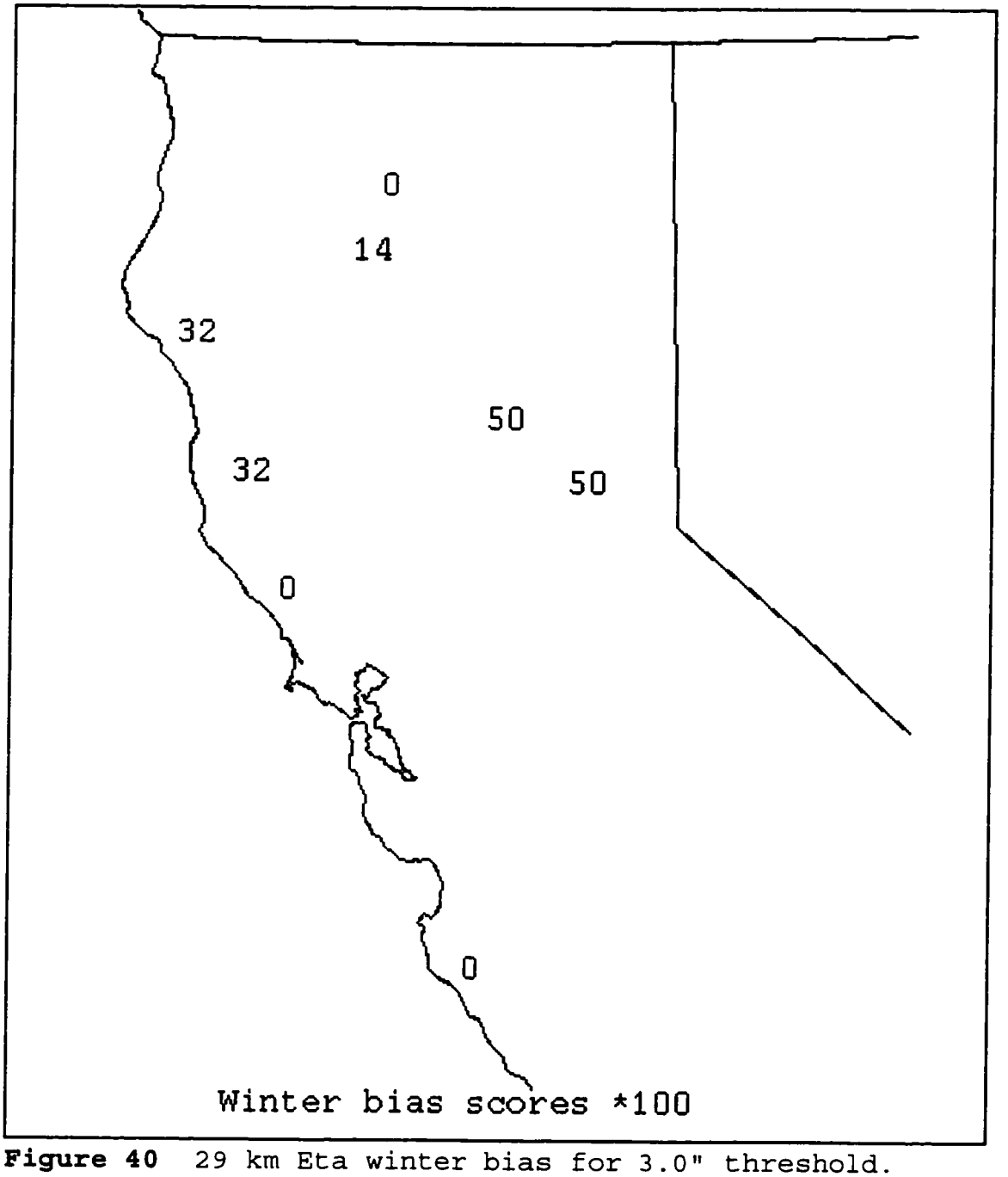

Figure 40 29 km Eta winter bias for 3.0" threshold.

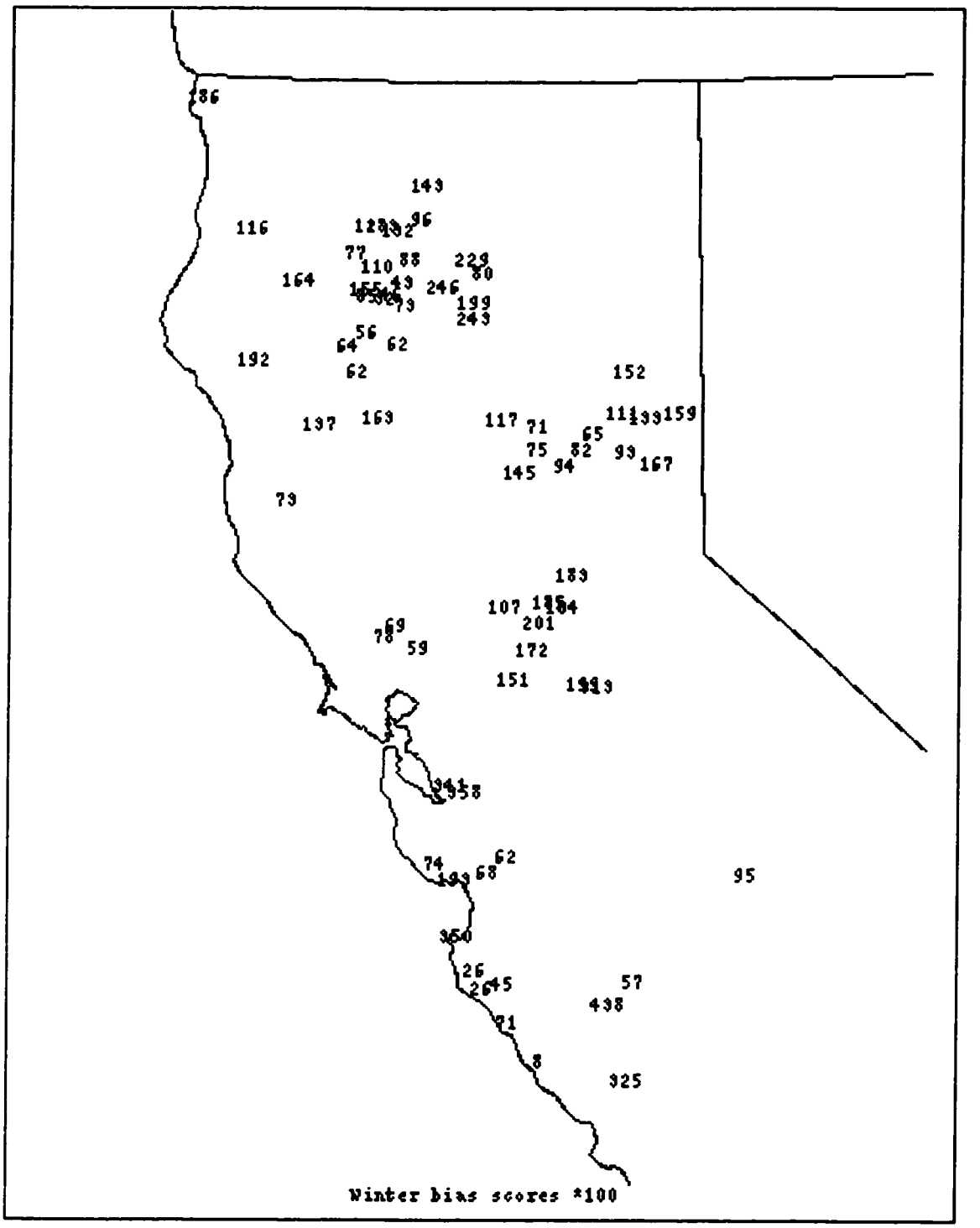

Figure 41 MM5 January 1997 24 hour precipitation bias*100 for 3.0" threshold.

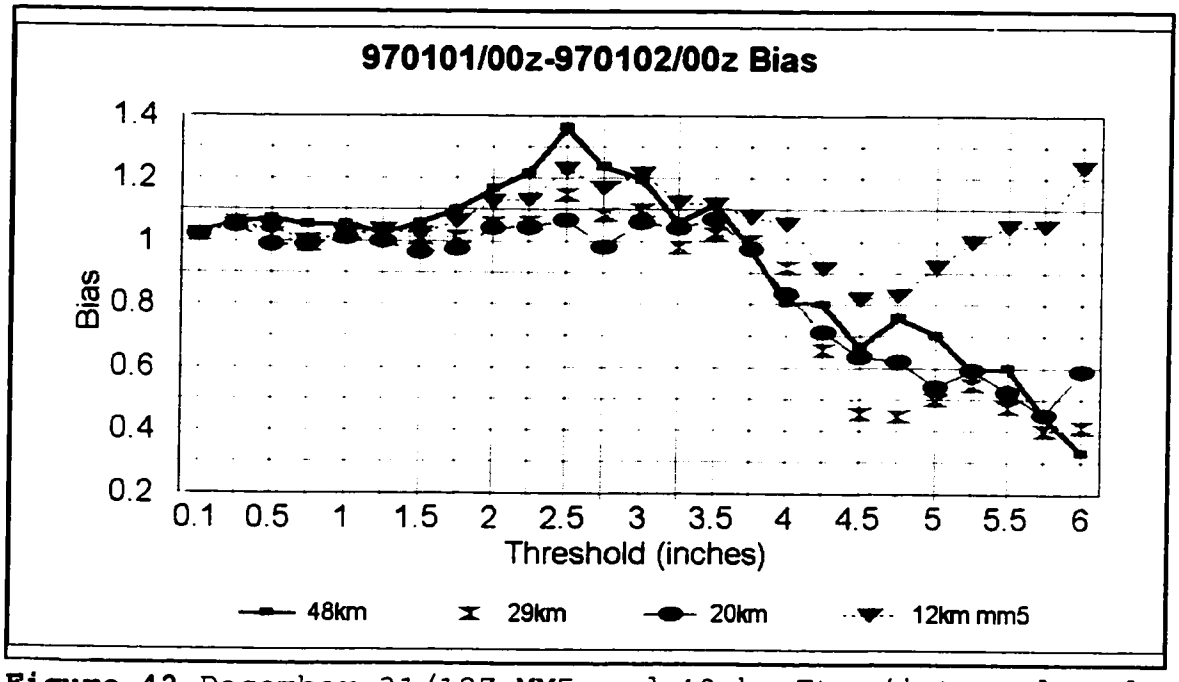

Figure 42 December 31/12Z MM5 and 48 km Eta (interpolated to 80 km), 31/15Z 29 km Eta (interpolated to 40/20 km) bias statistics. MM5 12-36 hr forecast. Eta 09-33 hr forecast.

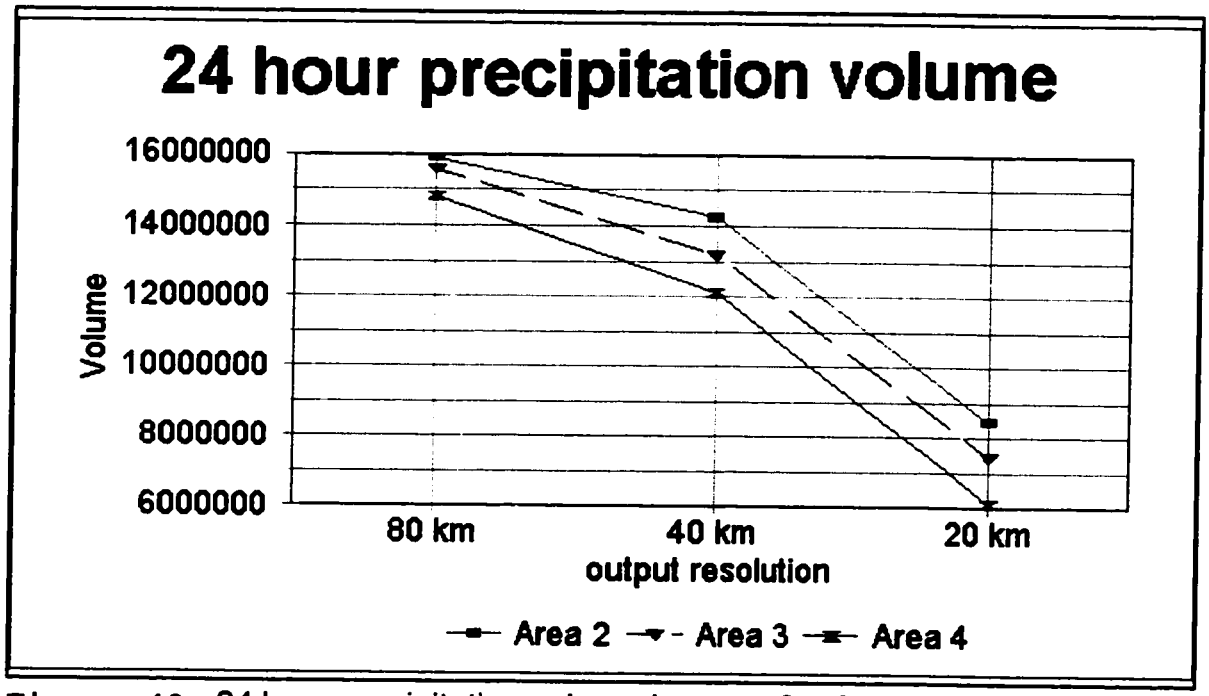

Figure 43 24 hour precipitation volume in areas 2-4 for the 48 km Eta, 29km Eta interpolated to 20 km and 40 km. Notice the greater volume for the courser grid.

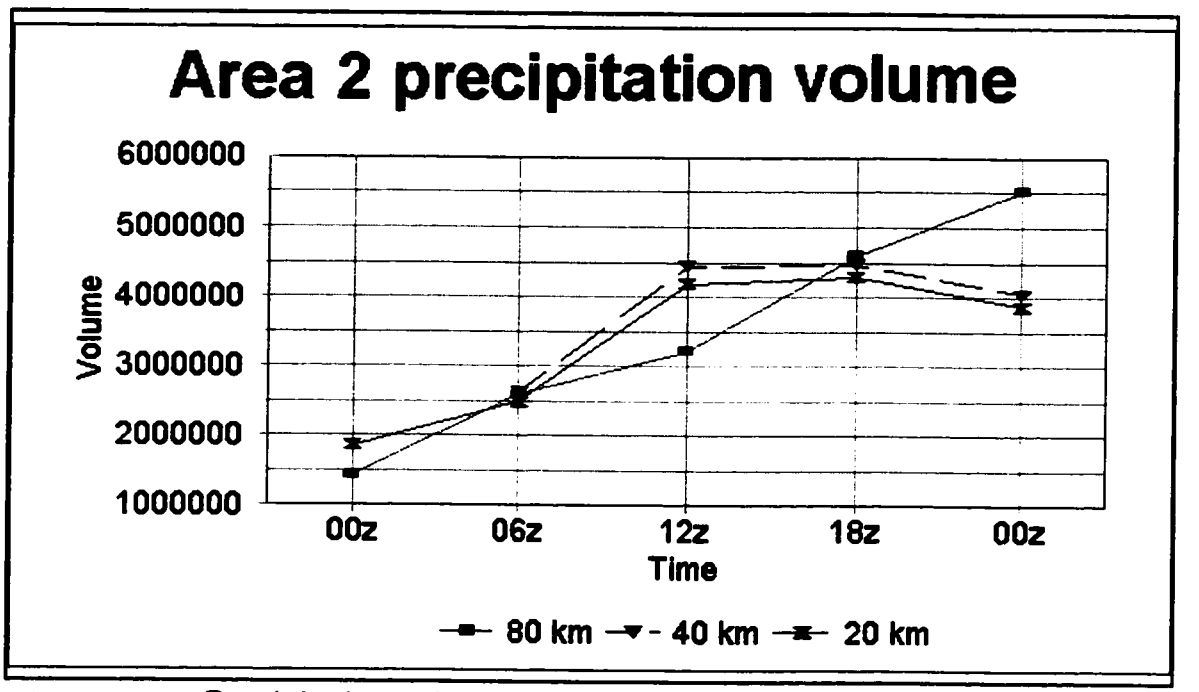

Figure 44 Precipitation volume six hour forecast for area 2. Notice the 80 km grid vs. 40/20 km grid time of maximum rainfall intensity.

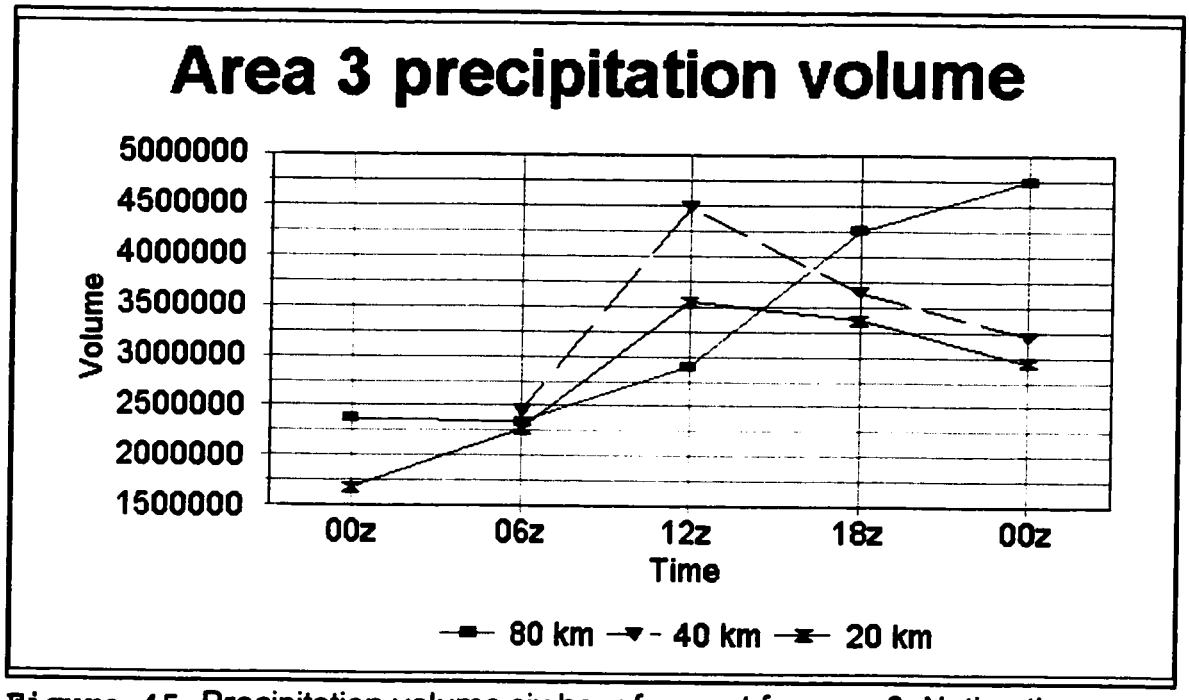

Figure 45 Precipitation volume six hour forecast for area 3. Notice the precipitation maxima at 12Z for the mesoscale Eta and at 00Z the next day for the Eta.

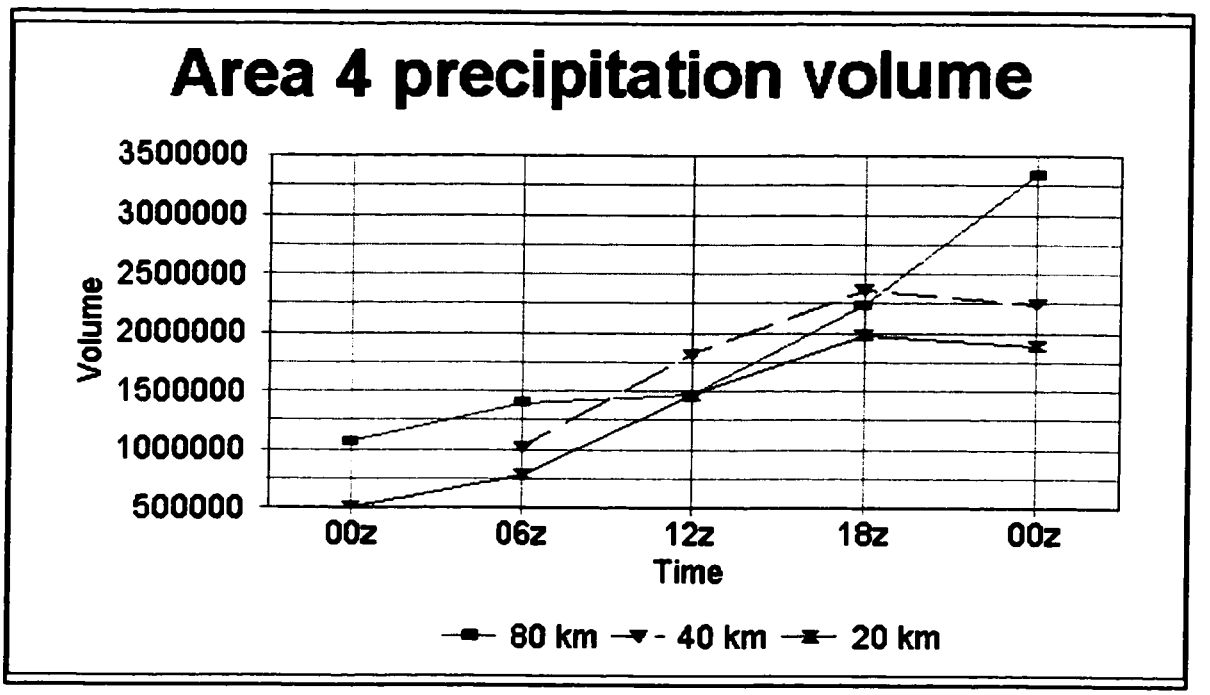

Figure 46 Precipitation volume six hour forecast for area 4.

IMAGE EVALUATION
TEST TARGET (QA-3)

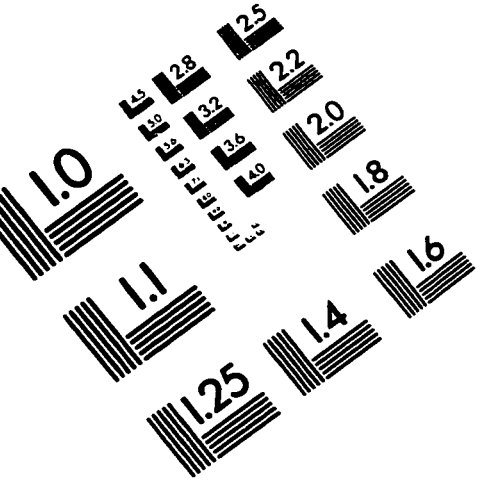

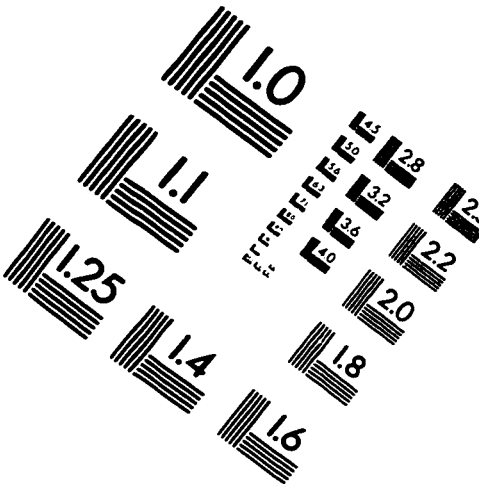

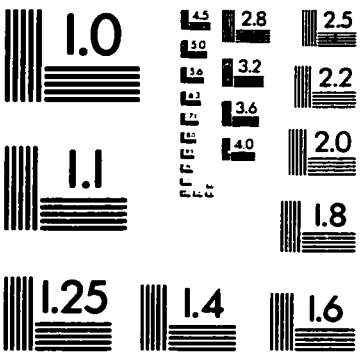

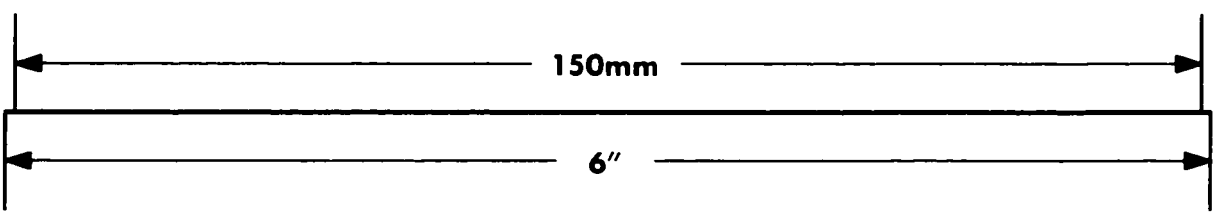

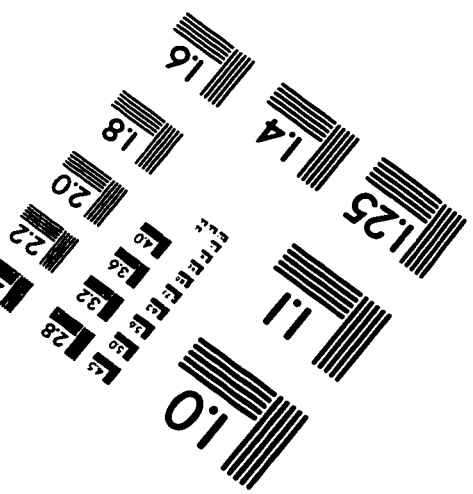

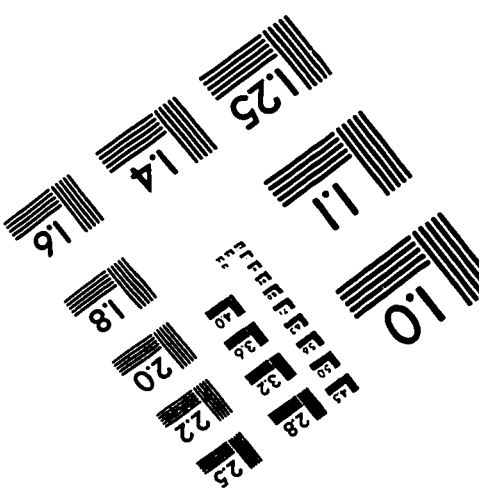

APPLIED IMAGE, Inc
1653 East Main Street
Rochester, NY 14609 USA
Phone: 716/482-0300
Fax: 716/288-5989